Jül-4362

Institute of Complex Systems
Strukturbiochemie (ICS-6)

Molecular Mechanisms of Signal Transduction in Two-Component Signaling Systems

Andrii Ishchenko

Mitglied der Helmholtz-Gemeinschaft

JÜLICH
FORSCHUNGSZENTRUM

Molecular Mechanisms of Signal Transduction in Two-Component Signaling Systems

Andrii Ishchenko

Berichte des Forschungszentrums Jülich; 4362

ISSN 0944-2952
Institute of Complex Systems
Strukturbiochemie (ICS-6)
Jül-4362

D 82 (Diss.,RWTH Aachen University, 2013)

Vollständig frei verfügbar im Internet auf dem Jülicher Open Access Server (JUWEL) unter
http://www.fz-juelich.de/zb/juwel

Zu beziehen durch:
Forschungszentrum Jülich GmbH
Zentralbibliothek, Verlag
52425 Jülich
Bundesrepublik Deutschland

Tel.: +49 2461 61-5220
Fax: +49 2461 61-6103
E-Mail: zb-publikation@fz-juelich.de

Contents

Introduction

Membrane proteins are one of the main components of cell membranes and serve for a variety of functions: transport, structure, signaling, cell communication, etc. Studies of membrane proteins are of high importance for understanding the key processes that maintain a cell in a viable state. With the help of membrane proteins cells grow, proliferate, exchange information with neighbors. Most of the cellular sensory systems are represented by membrane proteins. These proteins are particularly interesting for pharmaceutical applications and 70% of drugs are targeted to membrane proteins.

After the importance of studying membrane proteins was understood, a lot of methods were developed and adapted to address fundamental questions of their functioning. X-ray crystallography has become a method of choice for studying membrane proteins and complexes, since it allows researchers to obtain the atomic level structure of proteins. Structural information, then, often reveals the design of the active site. By crystallizing the protein together with the ligand one can trap it in an active state and explain, by such structures, the mechanism of functioning.

Despite the well-established importance and wide interest, the number of the structures of membrane proteins available at the moment is small. The rate of appearance of membrane protein structures is lagging considerably behind that for water-soluble proteins. The reasons for that are difficulties that researchers encounter at the stages of protein preparation and crystallization. Overexpression of a membrane protein in *E.coli* is a tough task. Normally, the expression levels would be very low. Also, solubilization and purification steps are not straightforward and require many routine screenings of conditions. Crystallization, as the last step of crystal preparation, remains the main stumbling block to the membrane protein structure. The proteins solubilized in detergents are usually unstable and don't retain native structure. They yield crystals of poor quality. New crystallization methods have emerged and developed during the last decade. One of these methods, the *in meso* approach [1–3], was used in this study.

Two-component signaling systems (TCSS) [4,5] comprise a class of proteins that has acquired recently a potential interest of researchers. In contrast to eukaryota, most prokaryotic signal transduction pathways use schemes of phosphate transfer involving two conserved components, a histidine protein kinase (HK) and a response regulator protein (RR). To the moment, hundreds of such systems were found in eubacteria, archaea and a few

eukaryotic organisms. Two-component systems serve as a general stimulus-response mechanism of coupling that allow organisms to feel and react to changes in many different environmental conditions (for a review see [4]). Though a lot of advances in the field of signal transduction in TCSS have been made recently, there is still a strong demand for robust model systems where the molecular mechanism of signal transduction can be studied. The complex of the two membrane proteins from halobacterium *N.pharaonis,* sensory rhodopsin II (SRII) with its cognate transducer (HtrII), is an example of the TCSS system, where the signal transduction was studied in detail. This complex is serving as a phototaxis receptor that helps bacteria to avoid harmful UV light. It is unique for combining two huge independent classes of membrane receptors – 7TM (7-transmembrne helices) and two-component signaling systems, being the first component of such system. Sensory rhodopsin II belongs to the family of archaeal retinal proteins, were members are represented by bacteriorhodopsin, halorhodopsin, sensory rhodopsin I etc. Another protein in the complex, halobacterial transducer II, is highly homologous to bacterial chemoreceptors and histidine kinases (HK). All chemoreceptors share a common modular design and modules are included depending on the function of the receptor. HtrII consists of a transmembrane domain, a linker domain (between two HAMP domains), a methylation region, involved in the adaptation to the intensity of light, and a kinase domain.

The X-Ray structure of SRII/HtrII gives a unique insight into the complex of two transmembrane proteins [6,7] (PDB code 1H2S, 2F95). These structures elucidate initial steps of signal transduction in SRII and a possible mechanism of signal transfer to HtrII. Another representatives of TCSS, NMR structures of the cytoplasmic domain of the osmotic sensor EnvZ from *E.coli* have shown the design of the kinase domain that is highly conserved among all histidine kinases [8,9]. Despite this structural information there is still no detailed molecular mechanism of functioning of the complex from the initial step of retinal isomerization until the phosphate group transition to the kinase CheA. This work is aimed to elucidate some of these steps in detail and to show by means of X-Ray analysis the key features of protein structures that are prerequisite for efficient signal transduction.

All halobacterial retinal proteins share common features of the signal transduction mechanism. One of these features is a proton transfer from the Schiff base to the counterion amino acid residue upon retinal chromophore isomerization. Various studies have shown that the mutation of the counterion to a neutral amino acid residue is critical for the function of most of them [10–12]. Asp75 is a Schiff base counterion in the case of SRII from archaea *N. pharaonis*. In the case of SRII/HtrII complex, physiological experiments have shown that

Asp75-to-Asn75 mutation doesn't inhibit the signal transduction that is seen as persistent rate of cell motion reversals upon light illumination. This fact is important for understanding the signal transduction mechanism in these systems. The structure of SRII-D75N/HtrII described in our work shows the differences in the hydrogen bond network of the mutant complex with respect to the wild type complex. Its comparison with the ground and M states of the wild type has helped to understand how the signal transduction process might be evolved in D75N mutant protein.

Extensive crystallization trials under various conditions have resulted into another finding that may be very important for understanding of the mechanism of functioning. Crystals of different space groups were produced and the structures in these space groups were compared to the previously published structures in the $P2_12_12$ space group. A striking difference in the arrangement of the SRII and HtrII proteins in the complex was observed. Whereas in the $P2_12_12$ space group the proteins form a crevice with an opening towards the cytoplasmic side ("V"-shape), in the newly obtained structure of $I2_12_12_1$ space group the proteins are roughly parallel to each other ("U"-shape). This thesis contains an analysis of the biological relevance of the protein complex quaternary structures.

The HAMP domain is a linker domain between the membrane and cytoplasmic parts of HtrII [13–16]. Though, it is abundant in different classes of proteins (found in more than 4500 different genes), its function is still unknown. Several structures of the HAMP domains have already been published [17,18]. However, there are several drawbacks in these structures that hinder understanding of the mechanism of functioning. These structures were obtained with the truncated HAMP domain, which does not include other parts of the membrane protein. Unfortunately, the structures presented in this work didn't reveal any sufficiently strong electron densities that could be used to build the structure of the HAMP domain. Possible reasons for that are discussed in the text. In order to get some structural information about the HAMP domain, some additional protein constructs were created, analyzed and set up for crystallization.

Another part of this work is devoted to the study of histidine kinases NarQ and NarX. Histidine kinase chemoreceptors are a large family of transmembrane proteins that are found in many prokaryotes [19–21]. They are another representative of two-component signal transduction systems. As in case of photoreceptors, they comprise a sensor kinase protein and a response regulator protein and they are involved in the regulation of many cellular processes. NarQ and NarX belong to the family of histidine kinase receptors and react to

nitrate or nitrite to regulate anaerobic respiration in various bacteria. Activation/deactivation of transmembrane histidine kinase chemoreceptors has become a new target for the next-generation anti-bacterial drugs [22]. Our study proposes some approaches that can be used in studying these very important proteins. First crystals of NarQ were obtained and optimization experiments are ongoing.

During this study the following X-Ray structures were obtained: structure of the complex SRII/HtrII-157 in $I2_12_12_1$ space group, structure of the SRII-D75N mutant in complex with HtrII-157, structure of the complex SRII/HtrII-135 in $P6_4$ space group, structure of SRII in a complex with HtrII-135-G83F mutant. Moreover, the membrane domain of the nitrate/nitrite receptor NarQ from *E.coli* was successfully expressed, purified and first crystals were obtained.

Acknowledgements

I’m deeply thankful to my supervisor Prof. Dr. Valentin Gordeliy, who has been mentoring me over my undergraduate and PhD work, for his support and valuable discussions. I appreciate the help of my friends and colleagues in Research Centre Jülich: Alex Volkov, Vitaliy Shevchenko, Dmitry Bratanov and Maria Silacheva. I would like to express special gratitude to Taras Balandin, whose help was essential for accomplishing molecular biology work, and Christian Baeken, who has produced SRII and has helped a lot in practical aspects of my life.

A large part of this work was done in cooperation with the lab of membrane transporters in IBS, Grenoble. Most of crystallization trials were set up there and it would be possible without the help from my colleagues: Alina Remeeva, Ivan Gushchin, Vitaliy Polovinkin, Pavel Chervakov and Petr Utrobin. Special thanks to Prof. Dr. Eva Pebay-Peyroula for the support of this collaboration.

The data collection was performed at ESRF in Grenoble and I’m thankful to ESRF staff and, in particular, to Dr. Alexander Popov for technical assistance and useful recommendations. Initial data treatment was done under supervision of Dr. Valentin Borshchevskiy.

I would like to acknowledge the help of Prof. Dr. Martin Engelhard, who was one of the initiators of the project and who has helped in manuscripts preparation related to this work. I’m grateful to Prof. Dr. Georg Büldt for the opportunity to work at ICS-5 in Research Centre Jülich and important insights on the results.

List of Abbreviations

SK	Sensor kinase
RR	Response regulator
ATP	Adenosine triphosphate
BR	Bacteriorhodopsin
DDM	n-Dodecyl-β-D-Maltopyranoside
ESI	Electrospray ionization
HR	Halorhodopsin
Hs	*Halobium salinarum*
HtrII	Cognate Transducer protein of Sensory Rhodopsin II
MALDI-TOF	Matrix-assisted laser desorption/ionization – time-of-flight
MO	2-mono-oleoyl glycerol
MR	Molecular replacement
MW	Molecular weight
Np	*Natronomonas pharaonis*
OG	Octyl-β-glucopyranoside
RT	Room temperature
SRII	Sensory Rhodopsin II
TCSS	Two-component signaling system
SB	Schiff base
SEC	Size-exclusion chromatography
HAMP1	First HAMP domain in NpHtrII sequence
HAMP2	Second HAMP domain in NpHtrII sequence
MCP	Methyl-accepting chemotaxis protein

1.Literature review

1.1. Two component signal transduction systems

Two-component signal transduction systems make bacteria able to respond to changes in extracellular environment. Many of such systems were found in both prokaryotes and even some eukaryotes (like plants, fungi and yeasts). No examples were found among animal species. Typical two-component system consists of a sensory protein from the family of histidine kinases and a coupled response regulator protein. This system transmits the signal from small ligands of the extracellular environment to the effector proteins in the cytoplasm [23,24]. The functional histidine kinase is always constructed as a homodimer. It is subjected to ATP-dependent autophosphorylation on a certain histidine residue in the cytoplasmic part of the protein and, afterwards, transfers the phosphoryl group to an aspartate residue on the cognate response regulator (RR). Thereby transcriptional, enzymatic or mechanistic properties of RR are changed. The RR is usually a cytoplasmic kinase protein [22,25]. These are the common features among this large family of signaling proteins (Figure 1.1). Moreover, for many two-component systems unphosphorylated sensor stimulates dephosphorylation of the phosphor-response regulator (also called transmitter phosphatase activity) [26,27]. The state of phosphorylation of the response regulator affects the function of its effector domain, which then calls an adaptive cellular response [5].

Such histidine kinase-mediated signal transduction chains are now found in the hundreds of species among prokaryotes, and evidences of their existence are reported for eukaryotes including yeast osmoregulation, fungi hyphal development, plant ethylene response and dictyostelium development [28]. Consequently, histidine kinases play an important role in signal transduction mechanisms among prokaryotes that is managed by serine/threonine and tyrosine kinases in eukaryotes [25].

The major problem in the understanding of the signal transduction mechanism in histidine kinases has been the lack of availability of structural information. The dimeric histidine kinases, constructed from multiple modules, contain highly flexible hinges between these modules and posses difficulties for structural analyses. The success in structural determination in the area has come after the domains of CheA and EnvZ were identified. CheA is a cytoplasmic histidine kinase involved in chemotaxis [29], and EnvZ is a transmembrane osmosensing histidine kinase [30]. Identification of domain boundaries finally allowed solving high resolution structures of their independent parts. The three-dimensional

structures of the kinase domains of the abovementioned two histidine kinases (EnvZ [9]; CheA [31]) were determined, showing that the topology of the histidine kinase domain doesn't have any resemblance to those of the previously determined structures of serine/threonine and tyrosine kinases. In contrast, they have defined a novel catalytic motif among other unique features. The structural studies also reveal that, although histidine kinases are composed of similar domains, they are diverse in their organization. These differences reflect their functions, localizations, and regulatory mechanisms in the cell [25].

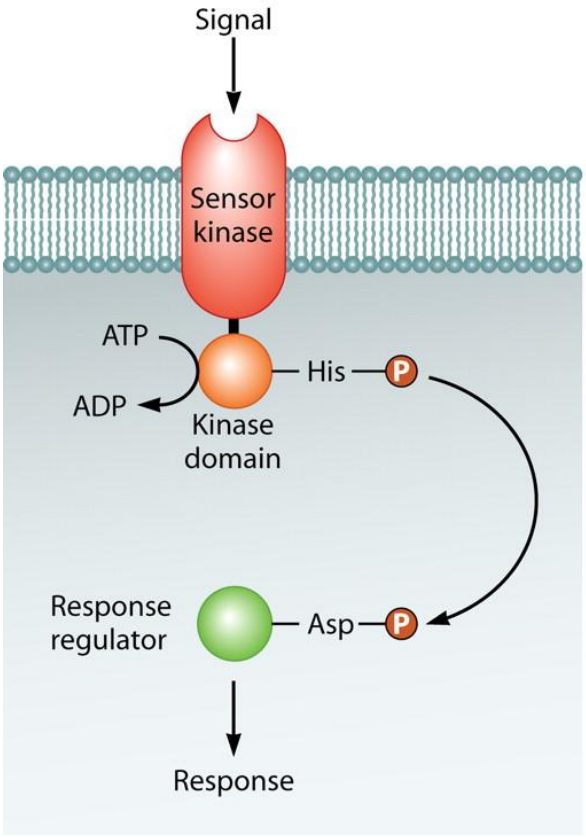

Figure 1.1 Organization of the typical two-component signaling system (TCSS) in bacteria. The typical TCSS is comprised of a single transmembrane sensor kinase (SK) as the first component and a single cytoplasmic response regulator (RR) as the second component. The sensory domain of the SK recognizes a specific signal from the environment. This can be a chemical ligand or a photon. The sensing of the ligand results in stimulation of the kinase domain and autophosphorylation in the output domain of the SK at a certain histidine residue. The receiver domain of the RR is close to the output domain of the phosphorylated SK. The phosphate is transferred to the conserved aspartate residue of the receiver domain. Phosphorylation of the RR, in turn, affects its output domain, resulting in conformational changes in the RR that aid to call the response in the cell, including transcriptional regulation of particular genes. From [32].

The main objective that is not achieved so far is to understand the mechanism of the signal transduction through histidine kinases. Undoubtedly, it is the major challenge for the future research in this area.

1.2. The complex of Sensory Rhodopsin II (SRII) with its cognate transducer

1.2.1. *General characteristics and function* in vivo

Rhodopsins are seven alpha-helical membrane proteins and are present in all kingdoms of life [33,34]. Although structurally very similar, their functions are quite diverse as they can act either as ion pumps, cation channels, or sensors [35,36]. This broad diversity made microbial rhodopsins the target of an intensive research and of biotechnical applications. This has been demonstrated in the new field of optogenetics which utilized channel rhodopsin and halorhodopsin, a chloride pump, as tools in neurophysiological research [37].

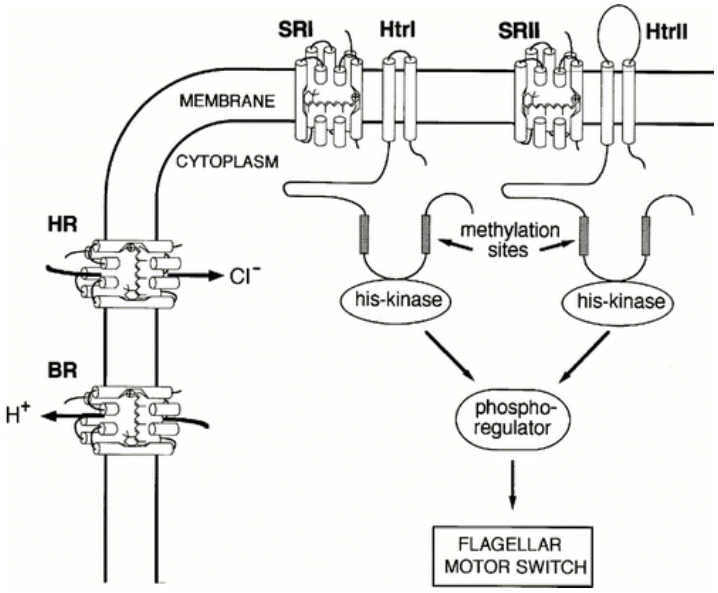

Figure 1.2 The four archaeal rhodopsins in H. salinarum. The ion-pumping rhodopsins BR (a proton pump) and HR (a chloride pump) are shown together with the sensory rhodopsins SRI and SRII with components in their two-component signal transduction chains. From [35].

The complex of the two membrane proteins from halobacterium *N.pharaonis*, sensory rhodopsin II (SRII) with its cognate transducer (HtrII), is an example of the two-component signal transduction system. This complex serves as a phototaxis receptor that helps bacteria to avoid harmful UV light. It is unique for combining two huge independent classes of membrane receptors – 7TM (7-transmembrne helices) and two-component signaling systems. This is the first component of TCSS that transmits the photophobic signal to the flagellar motor. This complex displays a 2:2 stoichiometry where two transducers are flanked by two receptors (Figure 1.3). The long rod-shaped cytoplasmic domain consists of two HAMP domains (present in Histidine kinases, Adenylyl cyclases, Methyl-accepting proteins and Phosphatases [38,39]), which are followed by a methylation domain involved in the adaptation processes and a signaling domain which harbors the CheW/CheA binding site [40].

The first HAMP domain (HAMP1, amino acid residues 83-135) and the second HAMP domain (HAMP2, amino acid residues 157-210) are connected with an α-helical linker (inter-HAMP). Despite high abundance of HAMP domains in different classes of proteins, their role and function is still unclear [16,17,38]. In order to understand the signal transfer from the receptor to the transducer it is mandatory to determine the exact structure of the binding surface connecting NpSRII with its cognate transducer. Currently, the structure of the membrane domain is determined [6,7], however for the adjacent proximal region only indirect experimental evidences [41–44] are available.

The whole process of signal transduction can be divided in the following steps. The complex captures photons of a specific wavelength and stores the energy of the photons in a chemical form in the active site of the protein consisting of retinal and neighboring protein residues. It uses the energy to create states, called signaling states, which have their distinct structural and spectral features. This leads to alterations in the SRII/HtrII interface. The changes in interaction between the receptor and the transducer are propagated to two distinct sites on the HtrII protein, first to a region called the signaling domain, causing alteration of autophosphorylation activity of a bound histidine kinase (CheA) and second to methylation regions, changing their susceptibility to methylation/demethylation (managed by proteins CheR and CheB). As a consequence, a new methylation level is set through the activity of methyltransferase and methylesterase enzymes. Methylation/demethylation processes reset the activity of CheA kinase to the prestimulus value in the case of continuous stimulation of the signaling process. Therefore, the overall output of this TCSS is a momentary change in the kinase activity that results into a momentary change in the level of phosphorylation of a cytoplasmic regulator protein (CheY). This process, in turn, causes a momentary change of the switching probability of the flagellar motor. The swimming reversal frequency in bacteria is normally measured as an output of the signal transduction [35].

The SRII/HtrII signaling complex is a unique system of two membrane proteins that allows studying the properties of signal formation and relay, from the photo-biophysics of initial stimulation of the receptors to the final output at the level of the swimming direction reversals, revealing underlying principles of sensory transduction and more generally the nature of dynamic intercommunication between membrane proteins [35].

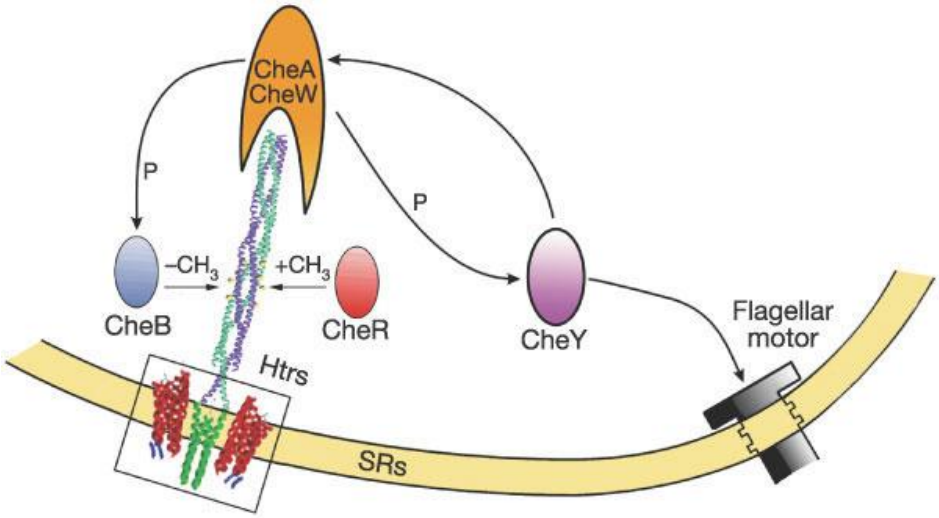

Figure 1.3 General view on two-component signal transfer in case of the SRII/HtrII complex. The activation of the transducer HtrII by its receptor SRII leads to a conformational change of TM2 that propagates to the tip of the coiled-coil cytoplasmic domain. The signal is transferred from the kinase control domain to the cytoplasmic kinase CheA by means of phosphorylation. Then, the signal is relayed to the flagellar motor through the mediator CheY. The result is the change in the rate of reversals of the flagellar motor's direction of rotation. From [7]***.***

Previously, the crystal structures (space group $P2_12_12$) of the wild type NpSRII/NpHtrII complex had been reported which display an overall "V"-shaped topology with the opening to the cytoplasmic side [6,7]. The structures contained HtrII truncated at positions 114 [7] and 157 [6] to optimize the construct geometry for formation of crystals in the cubic phase. Though, the structure of SRII contains nearly all amino acids except disordered C-terminus, only amino acids 23-82 were modeled for the HtrII protein. Computer modeling of the HAMP domain to the indention of the "V"-shaped structure did not show direct contacts of the receptor and the HAMP domain which is in contrast to presently available experimental evidences [41,42,45]. These clearly proved an interaction of TM2 with e.g. E-F loop. There could be several reasons for such a discrepancy, one of which could be the influence of crystallization conditions on the global arrangement of the proteins. There is so far a lack of information about how the structures of membrane protein complexes depend on crystallization conditions.

Conformational changes in SRII in course of the photocycle were initially studied spectroscopically and attributed to different intermediate states with characteristic absorption spectra. After isomerization of the retinal, NpSRII thermally relaxes back to the original state through a series of intermediates [46,47]. The M intermediate which is formed in 10 µs is central for formation of the active state. The formation of M-state is accompanied by deprotonation of the Schiff base and concomitantly the protonation of Asp75 (this residue is

the analogue of Asp85 in BR). Neutralization of the counterion complex Schiff base – Asp75 and subsequent M1-M2 transition plays an important role for signaling [48,49]. Therefore, it was expected that the substitution of Asp75 by neutral Asn75 will alter physiological properties. Nevertheless, the corresponding changes in the properties of the proteins were not observed in living bacteria. Interestingly, the analog mutation in *H. salinarum* (HsSRII-D73N) leads to constitutive activity [50,51]. The crystal structures of both wild type and D75N mutant complexes in its U-shaped structure provide an insight into the nature of transmembrane signal transfer.

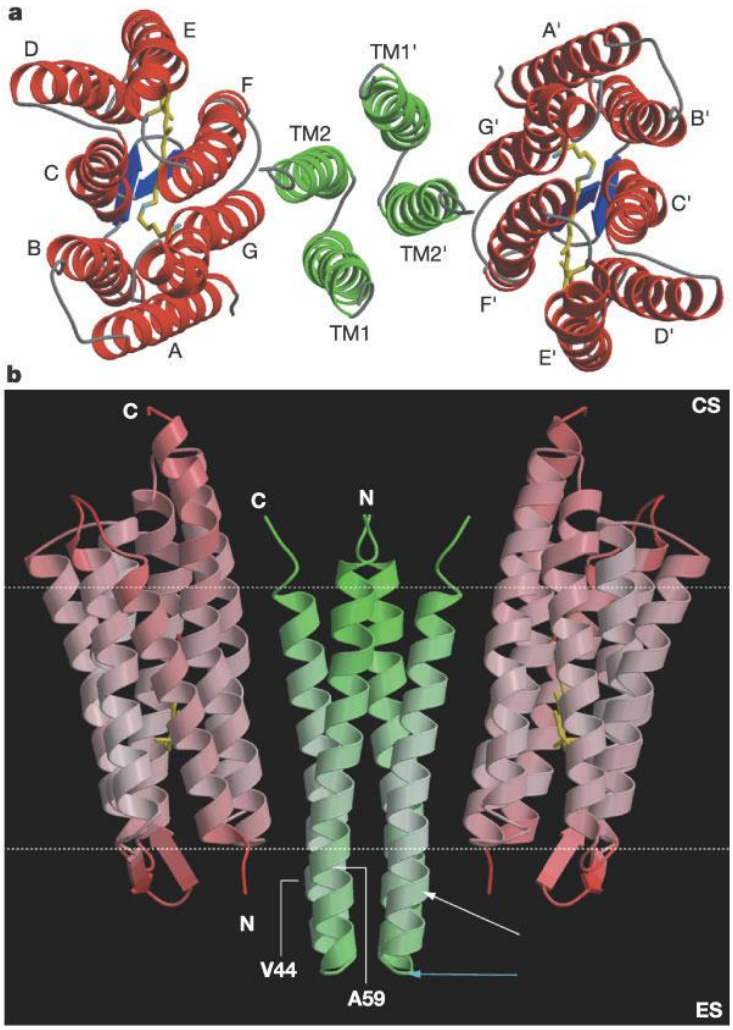

Figure 1.4 The structure of the "V"-shape of the complex. The structure was solved in the $P2_12_12$ space group. α-Helices are shown in red for the receptor and in green for the transducer; β-strands are shown in blue and coils are shown in grey. Dotted lines indicate hydrophobic core of the proteins. V44 and A59 are residues that form hydrogen bonds between HtrII and SRII. Only membrane part of HtrII could be built (residues 22-82), though the molecular construct contained residues 1-114. From [7].

1.2.2. Photocycle of Sensory Rhodopsin II. Intermediate states

The absorption spectrum of SRII from *N. pharaonis* displays two features that are different from the spectra of the other archaeal rhodopsins. First, the maximum of SRII is at 498 nm, lower wavelength as compared to BR (568) and HR (578). Second, the spectrum of absorption of the SRII protein shows vibrational fine structure at physiological temperatures [52].

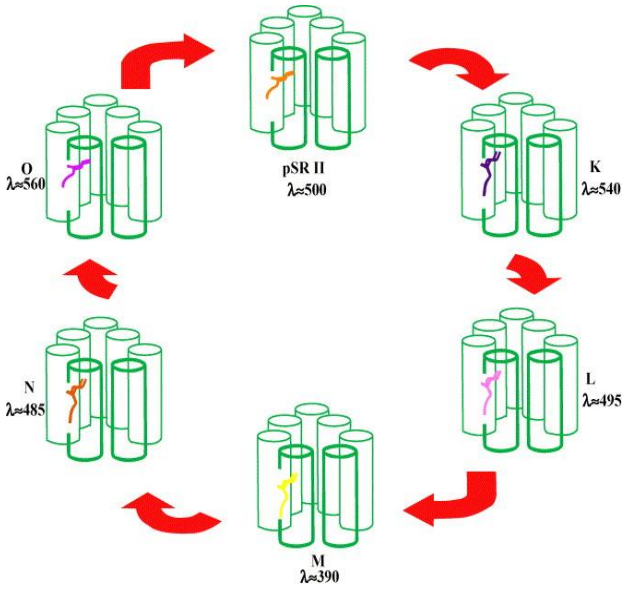

Figure 1.5 The photocycle of sensory rhodopsin II from N. pharaonis. The retinal chromophore is covalently bound to a Lys-205 in helix G via a protonated Schiff base (double C=N bond). The primary reaction, light-induced isomerization of the all-trans retinal to 13-cis configuration, is the followed by thermal reisomerization to the ground state via highly specific spectral intermediates as indicated by the color of the retinal and the λ_{max} of the intermediates. From [53].

The sequence of events, occurring after absorption of a photon by the protein is shown on the Figure 1.5. During the photocycle the retinal undergoes isomerization from *all-trans* to 13-*cis*. The energy, acquired by this process, leads to the sequence of structural changes in the protein that are characterized by the specific changes in the absorption spectrum of the protein. Five spectrally distinct species are formed [46]. The chromophore states correspond in their spectral properties to those of the BR photocycle, namely pSRII-510 (K), pSRII-495 (L), pSRII-400 (M), pSRII-485 (N) and pSRII-535 (O).

The spectrum of SRII has a maximum at 498 nm and two shoulders at 460 nm and 420 nm. Characteristic difference to BR is the absence of well-manifested L and N states. The M state is formed very fast and decays with a characteristic time of a few hundred milliseconds. In the K state absorption maximum is shifted by 10 nm to the red. Experimental information on the L state is quite poor. Primary reason is that it cannot be stabilized at low temperatures. The data obtained by dynamic FT-IR spectroscopy show that, as in the K state, the conformation of C14-C15 connection is different from the planar and structural changes have a greater amplitude than in the K state. The M state is characterized by the deprotonated SB and protonated Asp-75. In the M state the structural changes in the protein are the most

prominent. Slow decay of the M state is due to the lack of a proton donor. M state can be detected at temperatures below 220 K, while the IR spectra of M state are the same at low and room temperatures, indicating the identity of the structural changes. In the O state the retinal is in all-*trans* conformation. SB is again protonated. In addition, the carboxyl group of one of the glutamine or asparagine amino acids is protonated, while the other, also unknown, carboxyl group is deprotonated [54].

Intermediate states are, in the first place, spectroscopically distinct states, which reflect the changes in the immediate vicinity of the retinal. Structural changes far from retinal pocket do not produce changes in the absorption spectrum. During all the states of the photocycle from K to O the retinal is in the 13-*cis* conformation. The transition to all-*trans* happens upon transition from O to G.

While the shifts of the absorption maxima (λ_{max}) to the red and slightly to the blue in the K and L states, respectively, reflect changes in the strength of the salt bridge between the SB and the counterion complex [55], the much larger blue shift of the λmax upon M formation reflects deprotonation of the Schiff base by the Asp75 anion, thereby disrupting the salt bridge.

1.2.3. The role of HAMP domains in cell signaling

Microbes react to changes in the environment in a variety of ways. Changes of environmental conditions can open opportunities in ways of nutrition and possess potential danger to their lives. Correspondingly, bacteria and archaea use a certain set of sensory systems to feel their living conditions. These sensory systems have a fundamental role in the life cycle and their functional mechanism can be split into the following steps: detection of an extracellular stimulus, transmission of the stimulus across the cellular membrane and conversion of that information to a signal that triggers a change in behavior of the bacteria or gene expression of certain effector proteins [13].

A lot of signaling proteins from bacteria include HAMP domain signaling motifs. The name “HAMP” is used because they are found in such abundant classes of proteins as histidine kinases (HKs), adenylyl cyclases, methyl-accepting chemotaxis proteins (MCPs) and some phosphatases. In transmembrane receptors HAMP domains are typically located near the cytoplasmic side of the membrane. Their function is predicted to be the conversion of the transmembrane and extracellular sensory inputs to output response signals in the cells. All the signaling chemoreceptors function as homodimers. HtrII is an MCP-like phototransducer of

sensory rhodopsin II that is found in two archaeal halobacteria *Halobacterium salinarum* (Hs) and *Natronomonas pharaonis* (Np). It is a cognate signaling protein of the SRII receptor. The HtrII molecule has an MCP adaptation domain (ruled by the methylation process of certain glutamate residues) and kinase control domain preceded by two HAMP domains connected through a linker helix and two transmembrane helices. NpHtrII has no periplasmic domain and the transmembrane helices are connected via a short extracellular loop. Meanwhile, HsHtrII has a periplasmic domain that has been found to be involved in serine chemical sensing [13].

In vitro spectroscopy studies [14,43,44] have provided some structural information for the first NpHtrII HAMP domain. There is no structural information for the second HtrII HAMP domain and the mutational information for this system is also insufficient. Spin-labeling studies of an HtrII fragment containing membrane part, HAMP-1 and the inter-HAMP helix, reconstituted in complex with SRII into lipids, showed that the HAMP-1 domain is in equilibrium between two conformations: compact and dynamic [56]. The ionic strength of the buffer and temperature changed the ratio between the two forms, and the compact form was suggested to resemble the tight bundle reported for the HAMP domain from the putative gene Af1503 [38]. Trypsin cleaved a similar, solubilized HtrII fragment in the AS1 segment of HAMP-1, yielding a C-terminal fragment in which only the linker helix had a discernible NMR solution structure [13,57].

1.2.4. Known structures of HAMP domains and molecular modeling

HAMP domains are special types of coiled-coil motifs that are defined by a few conserved residues. These residues form characteristic hydrophobic heptad repeats and are predicted to form helical and non-helical secondary-structure elements. HAMP subunits are typically about 50 residues long, with two helices joined by a non-helical connector. Heptad repeats form a hydrophobic core between helices in a functional HAMP domain. The two HAMP domains of HtrII are connected with an α-helical linker normally called as inter-HAMP. HAMP secondary-structure elements have been given diverse names, and their boundaries are also variously defined. In this work the notations AS1 and AS2 for alpha-helices and CTR for the connector between them will be used as most common in literature [13]. The corresponding elements of the symmetry related HAMP will be designated with a prime.

Recently, Hulko et al. [18] have published a high-resolution NMR structure for a HAMP domain from a protein of unknown function from a thermophile organism (Af1503),

an important breakthrough that has paved the way for the following work on HAMP domains. The Af1503 HAMP structure exposed a parallel, four-helix cluster with each interhelical connector bundled up around the outside of the cluster in contact with the two helices from the single monomer (Figure 1.6). The AS1 and AS2 helices are offset by one helical turn in the cluster.

The main packing interactions occur between the characteristic heptad repeat hydrophobic residues. It was found that the structure-defining residues in the HAMP domain sequences occupy key positions in the Af1503 cluster structure. Using Tsr nomenclature, these residues are: P221 (AS1) and E248 (AS2) (both lie at the N terminus of the bundle), and A233 (AS1) (lies at the C terminus of the bundle). G235 is a conserved residue at the start of the connector. It forms a flexible hinge to make a sharp turn in the structure. L237 and I241 are typically hydrophobic amino acids whose side chains pack against the AS1 and AS2 helices to stabilize the bundle [18]. The latter residues are not conserved among all HAMPs.

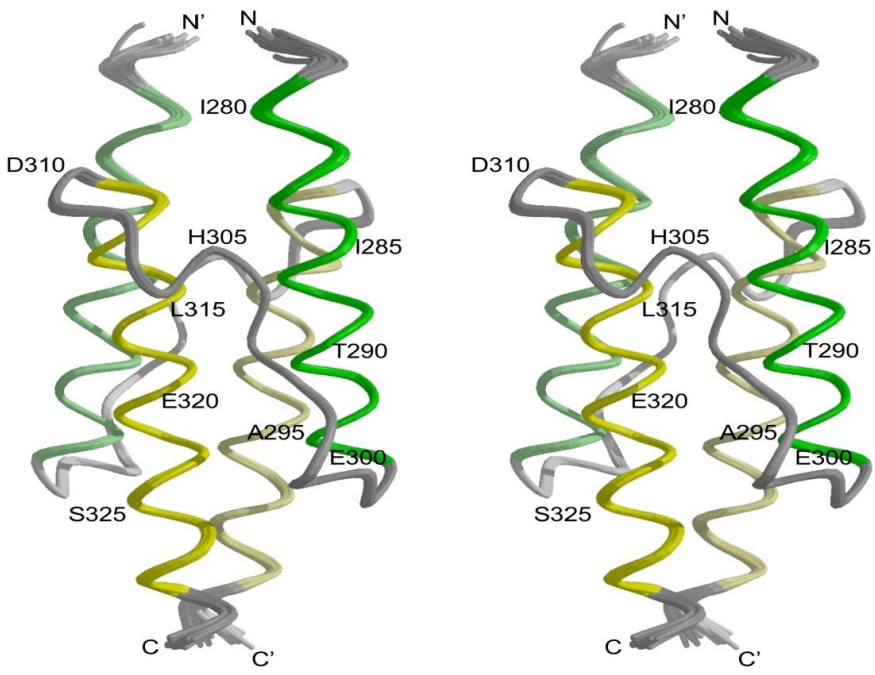

Figure 1.6 A stereo picture of the HAMP domain dimer. The structure was obtained by NMR spectroscopy (PDB code 2ASW). The solution structure of an archaeal HAMP domain Af1503 showed a homodimeric, four-helical, parallel coiled coil bundle with an unusual interhelical packing knobs-to-knobs, related to the canonical packing by rotation of the helices. From [18].

The Af1503 HAMP structural packing is not orthodox. The third position, usually occupied by a small, but not necessarily hydrophobic is not normally contributing to the structure of HAMPs. In Af1503 this residue also contributes to the HAMP domain packing. The new discovered possible HAMP domain packing was called x-da, or knobs- to-knobs. It

is characterized by the structure where the side chains of some hydrophobic residues protrude into the core of the HAMP cluster and make contact with their counterparts of the other subunit, whereas the side chains of the neighboring hydrophobic residues interact with similar residues in the other helix of the same subunit. Similarly, the less hydrophobic residues are in touch with the similar residues in the other helix from the other subunit. This packing arrangement is different from the more commonly observed a-d or knobs-in-holes packing of coiled-coil structures, although the heptad repeat pattern of hydrophobic residues is common to both [18].

The Aer2 protein of *Pseudomonas aeruginosa* contains three consecutive HAMP domains whose X-ray structures have been determined recently [17]. The first and the third Aer2-HAMP domains were found to have a cluster structure similar to that of Af1503-HAMP. Nevertheless, variations on the packing arrangements of the hydrophobic residues were also observed. These four-helix clusters, in which all AS1 and AS2 hydrophobic residues are involved in cluster-stabilizing knobs-to-knobs packing interactions are represent a widely spread HAMP structural state, which is normally called HAMP(A) [13].

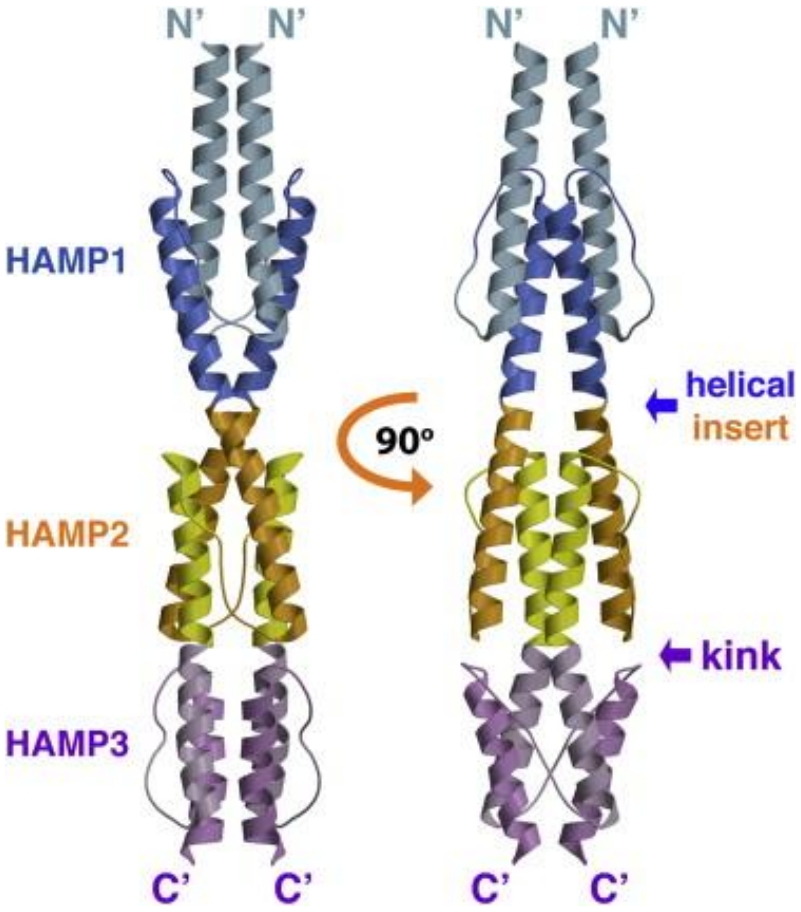

Figure 1.7 The crystal structure of the N-terminal domain of the soluble gas-sensing receptor Aer2 that contains three successive HAMP domains. Ribbon representation of the Aer2 (1–172) dimer with HAMP1,

HAMP2 and HAMP3 is shown. From [17]**.**

The second HAMP domain of Aer2 has a considerably dissimilar structure that may represent a possible alternative conformation of HAMP domains. This structure is denoted HAMP(B) and in literature is called a loose cluster or bundle. In the structure of HAMP-2 the four helices also have parallel orientations. In contrast to HAMP-1 and HAMP-2 these helices are less tightly packed and tilt apart from one another. They form a trapezoid shape where AS1 and AS1' are near each other at the top of the bundle, and AS2 and AS2' are closest at the bottom of the bundle (Figure 3b). The three C-terminal hydrophobic residues (L256, M259, L263) modulate the packing of the AS2/AS2' helices against one another in an arrangement different from that in the HAMP(A) bundle [17]. The different packing conformation is stabilized by the crucial hydrophobic connector residues: one (L237) packs against the last hydrophobic residue of AS2 from the other subunit (L263'); another (I241) packs against the first of the three C-terminal hydrophobic residues from the same subunit (L256) [13]. In general, HAMP-2 forms a unique fold for the HAMP domains never observed before and referred to as ridges-into-grooves interaction.

1.2.5. The molecular mechanism of signal transduction

The retinal chromophore switches from all-trans conformation to 13-cis and simultaneously shifts towards the central water cluster. The side group of Asp75 is rotated by about 90° from its ground state position, thereby losing the hydrogen bond to Thr79. Consequently, W3 becomes disordered and disappears in the M-state. Hydrogen bonds pentagon (Asp201-Oδ···W2···W1···W4···Arg72-Nε) does not exist anymore in the M-state because molecules W2 and W4 have vanished (Figure 1.8). Consequently, helices C and G have more freedom to move independently. The helical segment between Pro71 and Pro81 in the helix C is displaced towards the active center by 0.4 Å with respect to the ground state. Water molecule W2' shifts towards Asp75 and Arg72. Water W1, which forms a bridge from Asp201 to Asp75, vanishes in the M state. Thus, the signal is generated by retinal isomerization and then propagates to the interface between the receptor and the transducer. The signal propagation is driven by the rearrangement of the hydrogen bond network mediated by water molecules that leads to the movement of the receptor helices described above due to the loss of connectivity between C and G helices. These results are in agreement with those obtained for the symmetry $P2_12_12$ [6].

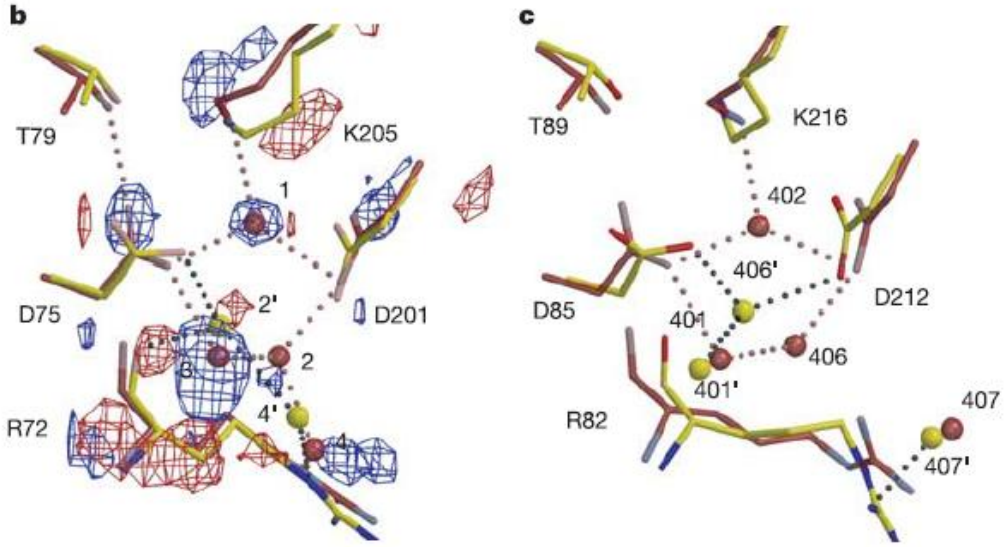

Figure 1.8 Structural changes in the vicinity of the retinal upon transition from the ground to the M state. Ground state is shown in red, M state is shown in yellow; a – changes in SRII, b – changes in BR. Difference density maps are contoured at 3σ. Primes denote water molecules of the M state. From [6]**.**

The movement of the helix G of NpSRII initiates the movement of TM2 in NpHtrII. The hydrogen bonds between receptor and transducer are shown to be the same in both the ground state and the M-state. A piston-like movement of the cytoplasmic end of TM2 by about 0.5 Å and rotation of 15° was observed and accompanied by alteration in the direction of Tyr199-Asn74 hydrogen bond. The similarity of the differences between the ground and the M-states in the new crystals shows an overall robustness of the signal transduction mechanism.

Structural changes in the positions of the helices observed upon the ground to the M-state transition are the same in both $I2_12_12_1$ and $P2_12_12$ crystals, though there is a small difference in the amplitudes of changes for some helices. One can determine two groups of helices that make cooperative movements (ABG and CDEF). Helix G moves towards the transducer and the extracellular side. The magnitude of the shift is not the same through the helix, being the biggest at the C-terminus (about 0.5 Å) [6].

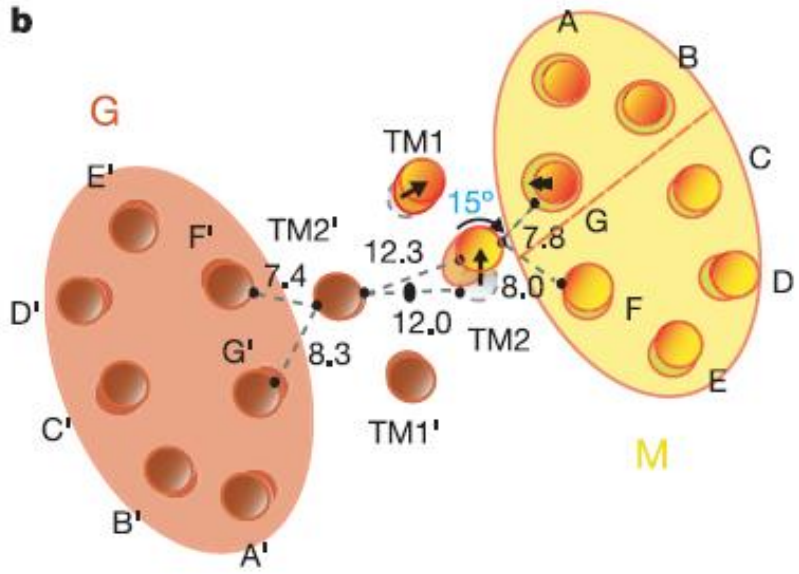

Figure 1.9 Structural rearrangements in the position of helices F, G, TM1 and TM2 observed in the membrane plane. The ground-state complex is shown in red and the late M-state complex in yellow; black numbers give distances between Cα atoms of the following amino acids in the ground and late M states: F(Leu 170) to TM2(Leu 77), ground state 7.4 Å, M state 8.0 Å; G(Val 203) to TM2(Leu 77), ground state 8.3 Å, M state 7.8 Å; TM2(Val 78) to TM2'(Val 78), ground state 12.0 Å, M state 12.3 Å. SRII can be divided into 2 sections: the first containing helices A, B and C and the second containing helices D, E, F and G. The arrows on TM1 and TM2 depict displacements parallel to the membrane plane in the late M state; the thick arrow on helix G depicts its 0.5 Å movement to the extracellular side. A clockwise rotation of 15° was observed for TM2. An in-plane displacement of 0.9 Å (black arrow) near the cytoplasmic membrane surface in late M state with respect to the ground state was also detected. The red line in the receptor on the right divides the molecule into the two functionally important domains ABG and CDEF. The inner red shaded circles of helices A, B and G depict their movements to the extracellular side. Illustration from [6].

Two possible mechanisms of TM2 communication with HAMP have been suggested in literature. The first is a crankshaft and gearbox mechanism that involves an axial rotation of TM2 segments around the axis of the helix in the plane of the membrane. The second is a piston mechanism that is manifested in displacements of the TM2 helix perpendicular to the plane of the membrane by 0.5 to 1 Å. The crankshaft and gearbox model arose from the NMR structure of a putative gene Af1503 [18]. In this study it was discovered that an x-da bundle should exist alternative to the orthodox a-d packing, differing by a about 26° counter rotation of the four helices [13]. Nevertheless, other structures of histidine kinases don't support this theory and are rather in favor of the piston-like mechanism.

Evidence for the piston motion mechanism in bacterial chemoreceptors has come from comparison of the apo- and ligand-bound structures of the Tar periplasmic domain, from disulfide formation rates of cysteine reporters in the TM segments of chemoreceptors and from the signaling changes caused by relocating the aromatic and basic anchor residues that

secure the position of TM segments in the membrane bilayer. Also, the recent results on the HAMP domain structure support this hypothesis[16]. Motions that move TM2 toward the cytoplasm enhance CW output activity, whereas shifts in the opposite direction enhance CCW signaling. Thus, outward piston-like movements in chemoreceptors simulate a repellent stimulus and inward displacements simulate an attractant stimulus. The small vertical shift is consistent with the calculated free energy change of ligand binding [13,23,58].

1.2.6. O-like D75N mutant of SRII

Conformational changes in SRII during the photocycle were initially studied spectroscopically and attributed to the different intermediate states, each with its own characteristic absorption spectrum. After the isomerization of retinal, NpSRII thermally relaxes back to the original ground state through a series of intermediate states [46,47]. The M intermediate, which is formed in 10 μs, is the key intermediate for the evolution of the active state. The formation of M state is escorted by a deprotonation of the Schiff base and accompanying protonation of Asp75. This residue is forming a salt bridge with the Schiff base. Asp75 is an analogue of Asp85 in BR. Neutralization of the counterion complex Schiff base – Asp75 and the following M1-M2 transition play an important role for signaling in SRII and SRII/HtrII complex [48,49].

Counterions of Schiff base, analogous to Asp75 in NpSRII, are found in all retinal containing proteins [59,60]. The most studied so far is the function of Asp85 in molecular mechanism of proton pumping in bacteriorhodopsin [61–65]. Asp85 acts as an acceptor of the Schiff base proton. Replacement of Asp85 by neutral Asn leads to dramatic changes in the photocycle and pumping activity of BR. These changes are different depending on pH of the buffer. At neutral pH the photocycle of the D85N mutant contains only L and N intermediates. No M state is observed in this case. Since the change of Asp85 to Asn85 decreases the net negative charge at the active cite, the pK_a of Schiff base is therefore decreased from 13 to around 8-9. Therefore, the proton is not tightly bound in the mutated protein and a mixture of protonated and deprotonated retinal forms with corresponding isomerization states can be observed showing absorbance peaks at 610 nm and 410 nm respectively [66]. Depending on conditions of illumination different manners of proton transfer were found for the D85N mutant of BR. Upon excitation with the blue light the protein stationary current is in the same direction as in the wild type protein. Two-photon excitation (yellow and blue) reverses the direction of pumping [67]. In halorhodopsin (NpHR) the homologous residue corresponding to Asp75 in NpSRII is Thr126. It was found to be not

crucial for the process of chloride pumping. The influence of T126V mutation on chloride affinity was found to be negligible and the time constants of the photocycle were not changed considerably [68]. Another phototaxis receptor, sensory rhodopsin I, exists as a mixture of two different functional forms depending on pH. At low pH it acts like a phototaxis transducer in the complex with HtrI. In high pH environment it is converted into a proton pump similar to BR. In this protein Asp76 residue acts as a Schiff base counterion and proton acceptor for the alkaline, BR-like form. In this case D76N replacement leads to spectral changes similar to that in BR. On the contrary, in the acidic form Asp76 is already protonated and D76N mutation has no substantial influence on the function of the protein [65].

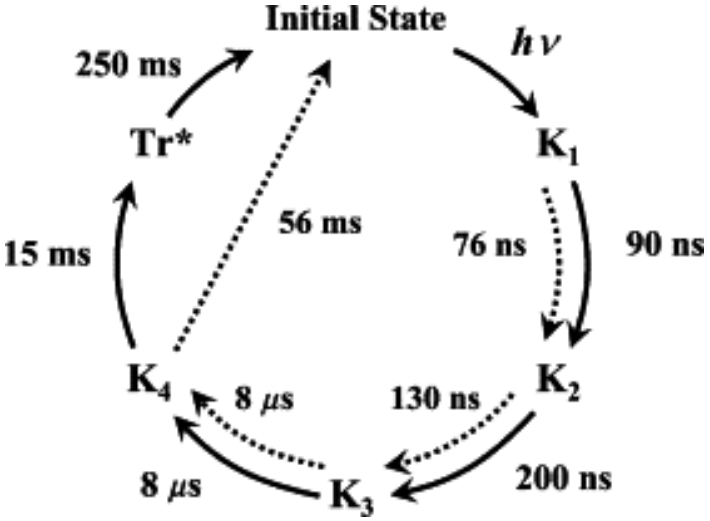

Figure 1.10 Proposed reaction schemes of photocycles of the D75N mutant of SRII (dotted arrows) and the complex SRII-D75N/ Δ NpHtrII (solid arrows). The numbers indicate the lifetimes of each of the intermediates. From [69]**.**

Two more proteins where the Schiff base counterion has a drastical influence on the phenotype are sensory rhodopsin II from *H. salinarum* (HsSRII) and human rod rhodopsin. In the HsSRII D73N and in the rod rhodopsin E113Q mutants constitutive activity of the pigments is observed [11,50].

Therefore, it was expected that the substitution of Asp75 by neutral Asn75 will alter physiological properties. Nevertheless, this was not observed experimentally [46,50]. Using transient grating analysis (TG) it was demonstrated that D75N-HtrII functions in phototaxis signaling despite the absence of a deprotonated Schiff base. The interpretation of this fact was suggested by authors. They propose that the retinal isomerization followed by proton transfer from the Schiff base to Asp75 may be necessary for signaling in the wild-type complex. Nevertheless, in D75N the Schiff base deprotonation is not obligatory, because Asp75 is replaced with a neutral residue imitating the protonated Asp75. The TG analysis has revealed four spectroscopically silent K-like intermediates (K1–K4) in the D75N protein with certain volume differences. The time constants for the interconversions were 76 ns, 460 ns, 130 ns, 8.0 ms, and 81 ms correspondingly (Figure 1.10).

Interestingly, the analog mutation in *H. salinarum* (HsSRII-D73N) leads to constitutive activity [50,51].

1.2.7. Signal abolishment in the G83F mutant of HtrII

Residue Gly83 in NpHtrII is important for maintaining the NpHtrII in a functional conformation. No phototaxis response was reported when Gly83 was mutated to cysteine or phenylalanine. Meanwhile, the phototaxis remained when Gly83 was replaced by alanine. The interpretation is that replacement of Gly83 with a more bulky residue eliminates the phototaxis response [70]. The same authors reported a large decrease compared to wild type in cross-linking efficiency in the dark was measured in G66C-G83F and L75C-G83F double mutants. It was suggested that the two helices TM2 and TM2‘ have become more separated or have become more flexible as a result of the G83F mutation. It was observed that the construct with two mutations G66C-G83F exhibited no detectable cross-linking in the dark and only a slightly detectable level after 3 min in the light. In NpHtrII containing mutations L75C-G83F, for which the efficiency could be measured, light still increases the cross-linking efficiency, showing that the NpSRII and NpHtrII are still coupled in a functional complex. The cells with HtrII-G83A mutation showed phototaxis responses similar to the response of the wild type whereas no phototaxis response was observed in the case of G83F mutation. The conclusion can be drawn that bulky residues at position 83 inhibit the signal transduction whereas small residues don’t. Another study has reported an absence of FRET signal between EF loop at position 154 and HtrII-G83F while in the case of wild type HtrII the signal was detected [42].

Worth noting that these findings are in line with the “V”-shape quaternary structure of the SRII/HtrII-G83F complex discussed in Chapter 3.7.

1.3. HAMP domain containing histidine kinases NarX and NarQ from *E. coli*

Nitrate (NO_3^-) and nitrite (NO_2^-) are exploited by bacteria as efficient respiratory oxidants in the phase of anaerobic growth. The two-component sensory systems NarX-NarL and NarQ-NarP act together in *E.coli* to control anaerobic gene expression in response to nitrate and nitrite. These proteins belong to the family of homologous nitrate reductases (Nar). Analysis of gene-deficient mutants has revealed that only one of the NarX or NarQ sensors is sufficient for NarL-dependent activation of narGHJI operon transcription. These observations provided an indication that the Nar regulators form a signal-responsive cross-regulation

network. Recent results show that this interaction network is asymmetric: although the NarQ sensor exhibited similar transmitter phosphotransferase activities for both the native NarP and NarX-connected NarL response regulators, the NarX sensor by contrast has shown a apparent predilection for phosphotransfer to NarL [26].

An extensive analysis of NarX and NarQ sequence was done by Dr. V. Stewart and coworkers [71]. The unique feature of response to nitrate and nitrite in *Escherechia coli* (and *Salomonella enterica*) is that they have both systems (NarX-NarL and NarQ-NarP) while other studied bacteria have only one of that.

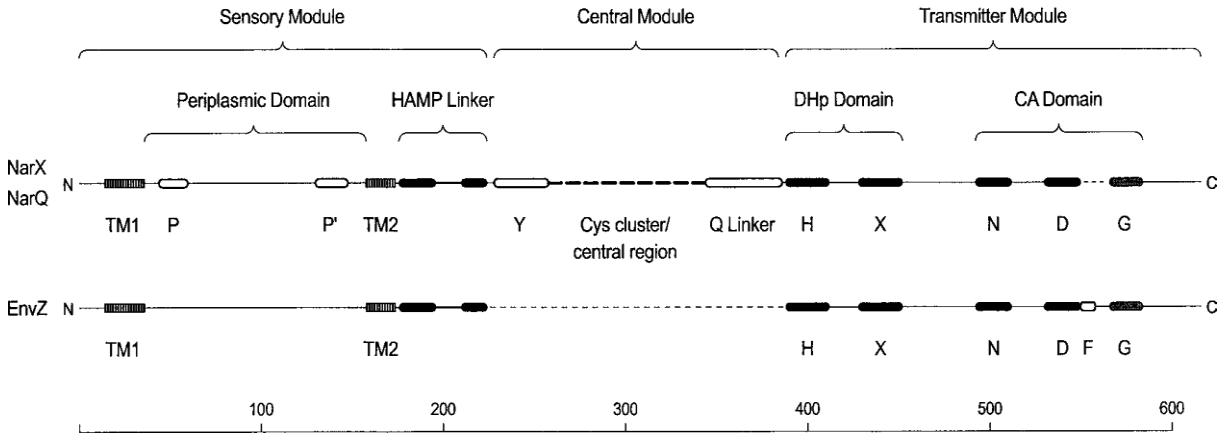

Figure 1.11 Sequence alignment of NarQ and NarQ chemoreceptors with the most studied MCP – EnvZ. Distinct domains including 2 transmembrane helices and the HAMP domain were identified. From [71]**.**

Crystal structure of NarX periplasmic domain was successfully solved [23]. The structures include apo- and nitrate-bound states and reveal a four-helix bundle. The all-helical fold is similar to that of the aspartate receptor Tar. The location of a single ligand binding site at the dimer interface is unique in NarX and is not found in other chemoreceptors. This binding site involves residues of both protomers. The important role of Arg54 in nitrate binding was found to be consistent with biochemical and genetic studies of NarX [71]. The nitrate binding is mediated by the hydrogen bonding with the side chains of Arg54 and Arg54' (Figure 1.12). This structure contrasts with aspartate binding by Tar where interactions between protein and ligand involve indirect hydrogen bonding involving water molecules. The nitrate occupies the unique binding site in NarX in quasi-symmetric manner. It different from the asymmetric binding of aspartate to chemoreceptor Tar, where only one of the two available binding sites is completely occupied [23].

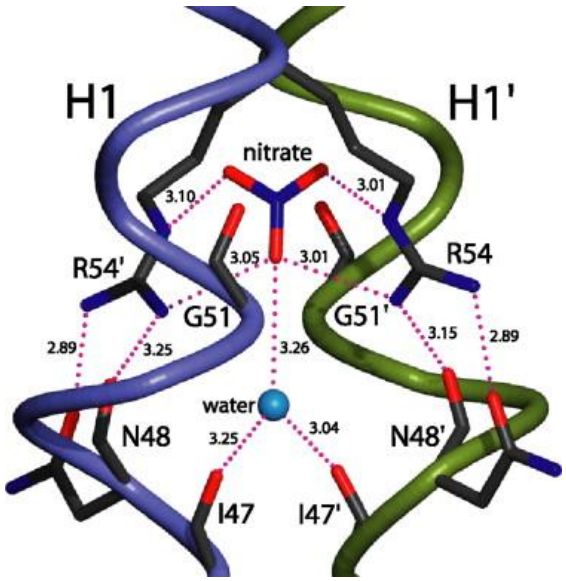

Figure 1.12 The extracellular nitrate-binding site of NarX. Two protein chains, H1 and H1', forming a homodimers are shown. Arg54 residue participates in ligand binding. The binding is symmetric. From [23].

The conformational changes that happen within the sensory domain of NarX after nitrate binding are similar of those in the chemoreceptor Tar, in which a displacement of about 1 Å between the N- and C-terminal helices of the periplasmic domain was also observed upon ligand binding. The structural alterations in NarX were found to occur symmetrically between the two monomers as the binding of nitrate is symmetric, whereas in Tar they appear to be localized in only one of the subunits due to asymmetric aspartate binding [23].

1.4. Crystallization of membrane proteins

Membrane proteins are the major functional components of cell membranes and constitute about one-third of the proteins encoded in the genome [72]. Study of membranes at the molecular level is of great importance for deciphering all cellular processes and drug design. Moreover, about 70% of currently available drugs focus on membrane proteins [73,74]. However, although the number of membrane proteins of known structure has increased recently, it is not yet comparable to the same indicator for the water-soluble proteins.

According to the database of membrane proteins of known structure (http://blanco.biomol.uci.edu/Membrane_Proteins_xtal.html) to date, only 360 of the more than 70 000 registered high-resolution protein structures are among the unique membrane proteins. This fact is usually accounted for by the amphiphilic nature of membrane proteins and difficulties associated with their instability outside of natural membrane environment. There are total 4 methods for crystallization of membrane proteins described in literature: standard crystallization of solubilized proteins (*in surfo*), crystallization from bicelles [75], crystallization from vesicles [76] and *in meso* approach [77,78]. As the first two methods didn't show wide applicability among various membrane proteins, the structures described in

this study were obtained mainly by the last method. It has proven to be a method of choice for crystallization of difficult targets as it allows crystallization in a native lipid environment. Despite a big success of the method, especially in crystallizing of GPCR receptors [79–81], the detailed mechanism of the crystallization process *in meso* is still unknown. This method yields crystals that belong to type I, where proteins are oriented in a parallel manner in layers, in contrast to conventional crystallization that gives crystals of type II (Figure 1.13). Normally, crystals of type I have much better quality and yield data of much higher resolution. Each crystallization target requires a massive screening of conditions that are optimal for the formation of high quality crystals. Moreover, by tweaking of the conditions, crystallization constructs and additives one can change phase properties and cell parameters of the resultant crystals.

In meso method was introduced by Landau and Rosenbusch in 1996 [3]. In this case crystallization occurs in a lipid matrix in a liquid phase (*meso* phase). Crystallization in the cubic phase was the first method to crystallize membrane proteins, in which a lipid mesophase was used instead of the detergent solution. It has been shown that lipid cubic phase reproduces the lateral pressure that the protein undergoes a natural membrane, resulting in less conformational freedom of the protein [82].

The most used lipid for *in meso* crystallization at the moment is unsaturated monoglycerol monooleoyl (C18:1c9; MO). When mixed with water it forms a variety of phase forms described on the Figure 1.14. In the process of *in meso* crystallization the protein solution is mixed with MO and the cubic phase is formed [1] (Figure 1.14). Normally, such solutions contain a lot of detergent coming from solubilization and purification processes. It is a well established fact that such additives as detergents can influence the lipid phase, change its properties, disturb or disrupt it. M. Caffrey with his colleagues have studied phase behavior after addition of various detergents [83]. The phase identification was done through SAXS measurements in the conditions identical to that of crystallization trials. The study has proved that addition of small quantities of detergents (glucopyranosides, dodecylmaltopyranosides, fos-cholines, CYMAL) has minimal or no effect on the phase stability. Larger amounts of detergents transferred the system into lamellar phase.

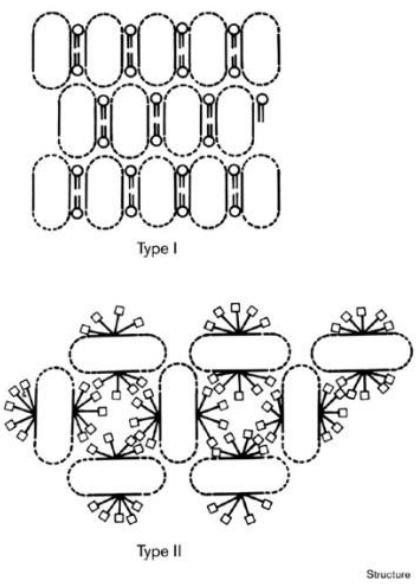

Figure 1.13 Type I and type II of membrane protein crystals. Type I is a stack of 2-D crystals where proteins interact with each other mainly by their hydrophobic surfaces. These crystals are usually formed by methods using lipid environments, i. e. bicelles, vesicles and in meso methods. Type II crystals are formed by interactions of polar hydrophilic areas of proteins that are outreaching detergent micelles in case of in surfo method. From [84].

LCP crystallization methodology was much upgraded within past few years by introducing phase preparation devices like a syringe mixer and 96-well sandwich plates. Consumption of protein and lipid for the crystallization trial has considerably reduced (up to 1 mg of protein per full sparse screening of conditions), and the whole process was much eased by introduction of robotic systems. A robot can typically dispense down to 20 nL of LCP per one crystallization trial and takes 5‑10 min to setup a 96-well sandwich plate [85].

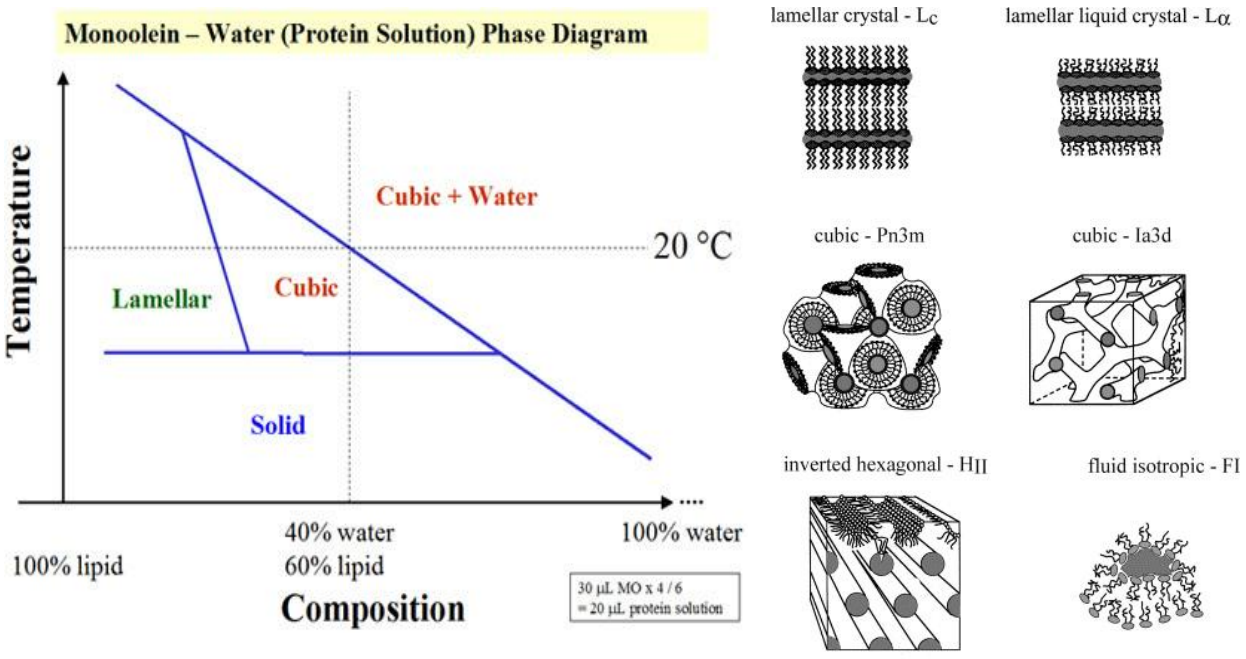

Figure 1.14 A simplified temperature-composition phase diagram for the lipid (monooleoyl) / water system with schematic representation of the various phases. From [78,86].

2. Materials and Methods

2.1. Materials and Equipment

Filters:

SFCA Bottle Top Filters, 150 mL, 0.22 μm pore size	Nalgene

Ultrafiltration and concentration:

Amicon® Ultra centrifugal filter units Ultracel®- 30K	Millipore, USA
Amicon® Ultra centrifugal filter units Ultracel®- 50K	Millipore, USA

Columns:

Glass Econo-Column®	Bio-Rad, USA
NAP™-5 Columns	GE Healthcare, USA

Membranes:

Nitrocellulose Membranes (pore size 0.45 μm)	Bio-Rad, USA
Dialysis membrane Spectra/Por® MWCO 12-14,000	Spectrum Laboratories, USA

Crystallization tools:

Gastight syringes	Hamilton (Reno, USA)
LCP sandwich set (Lauda-Königshofen, Germany)	Paul Marienfeld GmbH

Detergents

- **n-Dodecyl β-D-maltoside**

n-Dodecyl β-D-maltoside was used from Anatrace, Cleveland, USA distributed by Affymetrix, High Wycombe, UK; Purity >99% (HPLC); alpha isomer <2%, nonionic detergent for membrane protein stabilization and crystallization

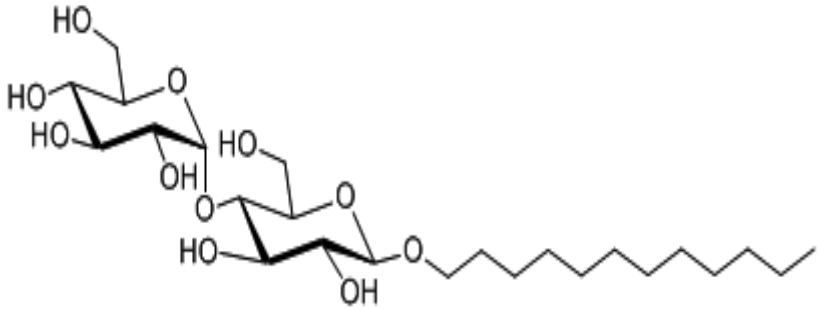

Molecular formula: $C_{24}H_{46}O_{11}$ Molecular weight: 510.6 g/mol

CMC (H_2O): ~ 0.17 mM (0.0087%)

CMC (0.2 M NaCl): ~ 0.12 mM

Aggregation Number (H_2O): ~ 78-149

dn/dc (H_2O): 0.1435 mL/gm

Micelle Size: 72 KDa

Purity: ≥ 99% by HPLC analysis.

Percent alpha: < 2 (HPLC)

Percent dodecanol: < 0.005 (HPLC)

pH (1% solution): 5-8

Solubility in water at 0-5°C: ≥ 20%

Conductance (10% solution): < 40 μS

- **n-Decyl β-D-maltoside**

n-Decyl β-D-maltoside was used from Anatrace, Cleveland, USA distributed by Affymetrix, High Wycombe, UK; Purity >99% (HPLC); alpha isomer <2%, nonionic detergent for functional purification and crystallization of membrane protein

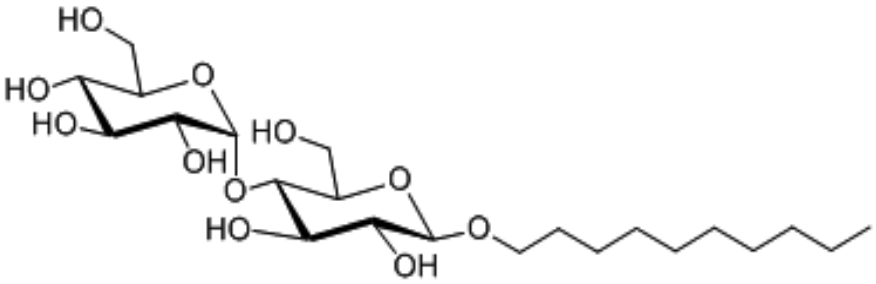

Molecular Formula: $C_{22}H_{42}O_{11}$ Molecular Weight: 482.6 g/mol

CMC (H_2O): ~ 1.8 mM (0.087%)

CMC (0.15M NaCl): ~ 1.8 mM

Aggregation Number (H_2O): ~ 69

dn/dc (H_2O): 0.1473 mL/gm

Purity: ≥99% by HPLC analysis.

Percent alpha: < 2 (HPLC)

Percent decanol: < 0.005 (HPLC)

pH (1% solution): 5-8

Solubility in water at 0-5°C: ≥ 20%

Conductance (10% solution): < 40 μS

- **Monoolein (1-oleoyl-rac-glycerol)**

Monoolein was used from NU-CHEK Prep, Inc., Elysian, USA, Purity >99%

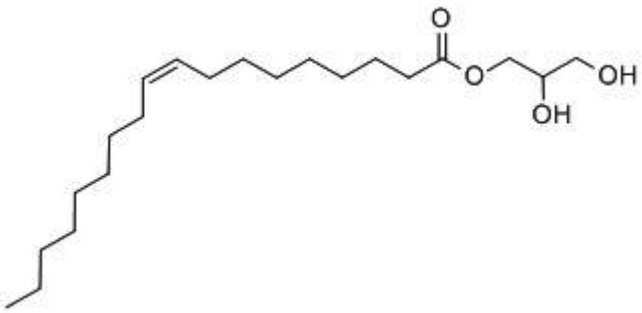

Chemical Name: MONOOLEIN

Synonyms: Aldo MO; Aldo HMO;MONOLEIN; MONOOLEIN; Mazol GMO; 1-MONOLEIN; Capmul GMO; Kessco GMO; 1-MONOOLEIN; Ablunol GMO

Molecular Formula: $C_{21}H_{40}O_4$

Formula Weight: 356.54

Melting point: 35-37 °C

Other chemicals

Acetic acid	Applichem
Agar, bacteriological grade	MP Biochemicals
Aluminum chloride hexahydrate	Molekula
Ammonium sulfate	Merck
Ampicillin	Applichem
Ammonium persulfate (APS)	Merck
L-(+)-arabinose	Merck/Alfa Aesar
Boric acid	Merck
Bromophenol blue	Merck
Calcium chloride dihydrate	Merck
Cobalt(II) chloride hexahydrate	Alfa-Aesar
Complete™ EDTA free	Roche
Coomassie™, Brilliant Blue R250	Merck
Coomassie™, Brilliant Blue G250	Merck
Copper(II) chloride dihydrate	Merck
Dithiothreitol (DTT)	Sigma
Ethanol 96%	Roth
Ethylenediaminetetraacetic acid (EDTA)	

di-sodium salt dihydrate	Applichem
Glucose	Applichem
L-Glutamic acid sodium salt hydrate	Sigma
Glycerol	Applichem
Glycine	Merck
HEPES	Merck
Hydrochloric acid	Merck
Imidazole	Sigma
Iron(II) sulfate heptahydrate	Merck
Magnesium sulfate heptahydrate	Merck
Manganese(II) sulfate hydrate	Merck
Methanol	Roth
Milk powder	Roth
Monovacenin	Nu-Chek-Prep
Phosphoric acid	Applichem
Polyethoxyethanol sorbitan monolaurate (Tween 20)	Sigma
Potassium hydrogen phosphate monobasic	Applichem
Rotiphorese™ Gel 30 (Acrylamide-Solution)	Roth
Sodium azide	Merck
Sodium chloride	Merck
Sodium dodecyl sulfate (SDS)	Caelo
Sodium hydrogen phosphate dihydrate dibasic	Applichem
Sodium hydroxide	Applichem
Sodium molybdate dihydrate	Sigma

Streptomycin	Applichem
Sucrose	Merck
Sulfuric acid	Merck
Tetramethylethylenediamine (TEMED)	Merck
Trichloroacetic acid	Merck
Tris HCl	Sigma
Trizma Base	Sigma
Tryptone	Applichem
Yeast extract	Applichem

Reagents

- Molecular weight standard for electrophoresis:

Page Ruler^{TM} prestained protein-ladder, Fermentas

- Standard reagent for western blot:

1-Step^{TM} NBT/BCIP, Thermo Scientific, USA

- Column-material for chromatography:

Ni-NTA-Agarose, Qiagen, Germany

Lipids for crystallization:

- *E.coli* polar lipid extract, Avanti Polar Lipids, USA

Crystallization kits:

- MemStart™, Molecular Dimensions, UK
- MemSys™, Molecular Dimensions, UK
- MemGold™, Molecular Dimensions, UK
- MemPlus™, Molecular Dimensions, UK

- NeXtal Cubic Phase I Suite, Qiagen, Germany
- NeXtal Cubic Phase II Suite, Qiagen, Germany
- NeXtal PEGs Suite, Qiagen, Germany
- NeXtal MemClass Suite, Qiagen, Germany
- Cubic™, Emerald Biosystems, USA
- Wizard I/II, Emerald Biosystems, USA
- Wizard III/IV, Emerald Biosystems, USA

Equipment

Incubator	Incu-Line, VWR, Germany
Orbital shaker	Multitron, Infors, Switzerland
Microfluidizer	M 110P, Microfluidics, USA
French® Press apparatus	Sim Aminco, USA
Roller Mixer	SRT6D, Stuart, UK
Spectrophotometer	V-1200, VWR, Germany
Peristaltic pump	SqiQ 400, Watson-Marlow, Canada
Thermomixer	Comfort, Eppendorf, Germany
Membrane pump	MZ 2C NT, VWR, Germany
Power supply	EPS 301, GE Healthcare, USA
Gyro-rocker	SSL3, Stuart, UK
Scanner	Epson Perfection V750 Pro, Japan
Äkta prime plus	GE Healthcare, USA
Mini Trans-Blot Electrophoretic Transfer Cell	Bio-Rad, USA
SE 250 Mighty Small II 10×8 cm Basic Unit	Hoefer, USA

FTIR spectrophotometer	Vertex 70, Bruker Optics, Germany
UV-Vis-Spectrophotometer	UV-2450, Shimadzu, Japan
Centrifuges	Optima L90K Ultracentrifuge with Rotor Ti70, Beckman, Canada
	Avanti J26 XP, Beckman, Canada
	Megafuge, Thermo, USA

High throughput membrane protein crystallization platform

Robot for in meso membrane protein crystallization, automated system for imaging crystallization probes, UV microscope for visualization of protein crystals, temperature controlled storing boxes for crystallization probes.

NT 8 Crystallography	Formulatrix, USA
Rock Imager 1000	Formulatrix, USA

Figure 2.1 The in meso crystallization robot Formulatrix NT8. The NT8 is a nanoliter-volume liquid handler with drop dispensing capability. The 8-tip head can aspirate and dispense drops from 100 nL to 1.8 µL.

2.2. Molecular biology methods

2.2.1. Plasmid DNA isolation

The commercial NucleoSpin® Plasmid method was used for isolation of plasmid DNA. The pelleted bacteria were resuspended in Buffer A1 and plasmid DNA was liberated from the *E. coli* host cells by SDS / alkaline lysis (Buffer A2). Buffer A3 was used for neutralization of the resulting lysate and created appropriate conditions for binding of plasmid DNA to the silica membrane of the NucleoSpin® Plasmid Column. Precipitated protein, genomic DNA and cell debris were then pelleted by a centrifugation step. The supernatant was loaded onto a column. Contaminations like salts, metabolites and soluble macromolecular cellular components were removed by washing with ethanol Buffer A4. Pure plasmid DNA was finally eluted under low ionic strength conditions with slightly alkaline Buffer AE (5 mM Tris / HCl, pH 8.5).

2.2.2. Amplification of DNA

DNA fragments were amplified with Polymerase Chain Reaction (PCR) [87]. Normally, a 20 µl reaction mix contained 20 ng of DNA matrix, 25 pmol of each primer, 5 nmol of each dNTP's and 0.5 U Phire® Hot Start DNA Polymerase (Fermentas). The amplification of DNA in the thermocycler was done with "Hot-start"-PCR in two-step manner. In the first step, 5 cycles of following conditions were made: 1) 15 s at 95°C, 2) 30 s at -3 to -5 degrees below primers' melting temperature and 3) 40-120 s (depending on the length of elongated DNA fragment), elongation stage at 72° C. In the second step, 25-30 cycles of following conditions were made: 1) 15 s at 95°C, 2) 30 s at primers' melting temperature and 3) the same time as in step 1, elongation stage at 72° C. Point mutations were also made with PCR [88].

2.2.3. Analysis and extraction of DNA from agarose gels

A horizontal gel-electrophoresis was used for analysis and extraction of DNA from agarose gels. The DNA probes in TAE buffer (Tris-base 2M, EDTA 50 mM and acetic acid till pH reaches 7.6) were applied to the 1-2% agarose gel running in TAE buffer. Staining of DNA bands was done by adding GelRed (Biotium) in 1:10000 dilution to TAE buffer. The DNA fragments were separated by applying 4 V/cm voltage to the gel. After cutting out of the band of interest, the Gel-Extractions-Kit (Qiagen, Hilden, Germany) was used for DNA extraction.

2.2.4. DNA restriction

DNA fragments were cut with corresponding restriction enzymes by 1 h incubation at 37° C. In most cases FastDigest® restriction enzymes from Fermentas were used together with FastDigest® buffer.

2.2.5. Ligation of DNA

Ligation of DNA fragments was done by incubation with T4-DNA ligase. 100 ng of cut plasmid DNA were taken together with 5-10X excess of insert DNA and 1 U of T4-DNA ligase with ligase buffer to total volume of 20 µl. Ligation mix was incubated overnight at RT. Deactivation of T4-ligase was done by incubation at 65° C for 10 min.

2.2.6. Transformation of plasmids into E. coli cells

Transformation of DNA was done into chemically-induced competent cells[89]. To prepare competent *E. coli* cells, a culture in 250 ml of SOB (SOB: 2% Bacto-trypton, 0.5% Bacto-yeast extract, 10 mM NaCl, 2.5 mM KCl, 10 mM MgCl2, 10 mM MgSO4) medium was incubated in a 2-liter flask at 18 C with vigorous shaking until an absorption at 260 nm equal to 0.6 was reached. Then, the broth was kept on ice for 10 min. Isolation of cells was achieved by spinning at 3000xg for 10 min at 4° C. The pellet was resuspended in 80 ml of ice-cold TB and kept in an ice-water bath for 10 min. The cells were pelleted by spinning as above. The pellet was resuspended in 20 ml of TB (10 mM Hepes, 55 mM MnCl2, 15 mM CaCl2 and 250 mM KCl). DMSO was added with gentle swirling to a final concentration of 7%. The centrifugation bottle was additionally kept in ice-water bath for 10 min.

At this point the cells became competent. They were dispensed by 100 µl into microfuge tubes and frozen immediately in liquid nitrogen. The frozen competent cells were stored at -80° C.

For transformation a plasmid solution (< 5 ul) was added and kept on ice for 30 min. Then the heat shock was applied at 42 C for 1 minute without agitation. After that the cells were transfer onto ice for additional 15 min.

To allow bacteria to acquire antibiotic resistance, the cells were incubated at 37° C for 1 hr in 800 µl of SOC (Add 1/100 vol. of filter-sterilized 2M glucose to SOB) medium. Bacteria were stroke on plates containing appropriate antibiotics. The plates were incubated overnight at 37° C.

2.3. Heterologous expression and purification of SRII in *E. coli*

Day 1

Buffer A: 150 mM NaCl, 50 mM Na-Pi (mixture of Na2HPO4 and NaH2PO4), 2 mM EDTA pH8.0

Solubilization buffer: 300 mM NaCl, 50 mM NaPi pH 8.0, 2% DDM

Starting with 30g of cells

1) 130 ml of Buffer A was added. Stirring 3-4h, 500 rpm, 4°C in darkness
2) Homogenization and addition of DNAse
3) French press
    a. French press cell was precooled
    b. After installation the French press cell was washed with buffer
    c. Pressure during cell lysis was kept between 900-1200 psi
4) Centrifugation 35000 rpm, 1h, 4°C
    a. Supernatant was discarded
    b. Pellets were solubilized in 2% DDM
5) Solubilization

The pellets were mixed with 150 ml Solubilization buffer

Stirring in darkness overnight at 500 rpm, 4°C

Day 2

Buffer B: 300 mM NaCl, 50 mM NaPi pH 8.0, 0.05% DDM

Washing buffer: 300 mM NaCl, 50 mM NaPi pH 8.0, 30 mM imidazole, 0.05% DDM

Elution buffer: 300 mM NaCl, 50 mM NaPi pH 8.0, 200 mM imidazole, 0.05% DDM

1) Centrifugation 35000 rpm, 1h, 4°C

Supernatant contains protein, pellets are waste.

2) Binding SR-II on Ni-NTA

   a. 10-15 ml of Ni-NTA were filled into glass column

   b. The resin was washed several times with H2O to remove ethanol

   c. The resin was washed 2 times with 2x column volume of buffer B

   d. Supernatant was loaded on Ni-NTA

3) Washing

After the protein was bound on Ni-NTA, it was washed with 500 ml of Washing buffer

4) Elution

The protein was eluted with Elution buffer. End volume was 20-25 ml.

Day 3

Buffer C: 10 mM Tris pH 8.0, 0.1% DDM

Buffer D: 30 mM NaCl, 10 mM Tris pH 8.0, 0.1% DDM

Buffer E: 500 mM NaCl, 10 mM Tris pH 8.0, 0.1% DDM

1) The eluate from the last step is diluted 1 to 10 with Buffer C.

2) Loading on the column

   a. The column was filled with fresh DEAE resin (15 ml).

   b. Resin was washed with H2O till ethanol was removed.

   c. Resin was wash with 2x resin volume of Buffer C.

   d. The protein was loaded on DEAE

3) Washing

Resin was washed with 500 ml of the Buffer D

4) Elution

Protein was eluted with buffer E.

The wings of the elution peak were cut to ensure high protein quality.

5) The absorption spectrum of the protein was measured

6) The protein was shock-frozen and stored at -80° C.

2.4. Heterologous expression and purification of truncated HtrII in *E. coli*

Day 1

For expression in 4.5 L scale 250 ml overnight culture (250 ml LB, 0.25 ml 100 g/l ampicillin) were mixed with 20 µl of pre-culture (in 20% glycerol) and incubated overnight at 37° C and 150 rpm.

1L LB medium:

10 g NaCl

10 g peptone or tryptone

5 g yeast extract

pH 7.2

Day 2: Expression

6 x 2l cultures (12 l LB, 12 ml 100 g/l ampicillin) in 5 l buffled flasks were inoculated with overnight culture to cell density at OD(600)=0.1 and incubated at 37° C and 130 rpm. The addition of 0.5 mM IPTG at OD(600)=0.8-1.0 induced expression and incubation was continued at 37° C and 150 rpm. Cells were harvested after 3 hours, washed in approximately 100-150 ml cell washing buffer (150 mM NaCl, 25 mM NaPi, 2 mM EDTA pH 8.0) and then resuspended in the same buffer, 5 ml per gram of cells. Then the cells were lysed using a microfluidizer with 900 KPa pressure. Membrane components were separated immediately by centrifugation (45 Ti rotor, 45 000 rpm, 4° C, 1h). Supernatant was discarded and the obtained pellet homogenized (5 ml per gram cells) in solubilization buffer (300 mM NaCl, 50 mM Na-Pi, 2% DDM pH 8.0) and moderately stirred at 4° C.

Day 3: Purification

Buffer 1: 50 mM Tris pH 8.0
100 mM NaCl
0.1% DDM

Buffer 2: 50 mM Tris pH 8.0
100 mM NaCl
0.1% DDM
250 mM Mesna or 100 mM DTT

Insoluble components were removed by centrifugation (45Ti or 70Ti rotor, 45 000 rpm, 4° C, 1h). The clear supernatant was loaded on a 20 ml Chitin-Beads column equilibrated in Buffer 1. After the washing step with Buffer 1, 20 ml of buffer 2 were added to the chitin beads and stirred overnight at 4° C.

Day 4

The suspension was filtered, the eluate was concentrated and dialysed against the buffer containing 150 mM NaCl, 20 mM Tris pH8.0, 0.1% DDM.

2.5. Biophysical methods for protein properties determination.

2.5.1. SDS-polyacrylamide gel electrophoresis (SDS-PAGE) and western-blotting (WB)

The denaturing SDS-polyacrylamide gel electrophoresis was performed (SDS-PAGE) by the method of H. Schägger and G. Jagow [90] for the analysis of proteins. For this purpose, SDS sample buffer (120 mM Tris pH 8.0, 6% (w/v) SDS, 35% (w/v) glycerol, 0.05 (w/v bromophenol blue) was added to the protein samples in a volume equivalent, shaken for 15 min and applied to 0.75 mm to 1 mm thick, 12-15% acrylamide gels. The separation of the proteins was carried out by applying an external voltage of 120 V (anode buffer: 200 mM Tris/HCl, pH 8.9; cathode buffer: 100 mM Tris/HCl, 100 mM Tricine, 0.1% (w/v) SDS, pH 8.25, the detection of the protein bands were visualized by staining the gel with Coomassie Brilliant Blue R250 (staining solution: 0.1% (w/v) Coomassie Brilliant Blue R250, 10% (v/v) acetic acid, 5% (v/v) methanol, destaining: 10% (v/v) acetic acid, 5% (v/v) methanol).

After separation by SDS-PAGE proteins were transferred to PVDF membrane (Macherey-Nagel, Düren) with a semidry blotter (30 min at 1.2 mA/cm2) (Anode buffer: 300 mM Tris/HCl, 100 mM Tricine, pH 8.7-8.8; Cathode buffer. 30 mM Tris/HCl, 300 mM 6-amino-n-caproic acid, pH 8.6-8.7, the membrane was incubated with 5% (w/v) dry milk in TBS buffer (5 mM Tris/HCl, 15 mM NaCl, pH 7.5) and blocked with the corresponding antibodies according to the manufacturer (1st antibody mouse anti-His IgG (Sigma), 2nd antibody goat anti-mouse IgG-Alkaline Phosphatase (Boehringer Mannheim). Visualization was done by adding NBT/BCIP solution (Pierce) that yields an intense, insoluble black-purple precipitate when reacted with alkaline phosphatases.

2.5.2. Size-exclusion chromatography (SEC)

Size exclusion chromatography is the commonly used experimental lab technique to separate proteins based on their molecular weight [91]. ÄKTA Prime purification system was used for automatic Ni-NTA purification and size-exclusion chromatography (SEC). Superose 6pg was used as a matrix for SEC analysis. After column packing, it was calibrated with a set of proteins that were purchased from commercial suppliers and for which the molecular mass was known. These experiments resulted into calibration curves shown below.

Vo – void volume

Ve – elution volume

Vc – column volume

$Kd = \frac{Ve-Vo}{Vc-Vo}$ [92]

Standards	Mw, Da	lg(Mw)	Kd	Ve, ml	Ve/V0	nm (DLS)	lg(nm)
V_t=				177,60			
Aceton	58	1,76	1,00	177,58	2,65		
UMP	324	2,51	0,90	166,00	2,48		
CytC	12400	4,09	0,92	168,43	2,51	1,80	0,26
RNAse A1	13700	4,14	0,84	159,65	2,38	2,10	0,32
CA	29000	4,46	0,74	149,21	2,23	2,60	0,41
bLAG-B	18400	4,26	0,73	148,15	2,21	2,90	0,46
OVA	44000	4,64	0,68	142,45	2,13	3,10	0,49
BSA	66000	4,82	0,62	135,57	2,02	3,70	0,57
ADH	150000	5,18	0,59	132,33	1,98	3,60	0,66
bAmylase	200000	5,30	0,55	127,33	1,90	5,90	0,77
Ferritin, pIV	443000	5,65	0,50	121,90	1,82	6,90	0,84
TGN	660000	5,82	0,41	112,20	1,67	8,70	0,94
Ferritin, pIII	886000	5,95	0,40	111,50	1,66	9,40	0,97
BD, peakI	9960000	7,00	0,07	74,50	1,11	44,10	1,64
Ferritin, peak I	32000000	7,51	0,06	73,28	1,09	50,10	1,70
V_0=				67,00			

Based on elution volumes of standards, two calibration curves were built. The first one (Figure 2.2) is showing logarithm of the particle size vs. Ve/Vo. The particle size was determined by dynamic light scattering. The linear approximation is quite good in the whole range. The next graph (Figure 2.3) is representing Kd vs. lg(MW). It was used for determination of the molecular weight of the eluted protein. It is clear that linear fit can be built only for $4<lg(MW)<6$. Since the physics of the separation process is based on the difference in size of the particles it is expectable that the size of the protein can be determined more precisely than the molecular weight. This fact can lead to problems when analyzing elution spectrums, especially in case of membrane proteins where detergent micelles are the main factor influencing on the size of solubilized protein and the size depends on the type of detergent.

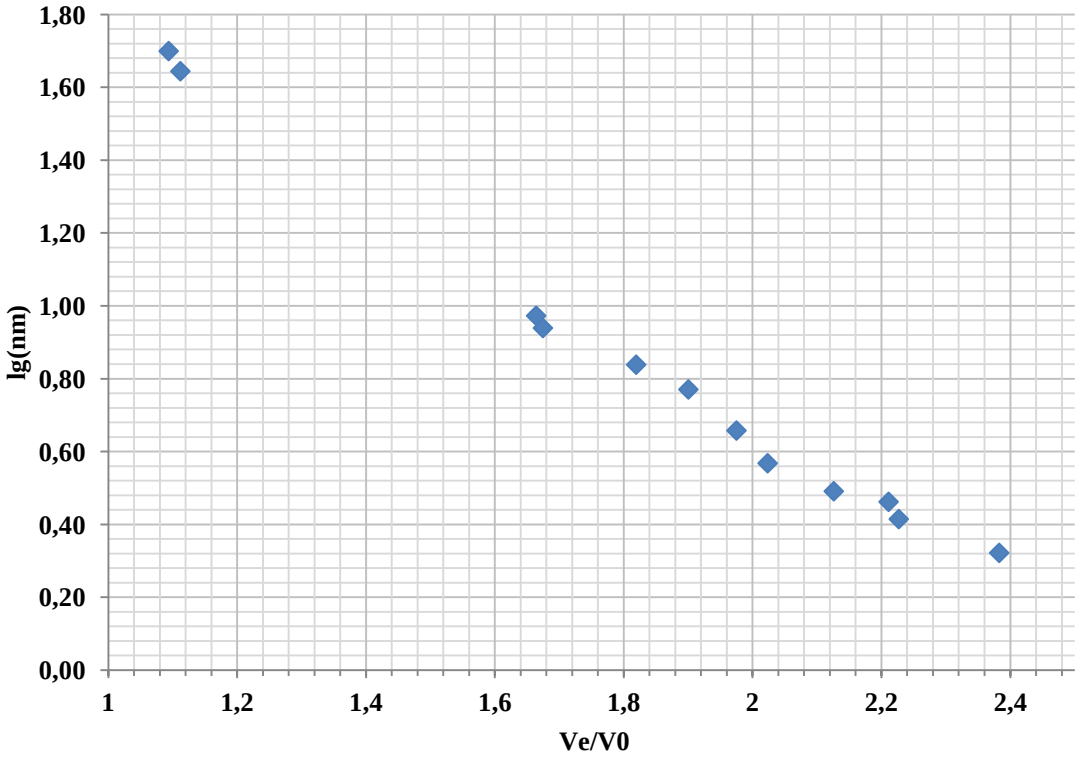

Figure 2.2 Calibration curve lg(particle size) vs. Ve/Vo

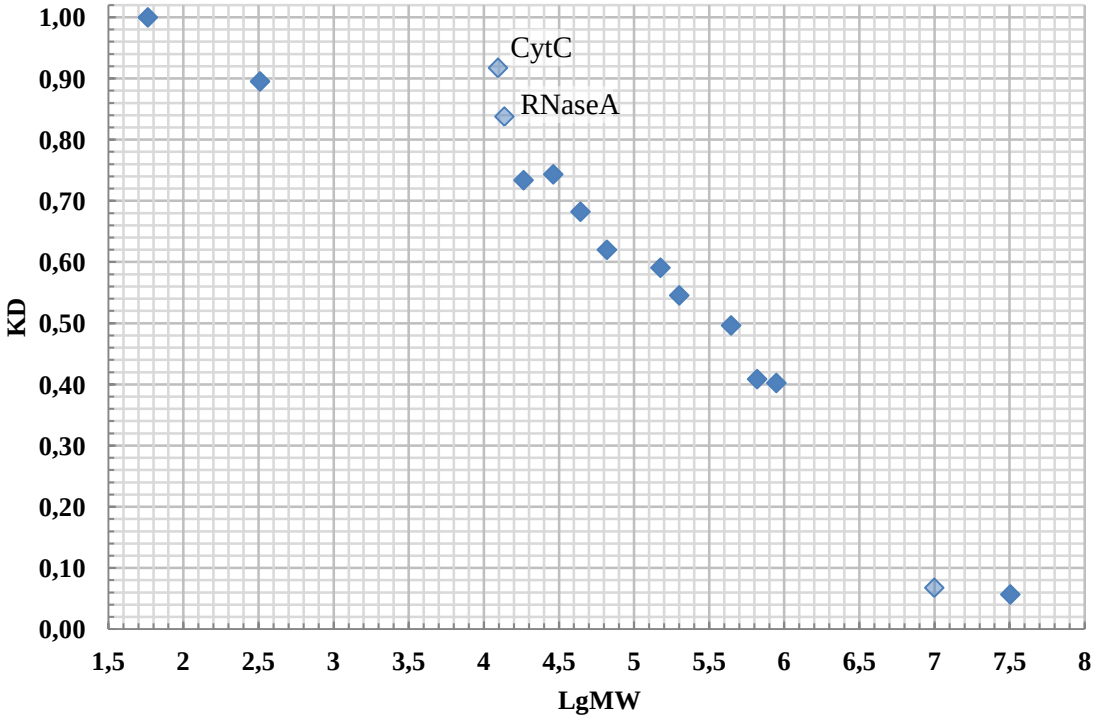

Figure 2.3 Calibration curve Kd vs. lg(molecular weight)

2.5.3. Mass-spectrometry (MALDI-TOF)

Matrix-assisted laser desorption/ionization-time of flight mass spectrometry (MALDI-TOF MS) is a relatively novel method for protein identification in which a co-precipitate of an UV-light absorbing matrix and a biomolecule is irradiated by a nanosecond laser pulse [93,94]. The vast majority of commercial MALDI mass spectrometers use a nitrogen laser with a wavelength of 337 nm and a pulse duration of ~ 10^{-9} sec. The matrix must have properties that provide reduced destructive properties of the laser radiation and the effect of the emergence of the so-called "soft" ionization without significant fragmentation of the analyte. Most of the laser energy is absorbed by the matrix, which prevents unwanted degradation of the protein. The ionized biomolecules fused with the matrix are accelerated in an electric field of the device and enter the flight tube. During the flight in the tube of the mass spectrometer, different proteins are separated according to their mass-to-charge ratio and come to the detector at certain times. This is the way to separate and distinguish chemically different proteins.

Mass spectrometric analysis of membrane proteins by MALDI-TOF was carried out on pure protein solutions and on PAGE gel extractions. Trypsin-digested samples were extracted from the gel, concentrated and desalted using Zip-Tip C18 columns using standard protocol.

Solutions:

1. Wetting solution - 50:50 acetonitrile (ACN) : water (H2O)

2. Sample preparation - 0.1% trifluoroacetic acid (TFA) in H2O pH <4

3. Equilibration solution - 0.1% TFA in H2O

4. Wash solution - 0.1% TFA in H2O

5. Elution solution - 0.1% TFA in 50:50 ACN:H2O

2.6. Crystallization of the SRII/HtrII complex

Starting material

1) NpSRII-His, C = 2-3 mg/ml; p.r< 1.3

2) NpHtrII-135, C = 2-3 mg/ml

3) Polar lipids of purple membranes

Procedure

Day 1 (Reconstitution)

1) Proteins were mixed at room temperature (1:1 molar ratio)

2) Incubated for 30 minutes at room temperature

3) Added NaCl to final concentration 150 mM

4) Added PM lipids (1:1 (wt:wt) lipid:protein ratio)

5) Added biobeads (10-20% of total volume)

6) Protein/lipid solution was shaken at 4° C in darkness overnight

Day 2

1) Reconstitution test

Centrifugation of 400 µl of solution 14 000 rpm for 10 minutes. If supernatant turns colorless then the reconstitution was successful.

2) Removed biobeads

3) Centrifugation 24 000 rpm, 40 minutes, 4° C, rotor Ti70

4) Removed supernatant

Resolubilization

Buffer: 150 mM NaCl, 25 mM NaKPi pH 5.1, 2% OG

Volume was calculated with respect to the final protein concentration ~0.6 mg/ml.

1) Resuspended the pellet by gentle stirring at 4° C.

2) Transferred to 50 ml Falcon tube

3) Shook at 4° C in darkness

4) Centrifugation 1h, 35 000 rpm, 4° C, Ti70

The solubilized protein must be in supernatant.

Cubic phase preparation

Detergent OG was added to the protein solution till the aimed concentration is achieved. Detergent concentration was checked by IR spectroscopy. The protein solution was added to monooleoyl in a ratio 1:1 (vol:vol) and several passes through interconnected

syringes for cubic phase preparation were performed. Cubic phase was ready for usage after 1-2 days.

2.7. Treatment of the X-Ray diffraction data

2.7.1. Determination of twinning fraction

To determine the factors of twinning diffraction data from 4 diffraction images was integrated in the program MOSFLM and Scaled in SCALA [95,96]. As a result, a few hundred reflexes related by twinning law were obtained. Twinning factor determined from the statistical analysis of the distribution of intensities of the reflections, using Britton plot [97] and the Yeates statistics [98], implemented in the program DETWIN [99], as well as the Internet resource University of California in Los Angeles (http://nihserver.mbi.ucla.edu/Twinning). Twin factors determined by various methods agree with each other within 5%. These methods have been used previously to determine the factors of twinning crystals BR [100], and it was demonstrated that the twinning factor, calculated from several hundred reflections, equal to the value determined from the full set of diffraction data measured from the same crystal. The quality of the diffraction of crystals and their twinning factor was used in deciding which of the crystals was used in further experiments at the synchrotron radiation source [101].

2.7.2. Determination of phases by molecular replacement

The term “molecular replacement” (MR) is usually used to describe the utilization of the structure of highly homologous protein to solve the unknown crystal structure of a target protein. MR enables the determination of the crystallographic phases by giving initial estimates of the phases of the new target structure from a previously solved structure. This method is opposed to the other main methods for solving the phase problem: experimental methods (which measure the phase from isomorphous or anomalous differences) or direct methods (which use mathematical relationships between reflections to derive a phase set for all reflections from phases for a small or set of reflections). The use of MR is now becoming more common as the data base of known structures expands. This method is especially helpful when the structures of protein families are solved, for instance, GPCR receptors. About 70% of the deposited macromolecular structures these days were solved using MR and at its best has the advantages of being quick and highly automated [102].

In case of the unit cell that contains more than one molecule, the best way to compare the diffraction patterns and to determine protein orientation is the usage of Patterson functions. Any Patterson function contains a set of peaks representing intramolecular vectors. For every molecule orientation found in the unit cell a single set of vectors will be found. The peaks of the set of intramolecular vectors should be within the biggest intramolecular distance r from the Patterson function origin. Contrary, the intermolecular vectors should be, in general, longer than intramolecular. They can be called a system of cross-vectors. The respective orientation of the molecules can be determined by comparing intramolecular Patterson functions inside the sphere with radius r [103].

Model orientation in the process of molecular replacement can be split in two steps: rotation search and translation search.

Rotational search

In the observed Patterson map peaks arising from different types of inter-atomic vectors are present. However, the model Patterson map doesn't contain all types of the peaks at the stage of the rotation search. Any inter-atomic vectors arising from non-crystallographic symmetry or from other molecules of a different type are not taken into account as normally only one search molecule is used at a time. Moreover, the translations that move the model molecule to the correct position with respect to the rotational symmetry operations are not known and the inter-atomic vectors arising from this symmetry are typically ignored. By default, the search molecule is placed in a P1 unit cell; in other words, the rotational symmetry is ignored. It is computationally most efficient to put the center of gravity of the model molecule to the origin of the unit cell [104].

The model Patterson map has only peaks arising from intra-molecular vectors and inter-molecular vectors between copies arising from lattice translations. The rotation search superimposes this `partial' Patterson map with the observed Patterson map. This can be imagined as a pattern-matching procedure. The search pattern is taken from the model Patterson map, while the observed Patterson map contains the search pattern where the angular orientation is unknown. In the observed Patterson map, the search pattern is concealed by other patterns that are not taken into account in the model Patterson and noise [104].

The rotation function is then given by:

$R=\int_U P_2(X2)P_1(X1)dX1,$

for the Patterson P1 and the rotated Patterson P2 within the volume U. This will have a maximum value when the two self-vector sets are equivalently oriented.

Translation search

By the analogy with the rotation function the translation function can be introduced by

$T(\mathbf{t})=\int P(\boldsymbol{u})P(\boldsymbol{u},\boldsymbol{t})d\boldsymbol{u}X1,$

The maximum of this function finds the best fit of the computed and correctly oriented cross-Patterson P(**u, t**) with the Patterson P(**u**). In the case of several copies of the subunits present in the unit cell one can position each of them step by step [105].

2.7.3. Model building and refinement

X-ray data quality was assessed using phenix.xtriage [106]. Starting from a molecular replacement solution from Molrep [107], using PDB entry 1H2S as a template, the structures were initially automatically built in Arp/Warp [108], refined in Refmac5 [109] and the final steps of refinement were done in Phenix [110]. The structures were validated using MolProbity [111].

2.7.4. Obtaining the structures of intermediate states

The structures of intermediate states were obtained by exploiting the same procedure as in [6]. Difference density maps $\Delta\rho = (|F_{ill}| - |F_{Gobs}|)\exp(i\varphi_G)$ were used to reveal major structural changes that occurred after illumination of the crystals, where $|F_{ill}|$ - the observed amplitudes from illuminated crystals, $|F_{Gobs}|$ - the observed ground-state amplitudes and φ_G are the phases calculated from the ground-state model. Refinements of intermediate states were performed by starting with a superposition of a fixed and a unfixed ground-state structure with occupancies varying in the range 0.2–0.8 by simulating annealing (using 3,000 and 5,000 K and a slow cooling protocol in CNS [112]). Extrapolated densities were calculated for refined models $\rho_{ex} = (1 - \alpha)|F_G|[\exp(i\varphi_G)] + \alpha|F_M|[\exp(i\varphi_M)]$ with different occupancies α for the intermediate state. Intermediate state occupancies were estimated from the best correlation as 50 ± 10% for late M state. This variation had no significant effect on the conformation for the intermediate state after refinement. After occupancy had been fixed, models were further refined and manually rebuilt in program Coot until convergence of *R* factors was reached [6].

3. Results and Discussion

3.1. Overall characteristic of the ground state structure of the SRII/HtrII complex

The structure of the complex of SRII-D75N mutant has revealed features that were not present in the structure of the wild type complex (see Chapter 3.2). The new quaternary structure of the complex was crystallized in the $I2_12_12_1$ space group, while all the previous structures of the complex were crystallized in $P2_12_12$. The influence of crystallization conditions has changed not only the space group of crystals but also the angle between protomers. The dramatic difference in the structures in two space groups may have a big influence on our understanding of the signal transduction mechanism in the SRII/HtrII complex. In order to check, whether the new shape of the complex is an effect of the new crystallization conditions or of the D75N mutation itself, we have crystallized the wild type complex. The ground and intermediate state structures were solved. These structures have shown the same respective orientation of SRII and HtrII as in the case of the mutation D75N. Moreover, the changes in the structure upon transition from the ground state to the M state were the same. In this chapter the ground state structure of the wild type complex SRII/HtrII in the $I2_12_12_1$ space group will be discussed.

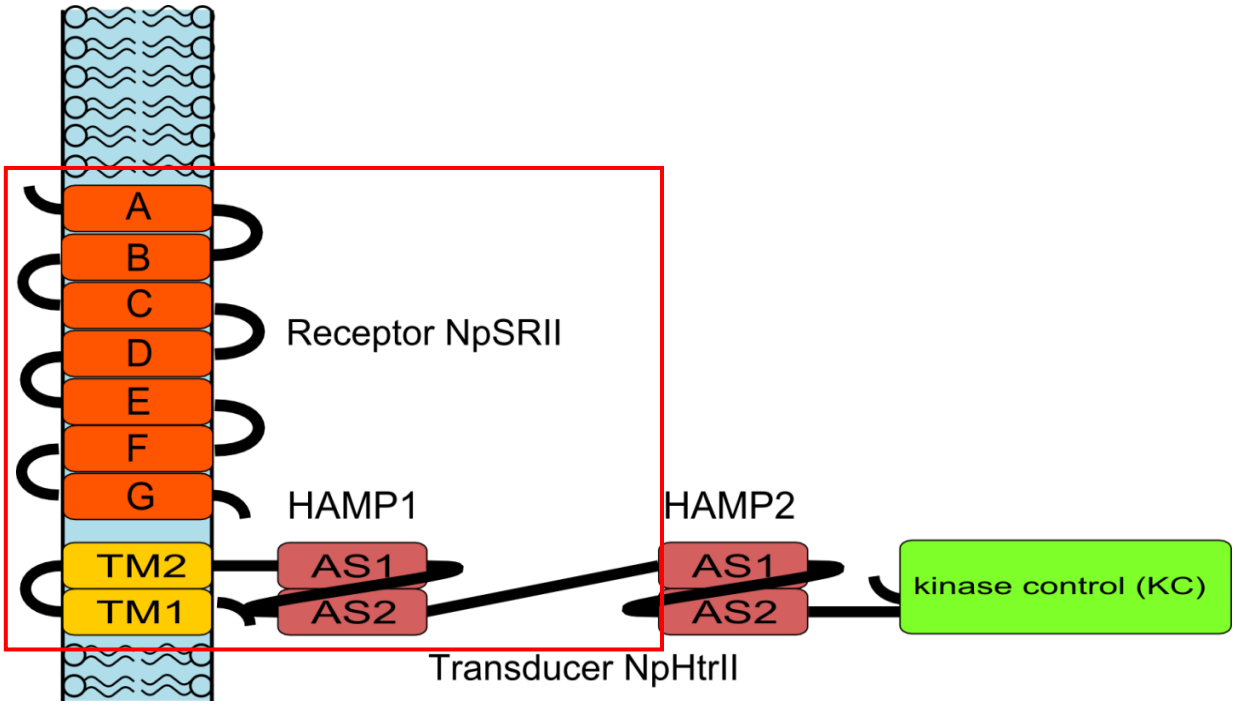

Figure 3.1 Structural multi-domain organization of the SRII/HtrII complex. The functional complex consists of two membrane proteins SRII and HtrII forming αββα topology, where two HtrII molecules are flanked by

two SRII light receptors. HtrII is organized as a sequence of domains that are conserved among histidine kinases: transmembrane domain, HAMP domain, adaptation domain, kinase domain. The red rectangle indicates the part of the complex that was crystallized. A-G, TM1 and TM2 are the transmembrane helices, and AS1 and AS2 are the helices of the HAMP domain.

The functional complex of membrane proteins SRII and HtrII is a homodimer, consists of two SRII molecules and two HtrII molecules. SRII contains 7 transmembrane α-helices named from A to G and HtrII contains two transmembrane α-helices named TM1 and TM2. As was mentioned before, HtrII comprises a membrane part and very elongated coiled-coil cytoplasmic part. This anisotropic geometry of the complex makes the formation of well-diffracting crystals from intact proteins very improbable (see Figure 3.1). The length of HtrII in the direction perpendicular to the membrane is about 250 Å that considerably exceeds the typical distance between layers in crystals grown from cubic phase. Therefore, truncated constructs of HtrII were crystallized in complex with SRII. These constructs contain the water-soluble N-terminus (amino acids 1-22), membrane part of HtrII (amino acids 23-82) and the first HAMP domain (amino acids 83-135). Previously published structures of the complex contained HtrII truncated at position 114 ([7], PDB code 1H2S) and 157 ([6], PDB code 2F95).

Figure 3.2 The crystal of the SRII/HtrII-157 complex in a cryoloop. The crystal belongs to $I2_12_12_1$ space group. Datasets were collected on macromolecular beamlines of ESRF in Grenoble: ID23-1, ID14-1, ID14-2, ID-29.

In an intensive crystallization screen we obtained two new crystal forms (Figure 3.2) of the SRII/HtrII complex displaying space groups with $I2_12_12_1$ and $P6_4$ symmetry in contrast to $P2_12_12$ published before ([6,7], PDB codes 1H2S, 2F95). In the case of the $I2_12_12_1$ space group the resolution for the both ground and M states was 1.9 Å. In this case HtrII was truncated at the position 157 and contained a 6xHis tag. Aiming to resolve the structure of the HAMP domain, the length of HtrII construct was truncated to 135 amino acids (discussed below). This complex was crystallized at similar conditions and data sets of 2.5 Å resolution in the $P6_4$ space group were collected (for statistics see Appendix I). No intermediate states data was collected in this case.

When comparing wild type structures solved in the $I2_12_12_1$ and $P2_12_12$ space groups it can be seen that the overall structure SRII is nearly the same and is highly similar to the structure of SRII alone [113,114] (see Figure 3.3 and Figure 3.4). SRII is a seven-helix transmembrane protein with molecular mass of 24.7 KDa. Most of the protein was built in electron density maps, except 6xHis-tag containing C-terminus which couldn't be resolved, probably, due to high flexibility. HtrII was truncated at the amino acid 157. This construct contains disordered N-terminus (amino acids 1-22), two transmembrane helices connected via a short extracellular loop (23-82), the first HAMP domain (83-135) and the helical linker between the two HAMP domains (136-157). Though the HAMP domain was present in the protein construct expressed, the electron densities in this region turned out to be very poor and discontinuous that didn't allow structural modeling of HtrII after Gly83-Gly84.

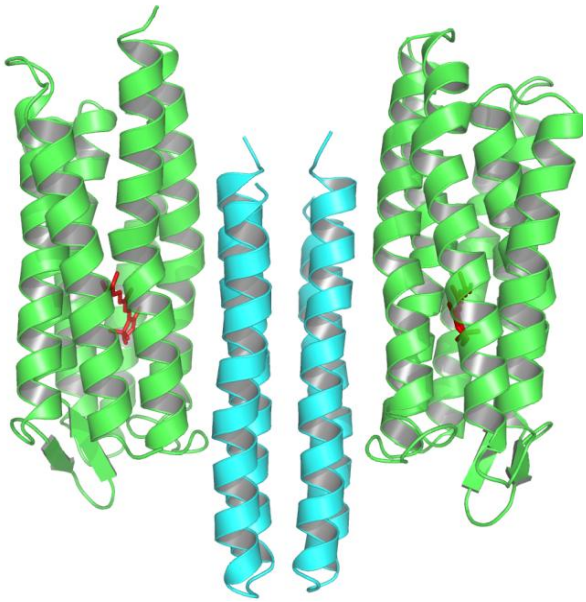

Figure 3.3 Overall view of the obtained structure of the SRII/HtrII complex.

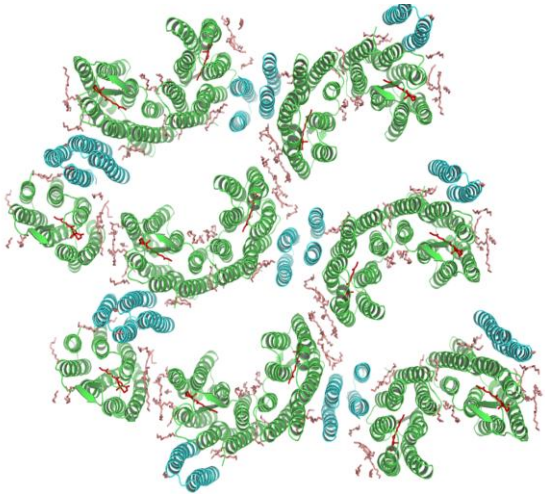

Figure 3.4 Crystal lattice of the SRII/HtrII complex in plane of the membrane.

The structure of the HAMP domain would be a big asset to the currently available structures of the SRII/HtrII complex. Despite a number of experiments, neither of the data sets yielded electron density strong enough for building HAMP. The reasons for this problem can be:

- the flexibility of TM2 helix in the point of two glycines (G83, G84),
- thermally unstable structure of the HAMP domain,
- unspecific interactions with neighboring proteins in the crystal,
- protein unspecific proteolysis in course of crystallization

It is worth noting that the TM1 helix structure is also not complete, built only up to amino acid 22, approximately at the same distance from the membrane as TM2. The structures in the $I2_12_12_1$ space groups contain two more amino acids on the C-terminus of HtrII in addition to 23-82 that were available in $P2_12_12$. This additional information was very important for modeling of the HAMP domain structure by homology and modeling of the interaction between the receptor and the transducer.

A number of hydrocarbon lipid tails were traced in the electron density (Figure 3.4). The interaction between proteins in the plane of the membrane is mostly mediated by these lipids. Modeling hydrophobic lipid tails as polycarbon chains has reduced R-factors and improved electron density maps considerably that was important for building of the complete model. The polar heads of the lipids couldn't be resolved.

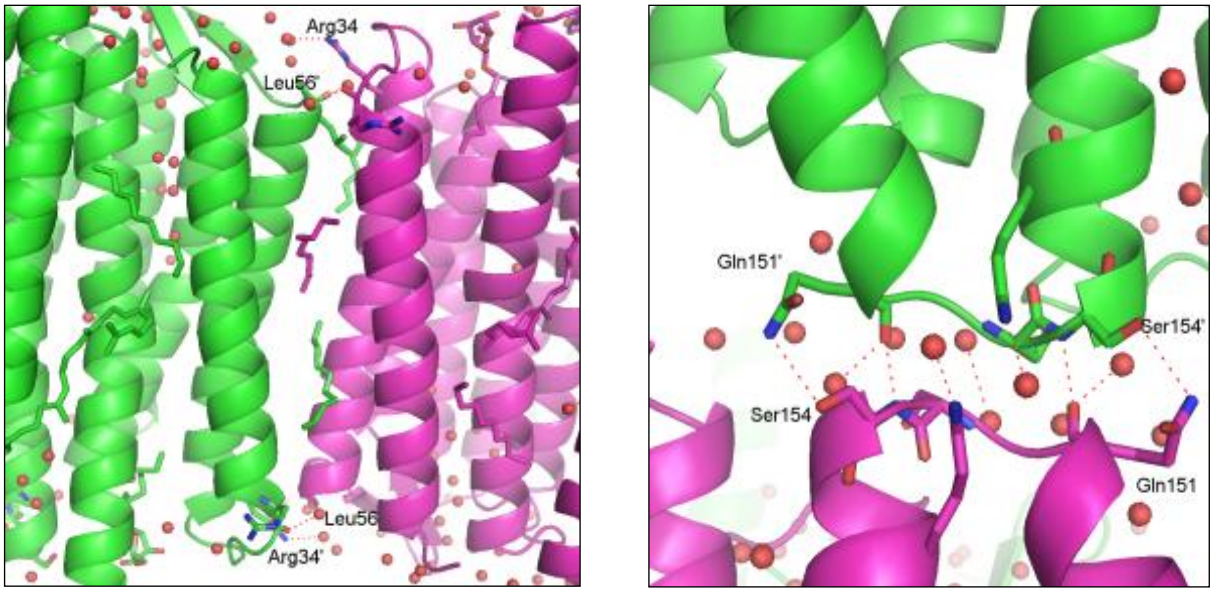

Figure 3.5 Adjacent proteins in the crystal are also interacting through several hydrogen bonds. Contacts in the EF loop are mediated by hydrogen bonding from Ser154 to Gln151 of the symmetry mate. A and B helices have interactions mediated by residues Arg34 and Leu56in the polar regions.

There are several places where adjacent proteins in the crystal form contacts. In the $I2_12_12_1$ space group EF loops of the neighboring proteins appear to be close to each other forming 2 hydrogen bonds from Ser154 to Gln151' (and the corresponding symmetric bond from Gln151 to Ser154', see Figure 3.5)

Strong similarity between the ground-state structure of NpSRII alone and the ground-state structure of NpSRII in complex with NpHtrII was also observed. The RMSDs of coordinates are 0.53 Å for the structure in space group $P2_12_12$ (PDB code 1H2S) and 0.45 Å for the structure in space group $I2_12_12_1$. There are only slight differences in flexible loop

regions, which include also the position of the C-D loop. An important observation concerns D193, which occupies the same position in the structure of the complex and in the present structure, contrary to its position in structures 1H68 and 1JGJ. These data emphasize the importance of identical crystallization conditions (in detail in [113]).

The structure of the active site is similar to that in 1H2S (Figure 3.6). The retinal molecule is covalently bound to Lys205 through Schiff base. The retinal is in all-*trans* isomerization state. The positive charge of the protonated Schiff base is equilibrated by the negative charge of the counterion Asp75. The hydrogen bonds network is organized through the Schiff base, Asp75, Asp210, Trp76, the water molecules W1, W2 and W3.

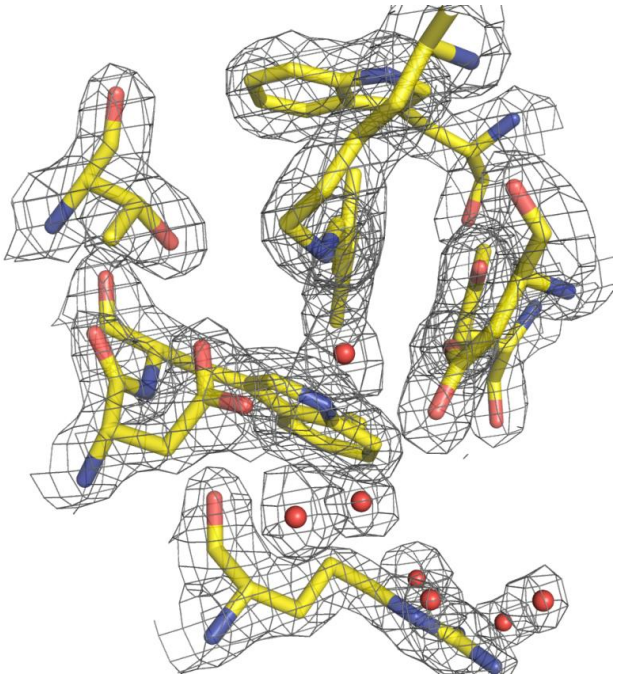

Figure 3.6 The active center of SRII in "sticks and balls" representation. Waters are shown as red balls, oxygen atoms are shown in red, nitrogen atoms are shown in blue. The map is contoured with 2σ cutoff.

In general, the structure of SRII and HtrII proteins is very similar to the structure obtained before in the $P2_12_12$ space group. Major difference is related to the mutual disposition of the proteins in a dimer. The $I2_12_12_1$ reveals a new "U"-shape of the complex (discussed in detail in Section 4.3). Having solved the X-ray structures of SRII and HtrII in different space groups we can conclude that the structure of the proteins remains the very similar with small RMSD regardless of crystal contacts and buffer contents.

As it is shown on the double distance matrix between structures in $P2_12_12$ and $I2_12_12_1$ (Figure 3.7), the largest RMSD is observed in the loop regions of SRII and on the C- and N-termini of HtrII. This result is very important as the position of the C-terminus affects the structure of the HAMP domain and it is different in the $I2_12_12_1$ and $P2_12_12$ space groups.

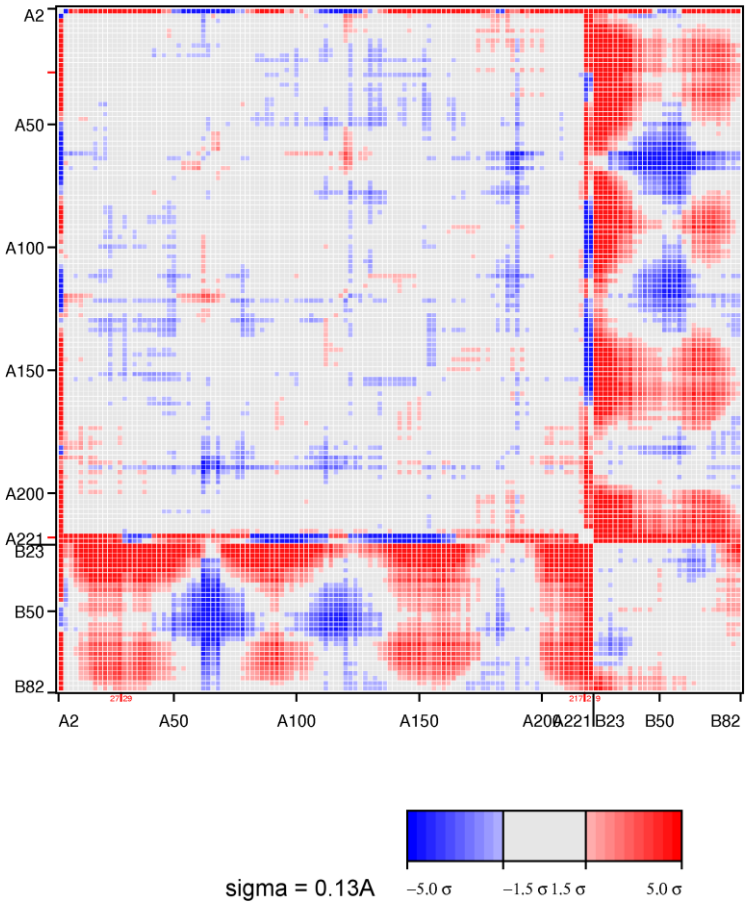

Figure 3.7 The double distance matrix plot showing differences in the ground state structure of the wild type complex in $I2_12_12_1$ and $P2_12_12$ space groups. Chain A corresponds to SRII, chain B corresponds to HtrII.

3.2. The structure of the D75N mutant. Implications from the structure

Isomerization of the retinal and Schiff base deprotonation are primary acts of the signal transduction in SRII. Asp73-to-Asn73 mutation is known to inhibit completely the signal transduction in SRII from *H.salinarum* [50] and similar Asp75-to-Asn75 mutation has barely any effect on the corresponding protein function in *N.pharaonis* [69]. Moreover, the corresponding mutation in other retinal proteins (like halorhodopsin, sensory rhodopsin I, and bacteriorhodopsin) has a drastical effect on the functionality of these proteins. Certainly, an explanation for the insignificance of the D75N mutation for signal transduction in the SRII/HtrII complex is required for probing existing paradigms of the molecular mechanisms of retinal protein functions. To create a molecular basis of the explanation of the fact that D75N mutation retains functionality of the NpSRII /NpHtrII complex, the X-ray crystallographic study was performed.

The D75N mutation was introduced into the gene by directed mutagenesis. The protein bearing the mutation was expressed as wild type SRII. The crystallization procedure was performed as for wild type complex. Crystals were fished and flash frozen directly without using a cryoprotectant. The X-ray data were collected at ESRF, beamline ID14-1.

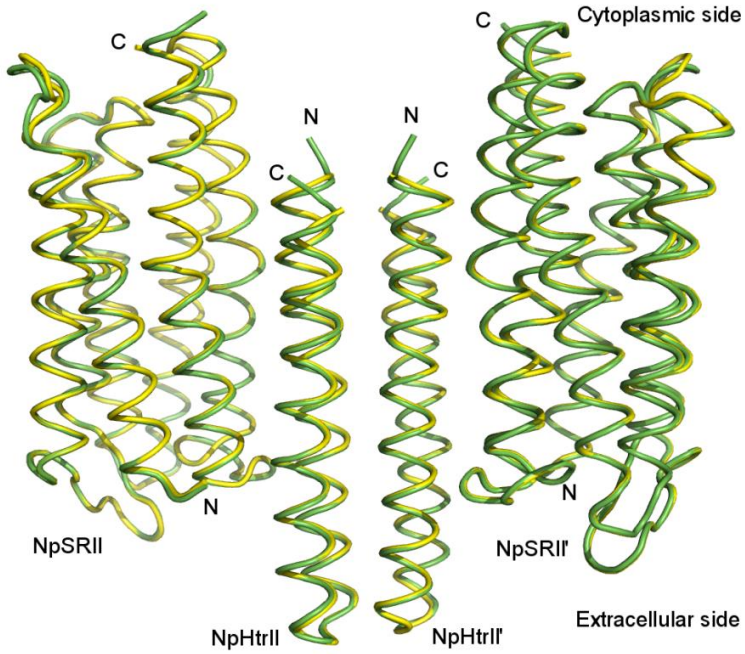

Figure 3.8 Fold of the receptor/transducer complex (side view). NpSRII-D75N/NpHtrII complex is shown in yellow and the wild type NpSRII/NpHtrII is shown is green. "N" and "C" letters denote N- and C-terminus of the proteins. The structures of receptors are overall identical, whereas some deviations were observed on the termini of HtrII. These deviations can be attributed to the different crystallization conditions and flexibility of the region. Coordinates and structure factors of NpSRII-D75N/NpHtrII have been deposited in the Protein Data Bank with the 4GYC accession number.

We have obtained the NpSRII-D75N/NpHtrII mutant structure from crystals grown by *in meso* approach diffracting to 2.0 Å. The crystals were plate-like, belonging to type I [115] and grew up to 1200x50x20 μm (see Methods and Appendix I for crystallographic statistics). Each asymmetric unit contains one NpSRII-D75N/NpHtrII heterodimer; one of the crystallographic axes is collinear to the natural 2-fold axis between transducer molecules in the 2:2 dimer (Figure 3.8). The complex is "U"-shaped as in all the other structures in $I2_12_12_1$ and $P6_4$ space groups (see below). Receptors are oriented head-to-head, forming several contacts within loops. Transducers of adjacent layers in crystals are not stacked one below another but are rotated and displaced due to the crystallographic screw axis perpendicular to the membrane in the center of the dimer.

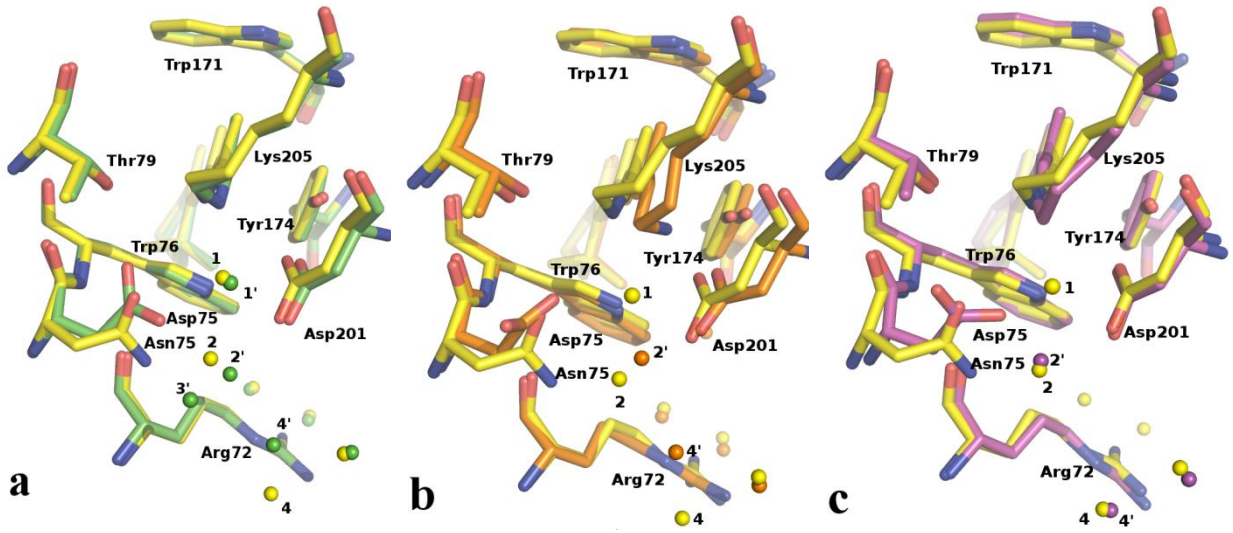

Figure 3.9, Panel a: Structural differences between the ground states of NpSRII-D75N and WT in the vicinity of the retinal Schiff base including water molecules,. Wild type molecule and waters (balls) are shown in green; NpSRII-D75N is shown in yellow. Primes denote water molecules in the wild type ground structure.

Figure 3.9, Panel b: Structural differences between NpSRII-D75N ground state and the K-state intermediate in the vicinity of the retinal Schiff base including water molecules. Ground state NpSRII-D75N and waters (balls) are shown in yellow, the K-state and waters are shown in orange. Primes denote water molecules in the K-state structure.

Figure 3.9, Panel c: Structural differences between NpSRII-D75N ground state and the M-state intermediate in the vicinity of the retinal Schiff base including water molecules. Ground state NpSRII-D75N and waters (balls) are shown in yellow, the M-state and waters are shown in magenta. Primes denote water molecules in the M-state structure.

Illustrations from [116]

In the mutant state we observe several conformational features resembling the M-state of the wild type (Figure 3.9a). Since Asp75 residue is replaced with a neutral Asn75, it has no connectivity to water molecule W1 and the Schiff base. It causes rotation of Asn75 side chain with respect to Asp75 and a shift towards Arg72. The hydrogen bond to Thr79 is lost. Water molecule W3 disappears breaking additional bonds in the hydrogen bond network. Water molecule W2’ is moved by 0.9 Å to the Schiff base. It forms a hydrogen bond with the nitrogen from Asn75 resembling W2’-Asp75 bond in the M-state. Water molecule W4’ is shifted in the mutant towards the extracellular part by 2 Å. Thereby the salt bridge between Arg72 and Tyr51 is broken. There is a slight movement of Arg72 residue towards the extracellular part, which can be expected from the absence of the charge at Asn75. Water molecule W1 is 0.3 Å shifted towards the Schiff base. All these rearrangements lead to a distortion of the G helix backbone with the RMS deviation from the wild type for the residues 196-206 as high as 0.12 Å with the maximum amplitude of 0.3 Å around the residue Asn201.

Comparing the structure of NpSRII-D75N with those of the ground and M-state of the wild type receptor it is obvious that the hydrogen bond network of the mutant is still able to preserve global arrangement of the α-helices (Figure 3.9c). In essence, this is an indication of the fact that the D75N mutant is resting in the ground state and not a model of the M state of the wild type protein. Inspecting the hydrogen bond network more closely one observes that the water molecule W3 is not present in the mutant. In the ground state of the wild type it forms a pentagon of hydrogen bonds together with W1, Asp75, Asp201 and Schiff base. Due to the absence of W3 two hydrogen bonds mediated by this water molecule, one bond to Asp75-Oδ and the second one to W2, are absent. The disappearance of two hydrogen bonds weakens the connection between C and G helices. However, reducing C-G interactions is not sufficient to trigger the rearrangement of the helices such that an M-state like conformation is reached. Indeed, in the M-state of the wild type complex in addition to W3, W1 is also not present. Furthermore, the hydrogen bonds connecting helices C and G through water molecules W2 and W4 are disrupted. Interestingly, also in the K state of the wild type the hydrogen bonds mediated by water molecules W1 and W3 are absent (Figure 3.9b). Apparently, the hydrogen bond network stabilizing the ground state structure is loosened and resembles that of the K-state.

Table 1. *List of hydrogen bonds in the active center for different states of the comlex.*

	NpSRII/NpHtrII ground state	NpSRII-D75N/NpHtrII ground state	NpSRII/NpHtrII M-state
W1•••Asp75/Asn75	+	+	–
W1•••Asp201	+	+	–
W1•••Lys205	+	+	–
W2•••Asp201	+	+	+
W2•••W3	+	–	–
W2•••W4	+	–	–
W2•••Asp75/Asn75	–	+	+
W3•••Asp75/Asn75	+	–	–

W4•••Tyr51	+	–	–
W4•••Arg72	+	+	+

Our data allow envisioning a molecular mechanism of signal transfer from the receptor to the transducer. Indeed, a general fundamental fact for retinal proteins is that upon absorption of a photon retinal isomerizes and the hydrogen bond between Schiff base and the adjacent water molecule W1 is broken resulting in its disappearance from the active cites. Additionally, side chains of the residues in the active cite become mobile as seen from increased B-factors. Second, the carboxylic group of Asp75 is rotated by 90° with respect to its ground-state position (already partially rotated in NpSRII-D75N) thereby losing its connection to the water molecule W3, which becomes disordered (already absent in NpSRII-D75N). Third, such reduction of the hydrogen bond network in the extracellular part of retinal pocket leads to further structural rearrangements. Indeed, water molecule W2 shifts towards Asp75 in the M-state of wild type NpSRII/NpHtrII complex. While in the ground state it is linked to water molecules W3 and W4 and to Oδ of Asp201, in the M-state only the bond to Asp201 remains intact. A new bond from W2 to Asp75 appears after the rotation of the side chain. Thus, only two hydrogen bonds are mediated through W2 in the M-state in contrast to three bonds in the ground state. Fourth, water molecule W4 shifts in the M-state towards the extracellular part by 2 Å and concomitantly breaking the hydrogen bond between W4 and Tyr51-OH that links Tyr51 with Arg72 (see Table 2). Finally, inter-helical connections between helices C and G are broken and the receptor splits in two loosely connected domains consisting of A, B and G α-helices and C, D, E and F, respectively. The movement of the helix G triggers signal propagation to the TM2 helix of the transducer.

As was discussed above, the NpSRII D75N mutant is different from the wild type protein mainly in the hydrogen bond network, which, in effect, weakens the helix C-helix G interaction, like it is also been observed for the structure of the K-intermediate. Apparently, in both insistences the protein is poised for reaching the active state. Infrared spectroscopic data indicated that upon its activation the conformational changes observed for the NpSRII-D75N mutant are almost identical to those observed for the wild type [117]. It is in line with the observation that this mutant displays wild type physiological behavior and gives additional confidence for the described above structural explanation of the unexpected consequence of D75N mutation. From electron paramagnetic resonance (EPR) data it was concluded that the D75N mutation shifts the ground state conformation of NpSRII-D75N and its cognate

transducer into the direction of the signaling state [118]. The present results and those from spectroscopic investigations could provide a reason why the corresponding HsSRII-D75N mutant shows constitutive activity. In this case, the neutralization of the counterion might trigger conformational changes large enough to stabilize the active state. Thus, our crystallographic data show that deprotonation of the Schiff base itself is not mandatory for the receptor activation. This does not mean the rest positive charge at the Schiff base does not influence the conformational changes since it still can interact with charges in more distant positions.

Obtained crystal structure of ground state complex of NpSRII-D75N/NpHtrII in the crystals of the $I2_12_12_1$ space group gives a new insight into the structure and possible molecular mechanisms of signal propagation of sensory rhodopsin II with its cognate transducer. We show the importance of the hydrogen bonds network inside SRII and propose a mechanism by which the energy stored in hydrogen bonds is transferred to HtrII. It should be stressed that these data do not contradict with the early proposed molecular mechanism of signal development in the membrane part of the NpSRII/NpHtrII complex [6]. In opposite, the present work provides its additional valuable support.

3.3. The structure of the M state intermediate. Signal transduction

An intermediate M state is important for understanding of the processes underlying signal transduction in SRII/HtrII complex. It was important to crystallize the signaling state in the same conditions as the ground state to check whether the molecular mechanism remains conserved. The M state structure was obtained by the procedure developed before and described in paper by Moukhametzianov *et al.* [6]. In brief, after collecting the ground state dataset the crystal was illuminated with the green laser for several seconds at room temperature. Then the crystal was flash-frozen again and the new dataset was collected from a different part of the crystal, from which the ground state was collected.

Having two data sets from different space groups ($I2_12_12_1$ and $P2_12_12$) we checked whether different space groups have a structural influence on the retinal binding site. As can be seen from Figure 3.7 there are almost no differences found for the ground state structures (Figure 3.12a) as well as that for the activated M intermediate (Figure 3.12b) indicating that the different crystallization conditions and space groups have little, if any at all, influence on the structurally important regions of the complex. This is substantiated if one analyzes the

transition between ground state and the M state (Figure 3.8). In $I2_12_12_1$ as in $P2_12_12$ the retinal chromophore switches from *all-trans* conformation to *13-cis* upon photon absorption and with Lys-Cε simultaneously shifting towards the central water cluster. The side group of Asp75 is rotated by about 90° from its ground state position, thereby losing the hydrogen bond to Thr79. Consequently, W3 becomes disordered and disappears in the M state. Hydrogen bonds pentagon (Asp201-Oδ···W2···W3···Arg72-Nε···W1) does not exist any longer in the M state because molecules W1 and W3 have vanished. Consequently, helices C and G have more freedom to move independently. The water molecule W2' is located close to Asp75 and Arg72. Thus, the signal is generated by the retinal isomerization and then propagates to the interface between the receptor and the transducer. The signal propagation is driven by rearrangement of the hydrogen bond network mediated by the water molecules that leads to the movement of the receptor helices described above. The main trigger of this process is the loss of connectivity between C and G helices.

One of the questions, which had to be taken with care, is weather the observed changes in the structure relate to real signal transduction mechanism or are just resulting from the radiation damage. The recent study [119] has shown that retinal isomerization and water molecules translocation can result from extensive X-ray illumination itself. To avoid the radiation damage, the exposed dose was always kept under reasonable limits and was the same for the ground state and the intermediate state data collection. If, nevertheless, any radiation damage did occur, it would be subtracted out and would not appear on difference Fo-Fo maps. As the data from the illuminated crystals is a superposition of ground and intermediate states, the Fo-Fo maps are the major experimental result to find and observe changes in the structure upon transition between states of the complex (Figure 3.11).

The conformational changes observed for free NpSRII and for NpSRII in complex with its transducer are quite similar in nature (Figure 3.12). Major movements are observed for helices F and G, which have been correlated to signal propagation from the receptor to the transducer. Additionally, an inward movement of the extracellular part of helix C is observed. Although these conformational changes are detected in both cases, in the case of NpSRII alone, they have almost twice-as-large amplitudes. Smaller changes in the complexed NpSRII cannot be attributed to crystal packing, as it is looser in the crystals of NpSRII‑NpHtrII, especially in space group $I2_12_12_1$. Thus, it means that the transducer opposes such structural rearrangements in the receptor. As this opposition leads to conformational changes in the transducer itself, it constitutes a signal transfer (in detail in [113]).

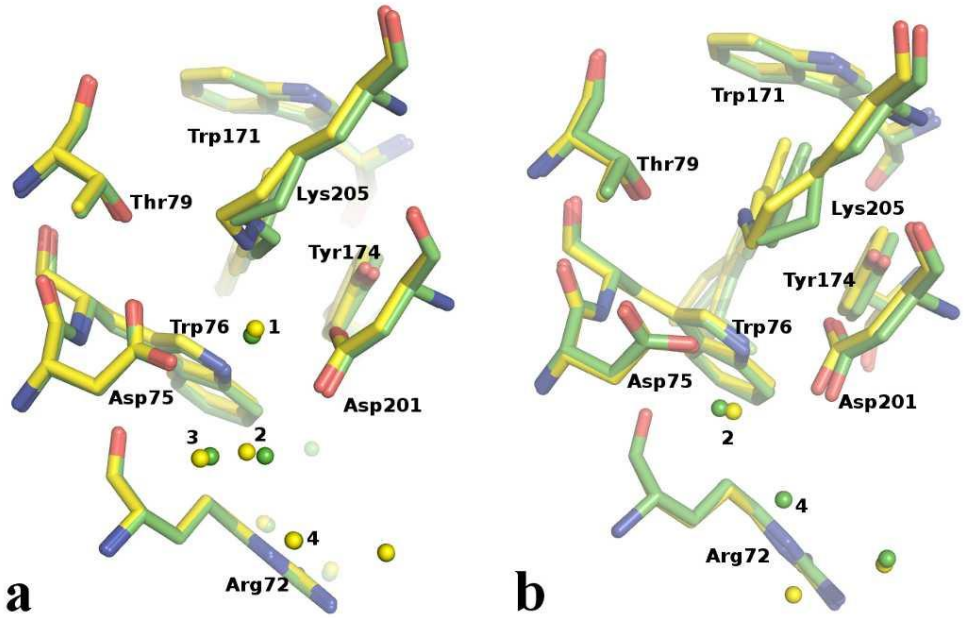

Figure 3.10 Structures of NpSRII active site. a) Structural differences between NpSRII ground state in I212121 space group (yellow) and in P21212 space group (green) and b) between NpSRII M state in I212121 space group (yellow) and in P21212 space group (green).

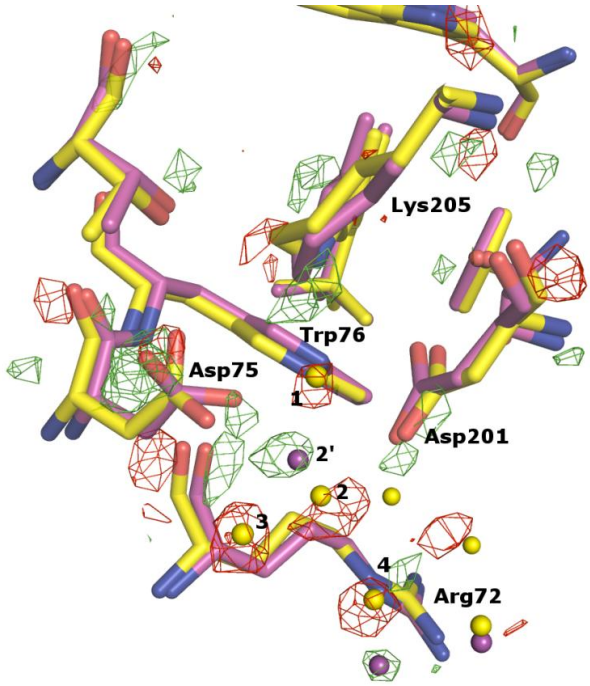

Figure 3.11 Structural differences between NpSRII ground state (yellow) and the M state intermediate (magenta) in the vicinity of the retinal Schiff base including water molecules, Lys205, Asp75, Asp201, Arg72, Thr79, Trp76, Trp171. Water molecules are depicted as spheres.

The structure of the M state is based on difference Fo-Fo Fourier maps, where the structure factor amplitudes are taken as difference between the amplitudes from the illuminated crystal and the ground state crystal, and the phases are calculated from the ground state structure. These maps reveal the rotation of Asp75 residue, displacement of water molecules and retinal isomerization.

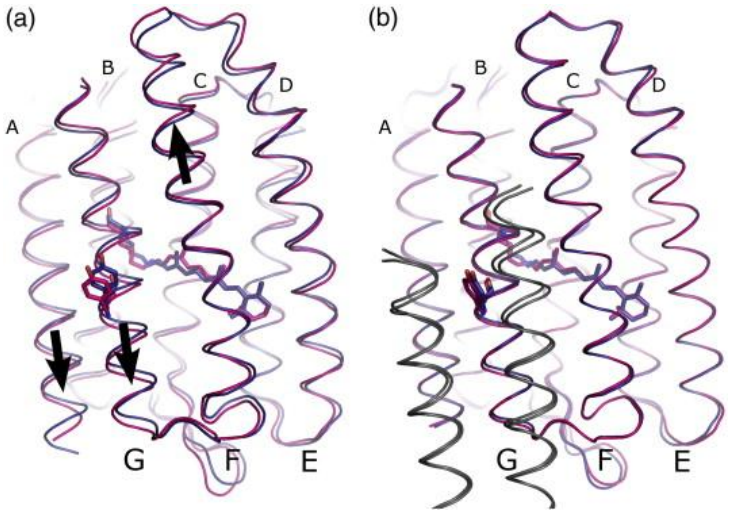

Figure 3.12 Overall structural rearrangements in NpSRII upon transition to the active state. (a) Structural rearrangements in uncomplexed NpSRII. (b) Structural rearrangements in NpSRII in complex with NpHtrII9 (Protein Data Bank ID: 2F95). The ground state is shown in blue, and the active state is shown in magenta. NpHtrII in (b) is shown in gray for both states. Lysine 205, retinal and tyrosine 199 are shown as ball-and-stick models. NpSRII helices are marked by corresponding letters (larger letters correspond to front helices and smaller letters correspond to back helices). Arrows show the movements of the corresponding helices. Alignment was performed by NpSRII backbone atoms. From [113].

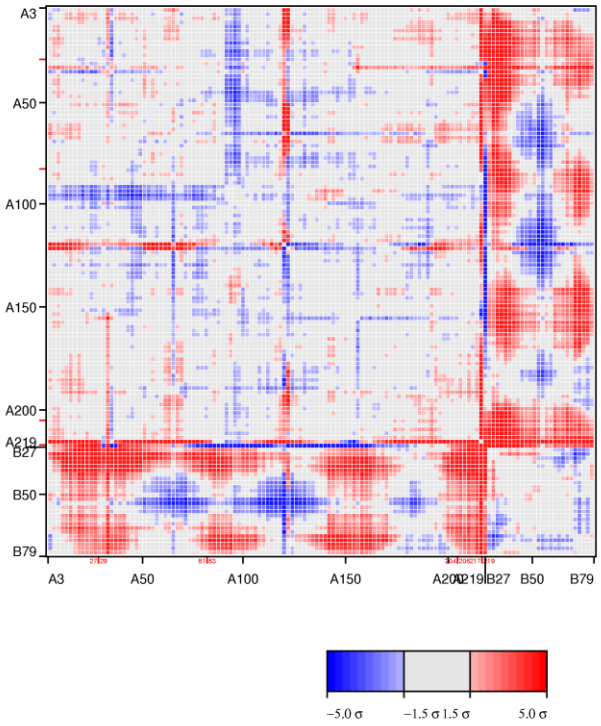

Figure 3.13 The double distance matrix plot showing differences between the ground state structure of the wild type complex and the M state structure in $I2_12_12_1$ space group. Chain A corresponds to SRII, chain B corresponds to HtrII.

The movement of the helix G of NpSRII initiates the movement of TM2 in NpHtrII. All hydrogen bonds between the receptor and the transducer observed for the ground state are still intact in the M state. A piston like movement of the cytoplasmic end of TM2 of about 0.5 Å and rotation of 19° (15° in $P2_12_12$) are observed and accompanied by alteration in the direction of Tyr199-Asn74 hydrogen bond.

The similarity of the differences between the ground and the M states in the new type of crystals shows an overall robustness of the signal transduction mechanism in the membrane part of the complex.

3.4. "U" and "V" shapes of the complex. Biological relevance

Having established that the fine structure of the complex in the two crystal forms is unperturbed, we analyzed the overall structures in the crystal lattices. It is evident from Figure 3.14 that the two receptors are oriented nearly parallel to the transducer and form a "U"-shaped structure in the new crystal form $I2_12_12_1$ comparing to the "V"-shaped structure with a crevice opened towards cytoplasmic side in the original $P2_12_12$ symmetry. The corresponding angles with helix G as base are 15° and 40°, respectively. These large differences might account for the altered HAMP domain-NpSRII binding interfaces. Probably due to crystal lattice interactions, electron density in this region is not available for both cases. However, the molecular dynamic calculation revealed interesting insights. Taking the known structures of HAMP domains [16,18,120] (PDB codes 1ASW and 3LNR) as base computer modeling indicates that only the "U"-shape structure facilitates an interaction of between NpSRII and the HAMP domain. The results show that the HAMP domain is turned by about 90º around the 2-fold axis of the dimer normal to the membrane with respect to the homology model (Figure 4). On the other hand, molecular dynamics calculations using "V"-shaped topology showed a hollow in between the HAMP domain and NpSRII, which leads to weaker interactions between these proteins.

"U" and "V" shaped conformations of SRII can be aligned by using the following orthogonal matrix (given by Coot):

```
|    0.9943,    0.1061, -0.003439|
|   -0.1059,    0.9892,   -0.1015|
| -0.007367,    0.1013,    0.9948|
```

The cosine of the angle is then given by (a1+b2+c3-1)/2 = (0.9943+0.9892+0.9948-1)/2 = 0,98915. This gives us an angle of 8.5°.

The surface of NpSRII reveals a unique group of charged and polar residues at the cytoplasmic ends of helix F (Lys-157, Ser-158, Arg-162, Arg-164 and Asn-165) and G (Asp-214) (Figure 4.7.2). For Ser-154 to Lys-157 an interaction with the transducer has been proven by ssNMR experiments [45]. From our model this patch of amino acids could interact with Asp85, Ser91, Asp115, Glu116 and Asp119 on TM2 via electrostatic interactions. Furthermore, Lys21 of TM1 and Asp214 of the helix G could form a salt bridge and might contribute to the overall stability of the complex conveyed by the HAMP domain-receptor interaction. It should be noted that these results on the "U"-shape of the complex explain well the spectroscopic data that shows that the EF loop interacts with the transducer [41,42,45].

Further evidence for the tight binding interface between the transducer and the receptor stems from calorimetric studies [43], solution NMR studies [44] and EPR experiments [14]. Thus, there is an ample experimental evidence for the tight interaction between SRII and the linker domain which is only possible in the "U"-shape assembly of the complex.

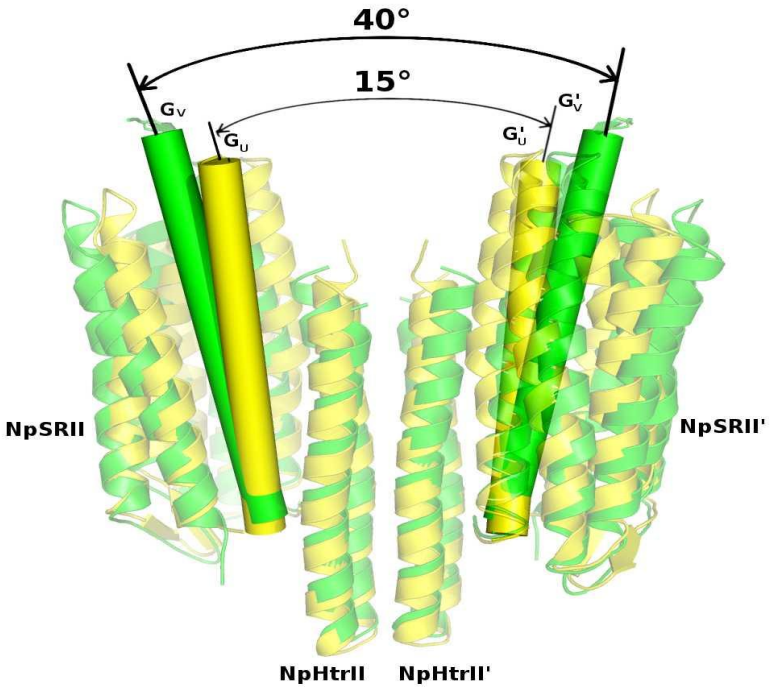

Figure 3.14 "V"- and "U"-shapes of the wild type dimer as seen along the membrane. Helices G are shown as cylinders. The angle is shown between two helices G belonging to different receptor molecules within a dimer. The structure solved in the $I2_12_12_1$ space group ("U"-shape, PDB ID 4GY6) is shown in yellow, the structure solved in the $P2_12_12$ space group ("V"-shape, PDB ID 1H2S) is shown in green. Primes denote symmetry mates.

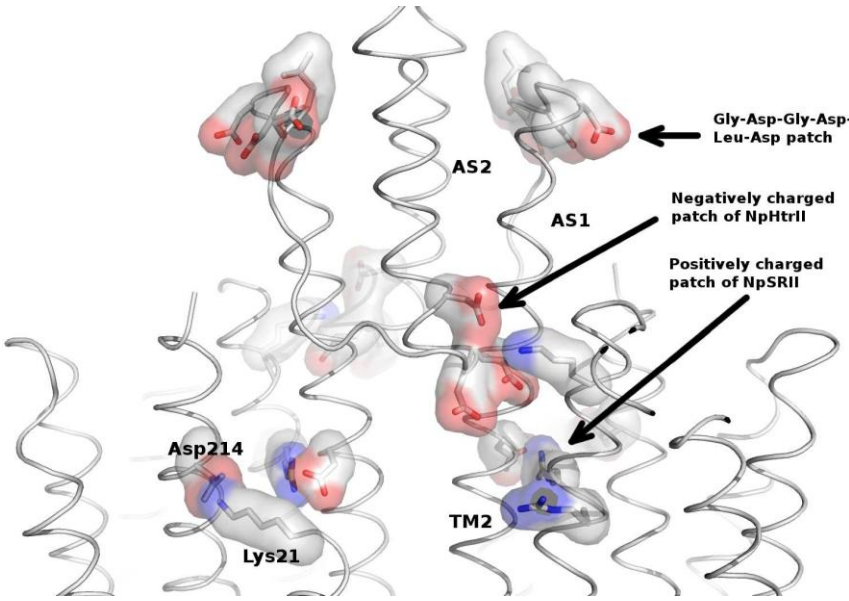

Figure 3.15 Electrostatic interactions between the receptor molecule and the HAMP domain. Interacting patches in the receptor and the transducer are shown and the G-D-G-D-L-D patch of the transducer proposed previously in literature as interacting with SRII. Positive charges are mapped in blue and negative are mapped in red. The expected salt bridges are: Asp214 (NpSRII) to Lys21 (NpHtrII), Lys157 (NpSRII) to Asp119 and Glu116 (NpHtrII).

Further evidence for the tight binding interface between the transducer and the receptor stems from calorimetric studies [43], solution NMR studies [44] and EPR experiments [14]. Thus, there is an ample experimental evidence for the tight interaction between SRII and the linker domain which is only possible in the "U"-shape assembly of the complex.

In contrast to the ground, in the M state the interaction between SRII and HtrII is considerably weakened (dissociation constants are 0.10 μM and 15 μM correspondingly) [121,122]. This effect can originate from a perturbation of the linker region but not from the membrane part of the proteins since interactions (especially, the hydrogen bonds interactions) are nearly the same in the both states. It is interesting that the HAMP domain itself ($NpHtrII^{G83\text{-}Q149}$) interacts with the receptor in the ground, but not in the M state. Since the "U"-shape provides quite constrained room for conformational changes of the HAMP domain; it may be that a transition from "U" to "V"-shape is involved in the signal propagation.

In accordance with the computer studies, the HAMP domain region itself corresponds to an asymmetric conformation [16]. It may happen that the "U"- and "V"–shaped complexes just correspond to symmetric ("U"-shape) and asymmetric ("V"–shaped) states of the HAMP domains and, therefore, correspond to different functional states (the ground and the active

ones). We suggest that the "U"-shape corresponds to a symmetric state where the HAMP domain is stabilized in the rotated confirmation via the aforementioned electrostatic interactions with the receptor. The HAMP domain turns by about 90º around the 2-fold axes which is made possible by a high flexibility of the linker between the TM2, especially to the presence of Gly83-Gly84 of the amino acid repeat. This hypothesis is supported by one more well established fact: the G83F mutation completely inhibits signal transduction [70]. Indeed, replacing a small glycine by a considerably larger phenylalanine would limit the ability of the HAMP domain to rotate relative to the membrane part of the transducer and therefore the ground state is forbidden. In line with this reasoning are the data on the crystal structure of the NpSRII/NpHtrII$_{1\text{-}135}$-G83F. Although, the crystallization conditions were the same as for the wild type "U"-shaped complex in the $P6_4$ space group, in this case the space group was $P2_12_12$ giving the "V"-shape structure similar to those observed before [7].

Further evidence in favor of functional significance of the "U"-shaped membrane protein NpSRII/NpHtrII complex was published recently [123]. The authors studied how photoexcitation of SRII affects the structures of the complex. They conducted two series of 90 nsec molecular dynamics simulations of the complex linked with a modeled HAMP domain in the lipid bilayer using published "V"-shaped structures of the ground and the M intermediate states [6,7] as starting models. The most significant finding was that the orientations of the two SRII molecules changed in going from the ground state to the M state: Their 'closed' ground state can be correlated to our "U"-shaped topology, whereas their more flexible M state might represent the "V"-shape introduced in this paper.

If we try to compare the energy of a photon with that necessary for "U"-to-"V" transition, we will see that is sufficient to trigger such changes. The estimation is based on the paper by C. Nielsen *et al* [124]. The Table 5 of this paper indicates the free energy of the hydrophobic mismatch for a protein with a radius of 15 Å. According to this table, the 3.4 Å mismatch corresponds to the free energy of 15 kT. Taking into account the size of SRII and the change in the tilt angle of 10° we assume that in our case the membrane mismatch is about 1 Å. Therefore, in our case $\Delta G = 15kT \times (1/3.4)^2 \times 2$ (for two proteins in one complex) = 2.6 kT. Worth noting that in reality ΔG will be smaller as we deal with a tilt movement and not a uniform spring-like deformation. The energy of the photon is about 100 kT but about 80% is thermally dissipated in protein. Nevertheless, the rest 20 kT of energy is sufficient to trigger such conformational changes.

Summarizing, the “U”- and “V”-shaped structures of the NpSRII/NpHtrII complex may be crucial for the mechanism of signal propagation spanning the membrane domain and feeding into the HAMP domain. This work represents the first evidence that different space groups might freeze different functional states of proteins. It is therefore of a great importance not only to analyze distinct structural differences but also to take the overall crystal packing and quaternary structures into account.

3.5. Structure of the signal transferring triple mutant of bacteriorhodopsin in complex with HtrII

Bacteriorhodopsin is a proton pump from archaea, highly homologous to SRII [125]. Its main function is production of charge gradient by means of proton translocation across the membrane. This gradient is in turn used by ATP synthases for ATP production. Bacteriorhodopsin’s structure and mechanism of functioning are well studied [125–127] and the best X-ray structures have resolution of 1.4 Å [126].

Despite of the high structural similarity between archaeal retinal proteins (SRI, SRII, BR. HR), their functions are totally different. Recently it was shown that three residues in BR replaced by the corresponding residues in SRII allow BR to effectively deliver the retinal photoisomerization signal to the SRII integral membrane transducer (HtrII) and induce robust phototaxis responses. A single replacement (Ala-215–Thr), bridging the retinal and the membrane-embedded surface, confers weak phototaxis signaling activity, and the additional two (surface substitutions Pro-200–Thr and Val-210–Tyr), expected to align bacteriorhodopsin and HtrII in similar juxtaposition as SRII and HtrII, greatly enhance the signaling [128].

In order to give structural insights on the mechanism of signal transduction from this triple mutant of BR (BR-3M) to HtrII the mutant construct of BR was created; the protein was expressed, purified, reconstituted into polar lipids together with HtrII and crystallized in mesophases. Detergent OG was used to change the parameters of mesophase with MO like a host lipid. MO/protein ratio (3:2) remained constant for all experiments, protein concentrations (as calculated for the BR-3M/HtrII) was varied as 25 and 35 mg/ml. Detergent concentration was varied from 1 to 5 % per MO (w/v). It should be mentioned that the complex of BR triple mutant and NpHtrII can only bear not very high detergent concentrations. Thus, for crystallizations with higher OG per MO concentrations (w/v) hexagonal crystals were formed but, as followed X-ray analysis demonstrated, they were not

the crystals of the complex but single BR. It can be explained as BR-3M/NpHtrII complex was dissociated by high amounts of OG [129].

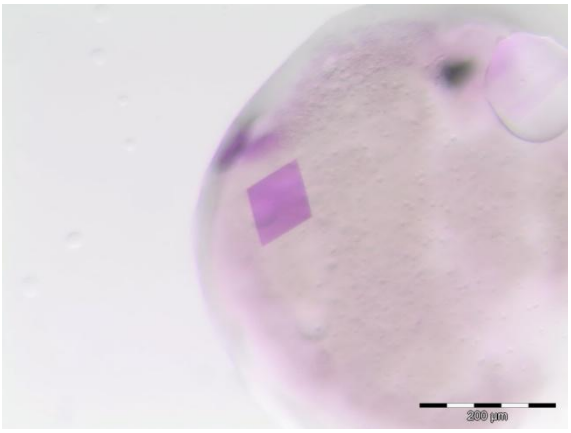

Figure 3.16 Rhombic crystals of proteins complex BR-3M/NpHtrII grown from mesophases with addition of OG. First crystals appeared after 1 month and diffracted to 3 Å. Crystals belong to space group $P2_12_12$ with unit cells parameters: a = 54.9, b = 88.6, c = 130.1 Å, α = 90º, β = 90º, γ = 90º.

Rhombic crystals of proteins complex were obtained by nanovolume crystallization from mesophases with OG and MO (w/v) in the presence of high concentration ammonium phosphate as a precipitant (2.4 – 2.8 M). For mesophase contained less amount of detergent crystals were grown to the size 20 – 30 µm, whereas for higher OG percentages per MO (w/v) crystals reached 100 µm in diagonal (Figure 3.16). The significant improvement of crystals size and quality in answer to increase the detergent concentration is understandable in terms of paradigm of crystallization from mesophases [129].

First crystals appeared after 1 month and diffracted to 3 Å. Crystals belong to space group $P2_12_12$ with unit cells parameters: a = 54.9, b = 88.6, c = 130.1 Å, α = 90º, β = 90º, γ = 90º. The asymmetric unit contains 2 complexes of BR-3M and HtrII.

BR and HtrII models were used for initial phase determination by molecular replacement. Only the membrane inserted part of the complex could be resolved in the electron density. The similar situation is observed in the case of SRII/HtrII complex. The electron densities after Leu82 of HtrII are very poor and the HAMP domain still couldn't be built.

A very interesting result was obtained while looking at the respective orientation of BR-3M and HtrII (Figure 3.17). As one can see, one transducer molecule forms a complex with BR-3M along the surface of F and G helices as it was expected from SRII/HtrII complex structure. Meanwhile, another HtrII molecule forms a complex with BR-3M along the surface of E and F helices that is much unexpected. This finding is the first evidence of two possible

binding schemes between BR and HtrII. Obviously, the preference for F-G helix surface is much stronger in case of SRII.

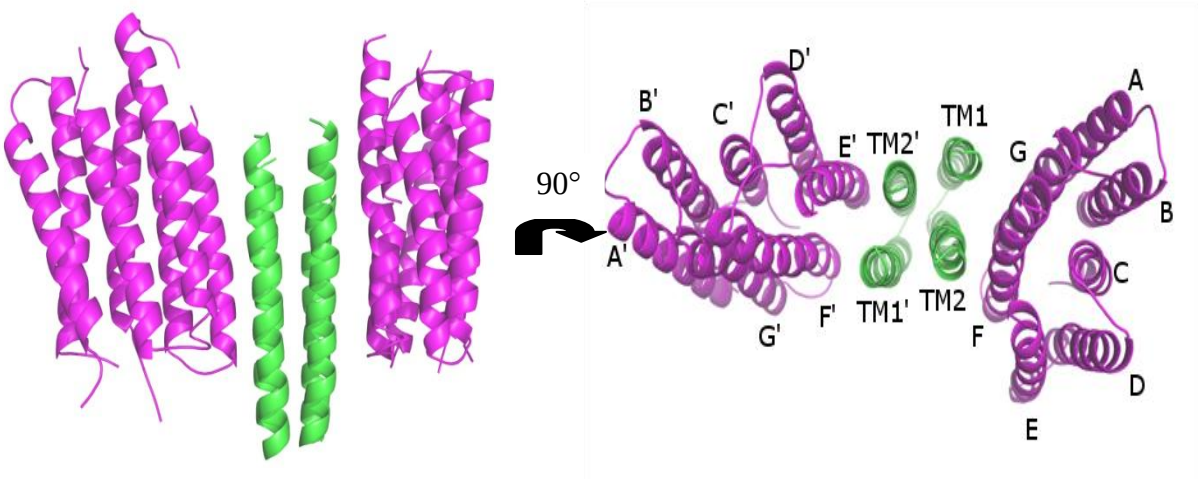

Figure 3.17 Structure of the BR-3M/HtrII complex. Left: view along the membrane plane; right: view perpendicular to the membrane plane. BR-3M is shown in purple, HtrII is shown in green.

3.6. Expression, purification and crystallization of truncated parts of HtrII

The geometrical parameters of SRII/HtrII complex do not allow crystallization of the complex in its native form. The transducer protein length in the direction perpendicular to the membrane is about 200 Å that is far beyond cubic phase possible lattice constants. Therefore, for crystallization purposes the HtrII construct was split into the membrane and water-soluble parts. Then, the membrane part was reconstituted into polar lipids together with SRII and crystallized using mesophases. Cytoplasmic part, which contains 2 HAMP domains, adaptation domain and kinase domain, was split into several parts taking into account predictions for domain boundaries and set up for crystallization separately, using approaches for water-soluble proteins. In this chapter constructs containing cytoplasmic parts of HtrII will be discussed.

The following constructs were created using different expression vectors: HtrII-1-135, HtrII-83-210, HtrII-83-157, HtrII-83-135 and HtrII-83-534. The first construct contains transmembrane part and the first HAMP domain. It was crystallized *in meso* in complex with SRII (see above). Four other constructs comprise water-soluble parts of HtrII: “HAMP1” + “inter-HAMP linker” + “HAMP2”, “HAMP1” + “inter-HAMP linker”, “HAMP1”, “HAMP1” + “inter-HAMP linker” + “HAMP2” + “methylation domain” + “kinase domain” respectively (Figure 3.18).

HtrII-83-534 gene was synthesized by MWG Company. Other constructs were derived from this DNA matrix by PCR. HtrII-83-135 and HtrII-83-157 were inserted into pTYB12 vector. The vector was transformed into BL21 Star expression strain. The expression was performed in auto-induction medium overnight at 37° C. The cells were harvested by centrifugation at 4500 RPM, 4° C for 30 min. Cell pellets were dissolved in cell buffer (see Methods and Materials section) and disrupted in a microfluidizer. After breaking, the cell debris were centrifugated again at 35 000 RPM, 4° C for 1 h, and the pellet was discarded. Soluble fractions were loaded on chitin beads column and the binding was performed overnight at RT. Intein cleavage and subsequent elution were induced by adding the buffer containing 40 mM DTT. Elution fractions contained considerable amount of precursor protein (target protein + intein) and intein itself (Figure 3.19). In order to get pure target protein either of the two strategies was applied: 1) size-exclusion chromatography 2) additional run through the chitin beads, were additives containing intein were bound to the resin. First method gave better result though it is more time consuming. The letter is straightforward and high-throughput but occasionally leads to the loss of considerable amounts of protein.

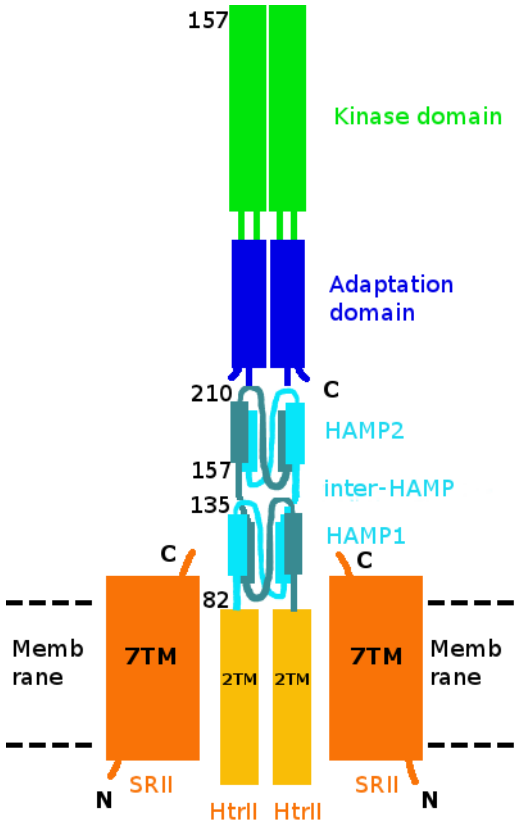

Figure 3.18 For crystallization purposes HtrII was split into several parts. Membrane part (containing residues 1-135 or 1-157) was crystallized in complex with SRII and has yielded crystals diffracting up to 1.7 Å. Cytoplasmic water-soluble part of HtrII was truncated between domain boundaries and different domains were expressed separately. The following constructs were made:

1. HtrII-1-135 (membrane + HAMP1)

2. HtrII-83-210 (HAMP1 + inter-HAMP-linker + HAMP2)

3. HtrII-83-157 (HAMP1 + inter-HAMP-linker)

4. HtrII-83-135 (HAMP1)

5. HtrII-83-534 (HAMP1 + inter-HAMP linker + HAMP2 + methylation domain + kinase domain)

Unfortunately, stability tests have shown that the both constructs containing only HAMP1 are not stable enough to be used for crystallization. The protein degrades quickly during storage at 4° C and after several freeze/thaw cycles. Nevertheless, some preliminary crystallization screening was performed but no crystals were obtained.

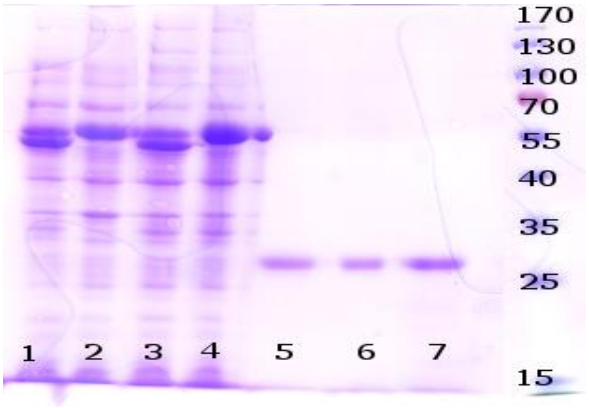

Figure 3.19 Expression of HtrII-83-135 in auto-induction medium.
1,3. Crude lysates in BL21 (DE3) and Lemo21 cells
2,4. Solubilized membrane fraction
5,6,7. Elution fractions

HtrII-83-210 and HtrII-83-534 were inserted into vector pStaby1.2. This vector was chosen as it has a specific plasmid stabilization system. In the StabyExpress system, the antidote gene (ccdA) is inserted into the plasmid DNA under the control of a constitutive promoter. On the other hand, the toxic gene (ccdB) is inserted in the chromosome of the SE1 bacterial strain. Expression of the poison gene is under the control of a promoter strongly repressed in the presence of the plasmid. When the plasmid is lost, the antidote is degraded and the production of the toxin is induced, causing cell death. Practically, this means that when during the pre-induction phase bacteria are grown, 100% of the bacteria will carry the vector. If they lose the vector, they will not obtain a growth advantage, but will die. Upon induction 100% of the bacteria will start producing the recombinant protein leading to higher yields of the target protein and less background caused by unwanted proteins (for details see StabyExpress Manual, Eurogenetec).

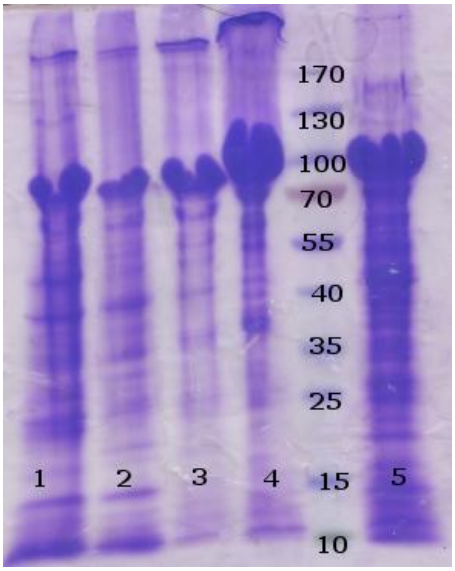

Figure 3.20 Purification of HtrII-83-534 under denaturing conditions.
1.Control in native conditions (300mM NaCl, 20 mM Tris pH8.3)
2. Control + 6M urea
3.Control + 6M GuHCl
4. Control + 6M GuHCl + 0.1% Tween20
5.Protein solution before purification

HtrII-83-210 and HtrII-83-534 were expressed in auto-induction medium ZYP-5052. In order to avoid formation of inclusion bodies and ensure proper protein folding, the cells were grown at 37° C until all glucose was consumed and induction by lactose was started. Typically, that corresponds to OD=2 and 3 hours of broth incubation. The cells were

harvested and disrupted in the same manner as for other constructs (see above). Target proteins were bound to Ni-NTA resin after incubation for 2 hours in the cold room. Subsequent washing of the resin and elution by 200 mM Imidazole solution were performed using ÄKTA Prime purification system.

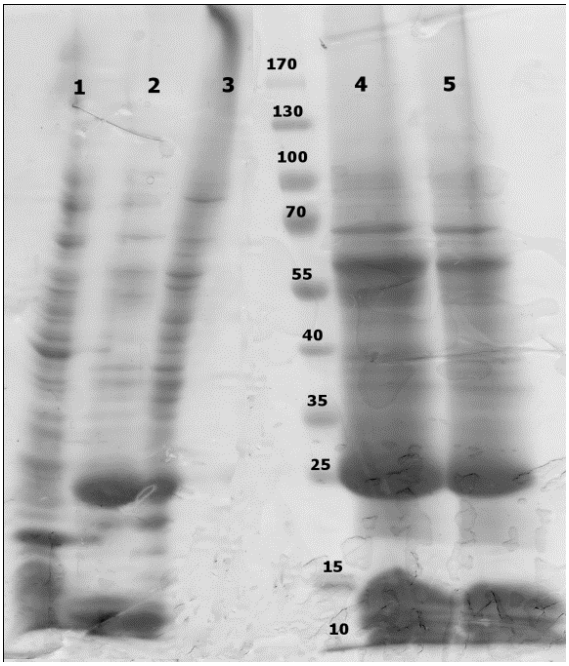

Figure 3.21 Purification of HtrII-83-210 and HtrII-1-135
1. Crude lysate HtrII-83-210
2.Protein HtrII-83-210 resolubilized after precipitation in ammonium sulfate
3.Insoluble pellet of HtrII-83-210 after precipitation in ammonium sulfate
4-5. HtrII-1-135 after purification of chitin beads.

While in case of HtrII-83-210 purification resulted into pure protein suitable for crystallization (Figure 3.21 represents PAGE gel of Ni-NTA purification), HtrII-83-534 couldn't be produced in unambiguously pure form. Elution fractions from Ni-NTA column contained major band corresponding to the protein of interest and a lot of impurities of different molecular weight. Additional analysis was performed in order to purify the protein under denaturing conditions (see Figure 3.20). As we can see, denaturing conditions indeed lead to more pure protein.

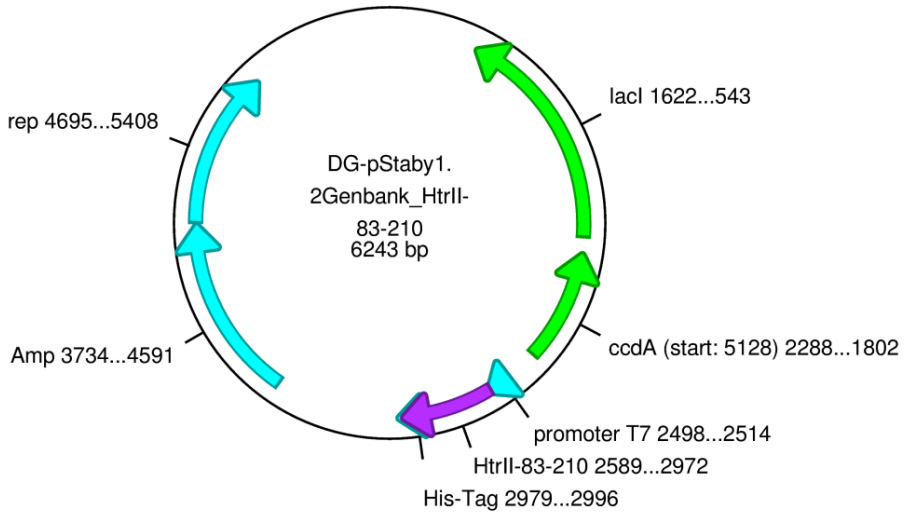

Figure 3.22 Plasmid map bearing HtrII-83-210. The construct was inserted into pStaby1.2 vector by NdeI and

XhoI restriction sites.

Additional purification of HtrII-83-534 was done using size-exclusion chromatography using Superose 6pg matrix on the column XK 16/100. The gel filtration was performed at 4°C. The major elution peak is positioned at 139.9 ml corresponds to K_d of the protein of interest. Unfortunately, PAGE analysis has shown that there was no good separation between target protein and other proteins in solution (Figure 3.23). Obviously, the protein runs as a complex together with side products or products of its own degradation. In overall, this construct turned out to be not suitable for crystallization experiments.

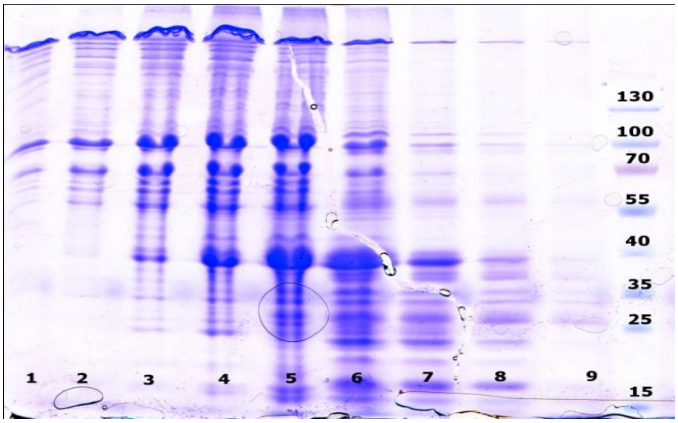

Figure 3.23 PAGE gel of SEC elution of HtrII-83-524 construct
Lanes 1-9 show serial elution fractions

For crystallization screening HtrII-83-210 was concentrated in a centrifugal membrane concentrator (MWCO 10 KDa) to the concentration of 15 mg/ml and submitted for crystallization to HTXLab in EMBL Grenoble. The crystallization was done as a sitting drop. Each trial contained 50 nl of protein solution mixed with 800 µl of mother solution. Crystallization was set up at 20°C. The following kits were used: Crystal Screen Lite & PEG/Ion; QuickScreen & Grid screens Ammonium Sulfate, Sodium Malonate - Sodium Formate; Grid screens PEG 6K, PEG/LiCl, MPD - Screen Mme (all from Hampton) and The Classics (from Qiagen). Unfortunately, neither of crystallization conditions yielded any crystals. A lot of trials contained precipitate that is an indication of poor protein stability.

The molecular constructs of the cytoplasmic parts HtrII could be expressed in high yield. Nevertheless, they turned out to be difficult to purify and to keep in a stable water-soluble state. Apparently, the conditions of the standard molecular biology buffers differ a lot from the environmental conditions of the cytoplasm in halobacteria. The amino acid composition of HtrII might have evolved to adapt to these conditions. This fact leads to the aforementioned problems. In turn, buffers with high ionic strength are not comparable with most methods of protein purification. Nevertheless, as the buffer conditions of the crystallization trial tend to the high molarity of the precipitant salt in course of crystallization,

at some point these conditions might become suitable for proper folding of the protein. These crystallization experiments are ongoing.

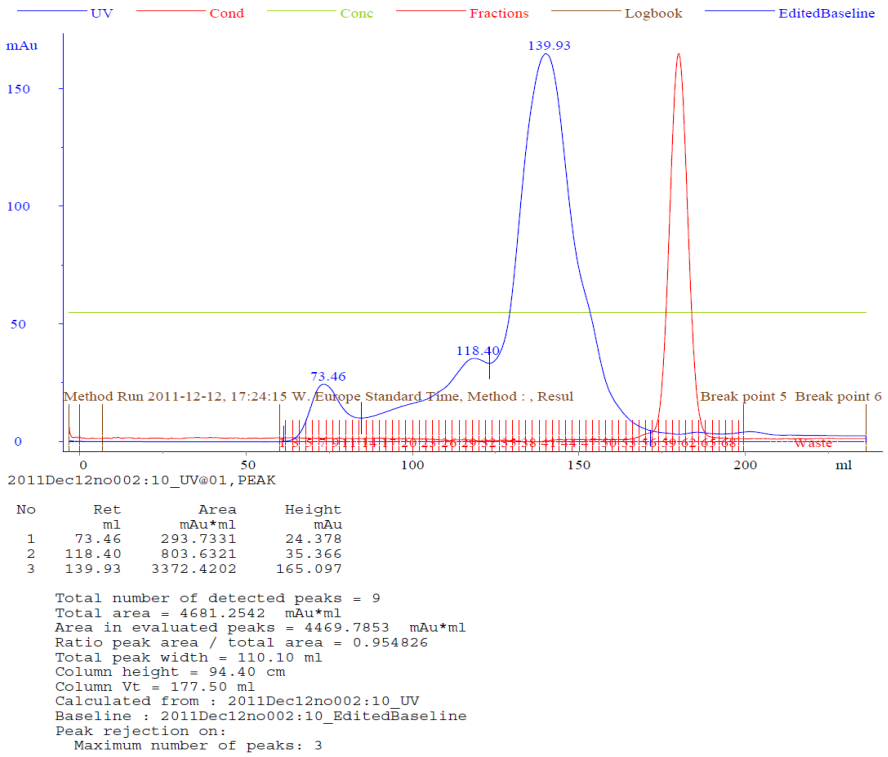

Figure 3.24 Elution profile of HtrII-83-534 construct purified using size-exclusion chromatography on column Superose 6PG, total volume 180 ml.

3.7. The structure of SRII in complex with HtrII-135 and G83F mutation of HtrII-135

Since the SRII/HtrII-157 construct didn't result into any reasonable electron densities in the HAMP domain area, it was decided to make molecular constructs of HtrII that could tackle with possible problems that led to the HAMP domain instability in crystals. One of these reasons could be the fact that HtrII-157 doesn't fit into water channel on the cubic phase. If we try to model the HAMP domain into the obtained structure of the complex we see that it only fits when being truncated after amino acid 135 (Figure 3.25). Therefore, any additional amino acids after position 135 would be unsuitable for proper HAMP domain folding. Moreover, only the space group $I2_12_12_1$ has cavity in this area big enough to accommodate the domain (Figure 3.26). In this sense $P2_12_12$ is much less favorable as in this space group HtrII molecules in a crystal are placed one under another in the neighboring layers thereby excluding space for the HAMP domain.

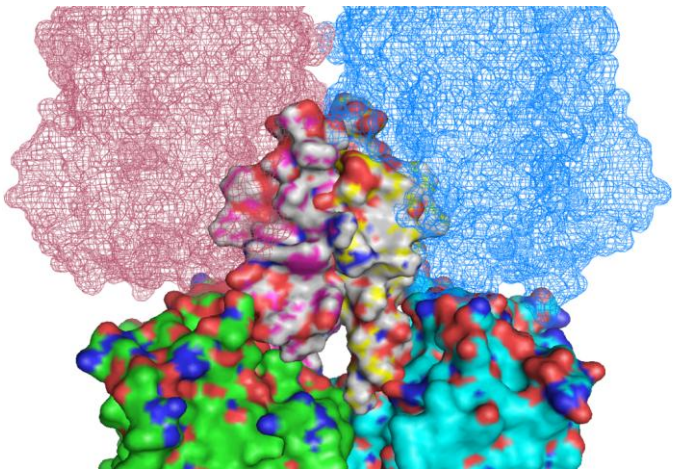

Figure 3.25 Space for the HAMP domain in $I2_12_12_1$ crystal lattice. The αββα homodimer of SRII/HtrII membrane part is shown as green and marine surface, HAMP dimer is shown as white surface and the complex in the next crystal layer is shown as red and blue mesh. The HAMP domain has some steric clashes

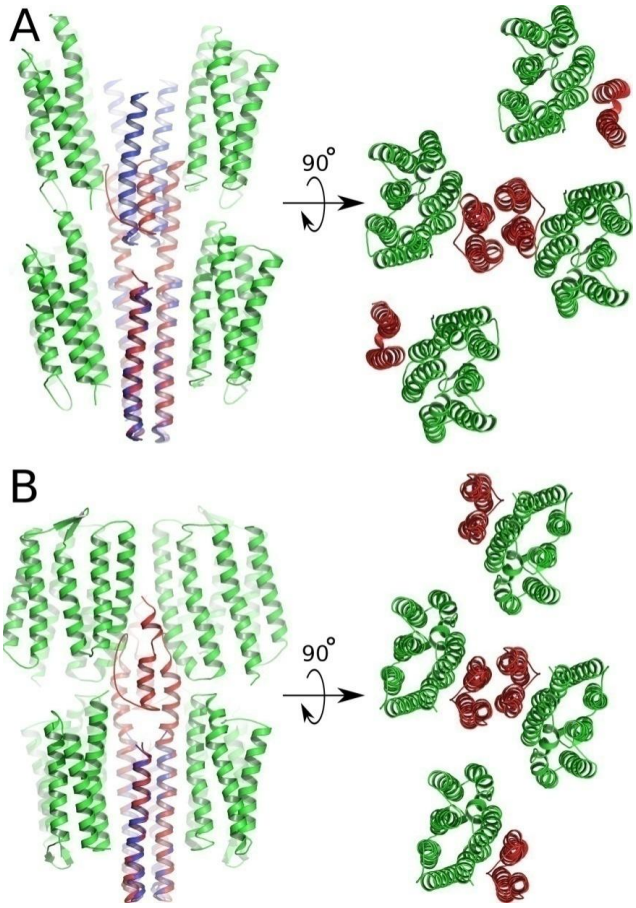

***Figure 3.26** a) "V"-shaped NpSRII/NpHtrII complex in P21212 space group. b) "U"-shaped NpSRII/NpHtrII complex in I212121 space group. Figures on the left show two subsequent crystal layers as seen along the membrane plane. Figures on the right show a single crystal layer as seen perpendicular to the membrane plane. NpSRII molecules are shown in green; parts of NpHtrII molecules resolved in the crystal structure are shown in blue. Models of NpHtrII that continue to the HAMP domain are shown in red. Residues 83-136 in these models are modeled by homology with NMR structure 2ASW. In a) a big steric clash can be seen between the model of the HAMP domain from one crystal layer and the corresponding NpHtrII molecule*

from the other crystal layer. There are no observed steric clashes between the model of the HAMP domain from one layer and NpSRII/NpHtrII molecules from the other layer in b) (Figure provided by S. Grudinin).

The pTXB1 plasmid with HtrII-1-135 gene was kindly provided by Prof. Engelhard (MPI Dortmund). Expression was performed according to the standard protocol of IMPACT kit (see Methods and Materials section). The protein was eluted by addition of 200 mM Mesna to the elution buffer and incubation for 1 day at room temperature. It was determined that elution at lower temperature or shorter incubation times is ineffective, and a lot of protein remains bound to the chitin beads. Mesna was removed by dialysis against 300 mM NaCl, 20 mM Tris and 0.1% DDM pH8 buffer. PAGE analysis showed that elution fractions may contain a lot of target protein bound to Intein or Intein alone (Figure 3.27). For additional purification of the target protein it was applied to the chitin column one more time. In this case Intein-containing impurities were bound to the resin while the target protein could be collected in the flow through. As a final step of purification, the reconstitution into polar lipids and buffer exchange has helped to remove any water soluble contaminants.

For crystallization the SRII/HtrII complex was reconstituted into the polar lipids of purple membranes. To do that, equal amounts of protein and lipids (wt/wt) were mixed with biobeads (approx. 30% of volume) and left on shaker overnight. After reconstitution the protein was concentrated by centrifugation to 30 mg/ml and mixed with equal amount of MO. The cubic phase was formed after 1 day and then dispensed using Formulatrix NT8 robot and kits from Hampton and Qiagen. First crystals appeared after 2-3 weeks and continued to grow for 3-4 months. The largest crystals exceeded 200 Å in size and diffracted to 2 Å.

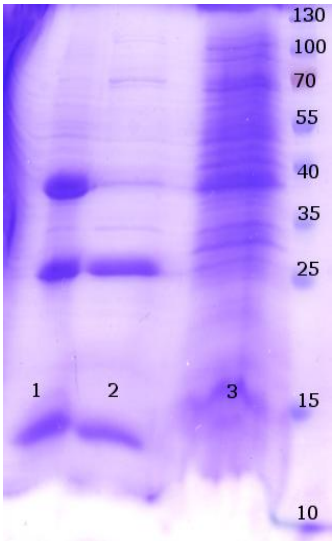

Figure 3.27 Expression of HtrII-135
Lane1: Chitin beads after elution
Lane 2: Eluted protein
Lane3: Flow through

The structure was solved in $P6_4$ space group. In this space group twinning is possible but it was detected to be on negligible level (about 5%). All the features of previously solved structures remained the same including the structure of the active site and the "U"-shape.

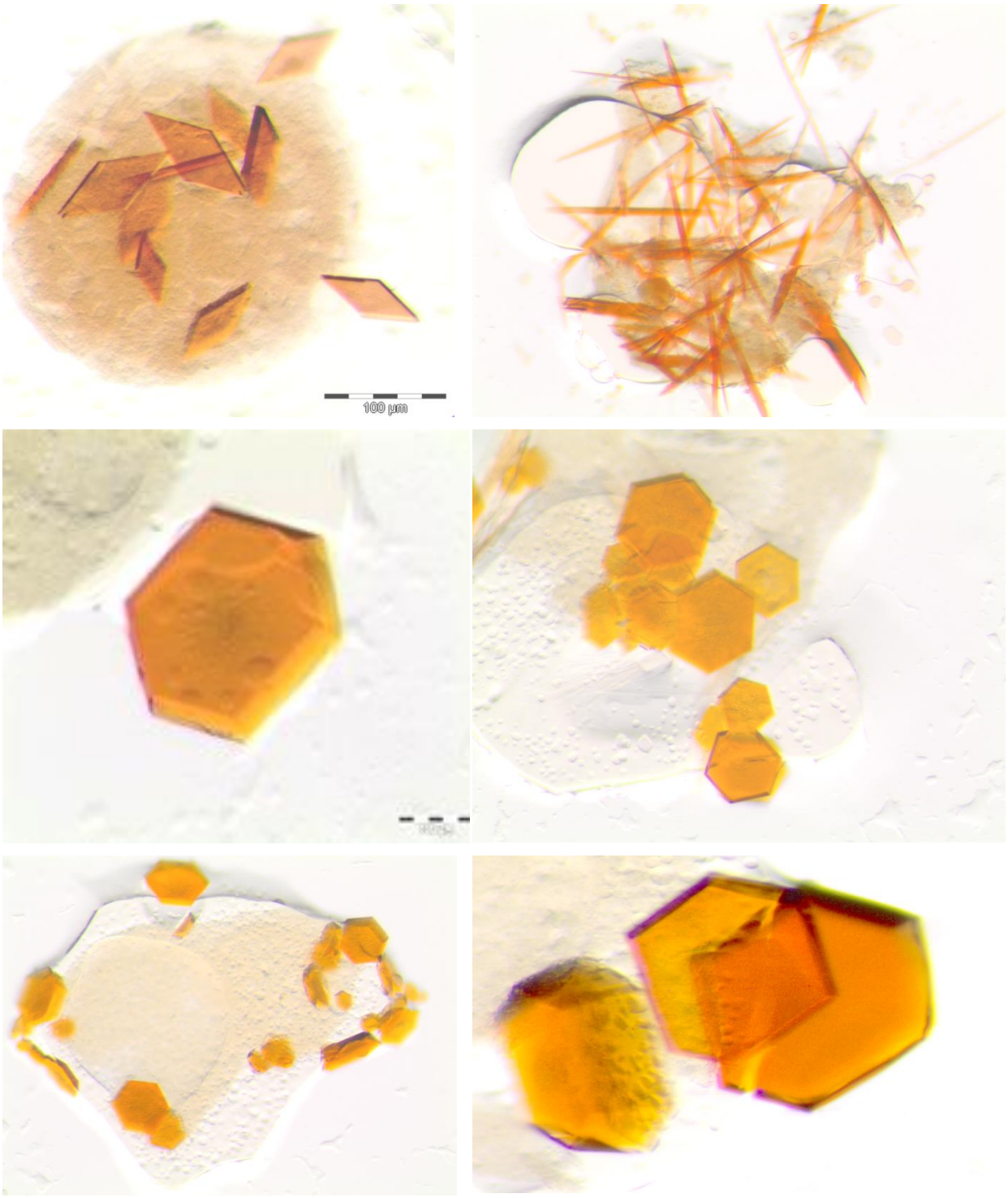

Figure 3.28 Different crystal forms of SRII/HtrII-135 complex. Hexagonal, rhombic and needle-like crystals were observed. The best crystals were obtained in the conditions were ammonium sulfate was used as a

precipitant. The pH range varies from 5 to 8.5. Typically, hexagonal crystals were of the best quality comparing to other types. The resolution of the datasets from plate-like and rhombic crystals was marginal.

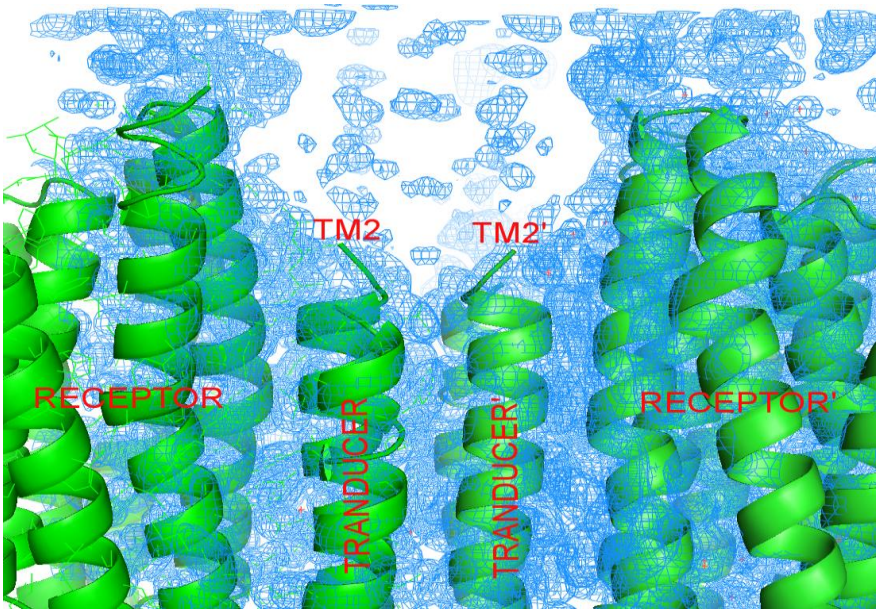

Figure 3.29 Electron density in the HAMP domain area in the crystals of SRII/HtrII-135 complex in $P6_4$ space group contoured at σ=1.0. The structure of TM2 ends with Gly84.

Unfortunately, the new crystal form also didn't provide any information about the structure of the HAMP domain. Since further truncation of HtrII was not possible without disturbing native HAMP1 domain structure that ends at amino acid residue number 135, other strategies had to be implemented.

As it was mentioned before, two glycines in HtrII just before the HAMP domain sequence may result into domain's flexibility. Moreover, it is known that G83F mutation impairs signal transduction.

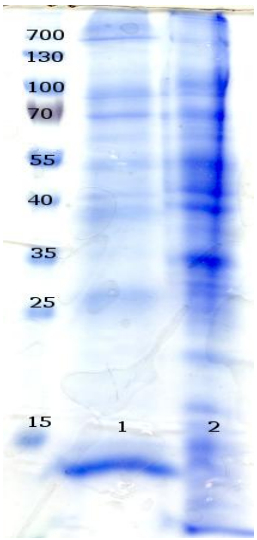

Figure 3.30 Expression of HtrII-135-G83F
1. Elution fraction of HtrII-135-G83F after addition of 40 mM DTT
2. Flow through

The G83F mutant of HtrII-135 molecular construct was designed, the mutation was introduced using conventional PCR method. Crystallization was performed using the same

procedure as for wild type complex. The optimal concentration of the protein was chosen to be 20-30 mg/ml as for the wild type HtrII. Two types of crystals were observed: hexagonal and needle-like crystals. Crystal growth took 1-2 months. Hexagonal crystals of the complex NpSRII/NpHtrII-G83F appeared at the similar conditions as the crystals of wild type complex – precipitant 1.4 M Ammonium sulfate, pH 5.2-8.2. Needle-like crystals were obtained in crystallization probes with 2.2-2.8 M Ammonium phosphate as a precipitant, pH 7.0-7.6. Crystals were harvested from LCP-sandwich and used for X-ray data collection. The crystals of NpSRII/NpHtrII-G83F from nanovolume crystallization from mesophases diffracted to 2.7-3.0 Å resolution.

Though, crystals appeared in the same crystallization conditions, they belonged to $P2_12_12_1$ space group and contained two molecules in the asymmetric unit. Surprisingly, in this case the quaternary structure appeared as "V"-shape. This is an indication of importance of the mutation for the structure of the complex. Nevertheless, the electron densities still didn't allow building the structure of the HAMP domain.

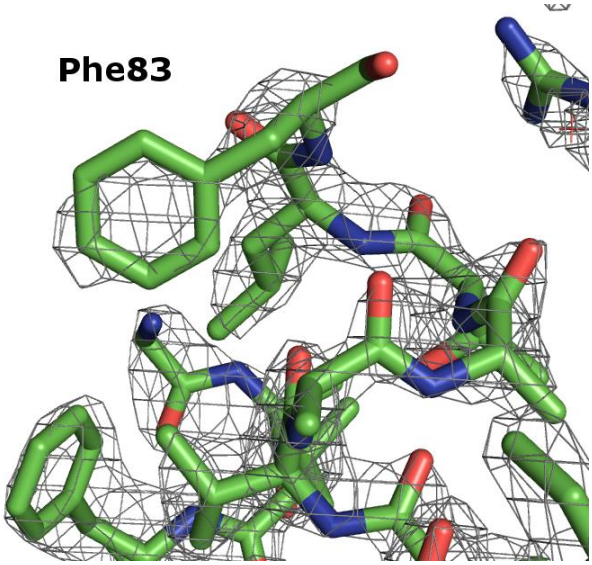

Figure 3.31 Electron densities in the C-terminus of HtrII. Gly83 was mutated to Phe83.

The "V"-shape structure of the complex may represent some of the intermediate states (see Chapter 3.4). Taking this into account the new finding makes sense. It is known that G83F somehow disturbs the signal transduction mechanism in the SRII/HtrII complex. The reason for that could be that the proteins get fixed in a constitutive signaling state and, consequently, get crystallized in that state thereby forming the "V"-shape quaternary structure.

3.8. Expression, purification, characterization and crystallization of chemoreceptors NarQ and NarX

In order to get an insight on the initial steps of signal transduction in chemoreceptors, the membrane domains of nitrate/nitrite sensing proteins NarQ and NarX were expressed, purified and crystallized. As *in meso* crystallization method implies restrictions in the size of the protein perpendicular to the membrane and in order to reduce possible thermal fluctuations, the molecular construct that was expressed contained only amino acid range 1-231 in case of NarQ and 1-225 in case of NarX. These ranges comprise the extracellular sensory part, transmembrane domains and the intracellular HAMP domains. The genes were taken by PCR from a single colony of *E.coli* BL21 strain using following pairs of primers: AGACATTGCTGACTGTTGGCCATAATAAAA and GGTGCCACTGCTCTGAGATGACATATAC (NarQ); GATAAGCTGTTTTACGCCAGTTCGCAGCATC and GTATACTTCAGCCAATAGCCGAGAATACTGCCATT (NarX). After genes were extracted from the genome, they were cloned into pStaby1.2 expression vector. To do that an addition PCR was performed that introduced NdeI and XhoI restriction sites. Plasmid with the gene was transformed into SE1 strain that was used for expression.

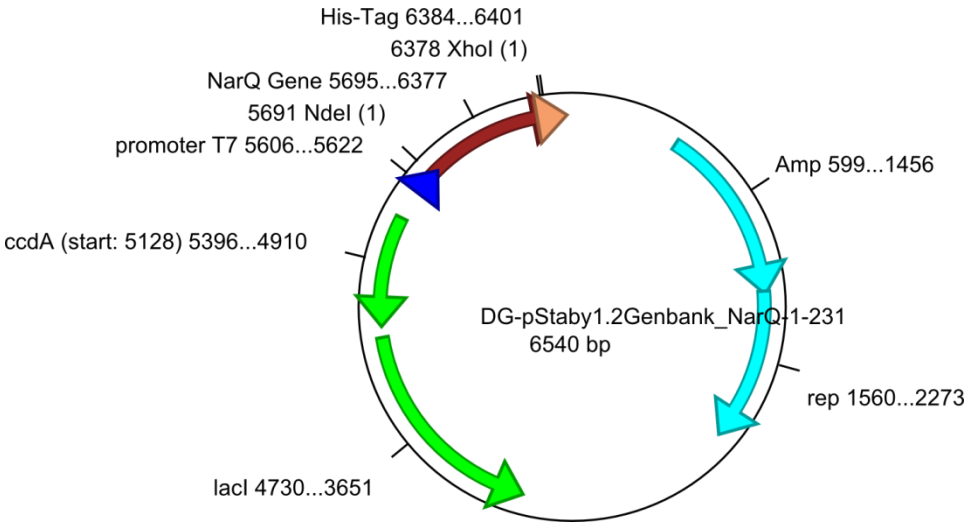

Figure 3.32 Plasmid map of the construct NarQ-1-231. The gene fragment was inserted by NdeI and XhoI restriction sites. Plasmid possesses anti-ampicillin resistance gene and special plasmid stabilization gene (ccdA).

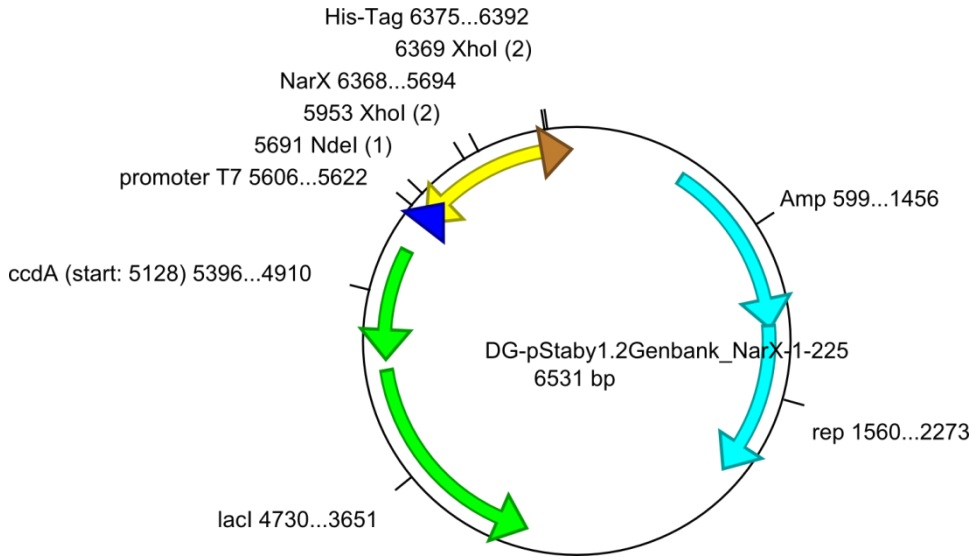

Figure 3.33 Plasmid map of the construct NarX-1-225. The gene fragment was inserted by NdeI and XhoI restriction sites. Plasmid possesses anti-ampicillin resistance gene and special plasmid stabilization gene (ccdA).

NarQ and NarX proteins were expressed using auto-induction medium developed by William Studier and colleagues [130]. Among all available auto-induction medium protocols the ZYP-5052 medium was chosen. The medium composition is as follows:

ZY: 1% tryptone, 0.5% yeast extract, autoclaved

20xNPS: 1M Na_2HPO_4, 1M K_2HPO_4, 500 mM $(NH_4)_2SO_4$, autoclaved

50 x 5052: 25% glycerol, 2.5% glucose, 10% alpha-lactose monohydrate, sterile filtered

1000X trace metals: 50mM $FeCl_3$, 20mM $CaCl_2$, 10mM $MnCl_2$, 10mM $ZnSO_4$, 2mM $CoCl_2$, 2mM $CuCl_2$, 2mM $NiCl_2$, 2mM Na_2MoO_4, 2mM H_3BO_3, Made in 60mM HCl, autoclaved

$MgSO_4$ 2 mM, autoclaved

In order to get ZYP-5052 928 ml ZY was added to 50 ml 20xNPS, 20 ml 50x5052, 2ml $MgSO_4$ and 0.2 ml 1000X trace elements with appropriate antibiotic.

Precultures were grown overnight in LB or 2xYT medium and diluted 20-30 fold to obtain starting main culture. The broth was incubated in shaker at 37° C for two hours and after that the temperature was decreased to 30° C and incubated so overnight. The cells were harvested in the morning by spinning down in the centrifuge at 5000 rpm. The yield was 2-3 mg from a 1 l of cell culture. Then, the cells were either frozen in liquid nitrogen for storage or disrupted in a microfluidizer after dilution in PBS buffer with addition of one tablet of

EDTA-free protease inhibitor cocktail Complete (Roche). After disruption cellular membranes were collected by centrifugation at 35 000 rpm.

The protein was extracted from the membrane by overnight solubilization in 300 mM NaCl, 50 mM NaPi and 2% DDM pH8.0. Then, the protein was applied to Ni-NTA column; binding was achieved in 1-3 hours. The resin was extensively washed with the washing buffer (300mM NaCl, 20 mM Tris, 0.1% DDM pH 8.0). The elution was done in elution buffer (300mM NaCl, 20 mM Tris, 200 mM Imidazole, 0.1% DDM pH8.0). Imidazole was removed by dialysis against 300mM NaCl, 20 mM Tris, 200 mM Imidazole and 0.1% DDM pH8.0.

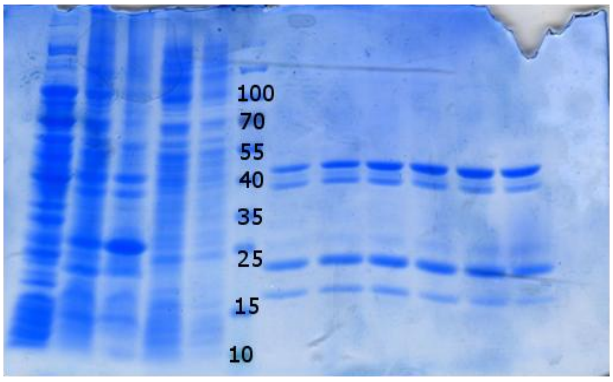

Figure 3.34 PAGE analysis of the purification process of the construct NarX-1-225
1. Cytoplasmic fraction
2. Membrane before fraction before solubilization
3. Membrane fraction after solubilization
4. Supernatant after solubilization
5. Ni-NTA column flow-through
6-11. Elution fractions from Ni-NTA column.

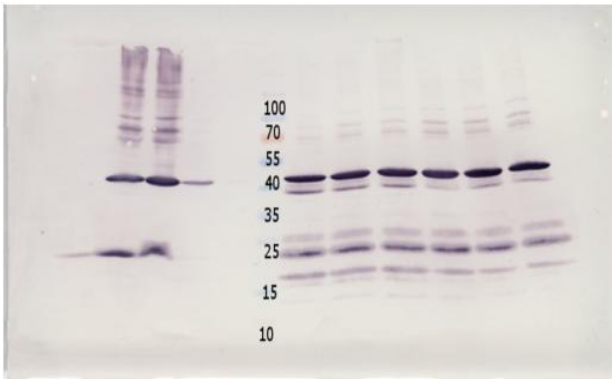

Figure 3.35 WB analysis of the purification process of the construct NarX-1-225
1. Cytoplasmic fraction
2. Membrane before fraction before solubilization
3. Membrane fraction after solubilization
4. Supernatant after solubilization
5. Ni-NTA column flow-through
6-11. Elution fractions from Ni-NTA column.

White pellet was observed in elution fractions from Ni-NTA purification and after dialysis. Though this pellet contains target protein, the major mass of the protein was still in the solution. The same pellet was observed in test purification using OG as solubilizing detergent (not discussed here). The conclusion is that the protein might not be sufficiently stable in these detergents and additional detergent screening would be necessary. The pellet was not observed when relatively harsh detergents were used (NLS, SDS).

The identity of the protein was verified by MALDI-TOF mass spectrometry (for detailed sample preparation description see Methods section). In brief, two methods were used: in-gel digestion and extraction and intact protein analysis. The following figure presents the MALDI-TOF spectrum of intact NarQ-1-231 solubilized in 2% DDM.

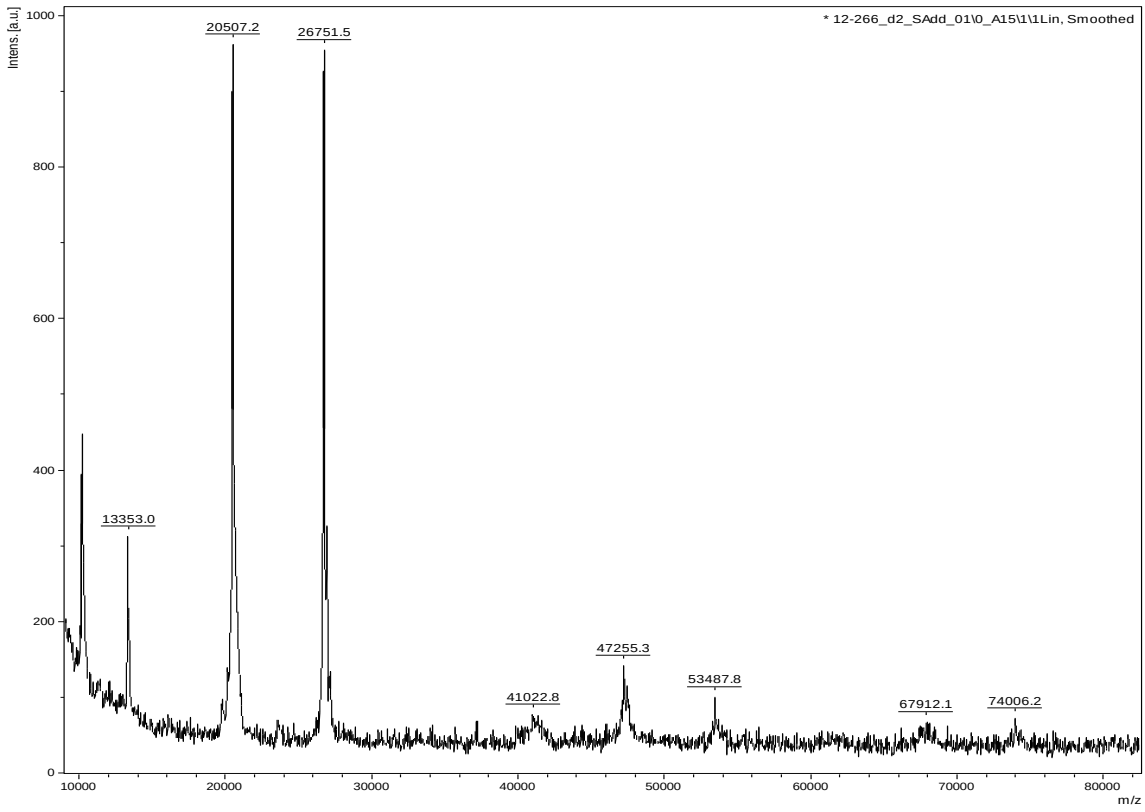

Sample	observed mass (Da)	expected mass (Da)	mass deviation (Da)	mass accuracy (ppm)*	interpretation
NarQ-1-231	**26751.5**	**26779.97**	28.5	1064	**In agreement**
	20507.2				**Truncated form of the protein (?)**
	13353.0				**Double charged ion of 26751.5**
	10216.2				**Double charged ion of 20507.2**

For initial crystallization screening NarQ-1-231 was concentrated in a centrifugal membrane concentrator (MWCO 30 KDa) to the concentration of 15 mg/ml and submitted for crystallization to HTXLab in EMBL Grenoble. Crystallization was set up at 20°C. The following kits were used: Crystal Screen Lite & PEG/Ion; MembFac & Natrix; QuickScreen & Grid screens Ammonium Sulfate, Sodium Malonate - Sodium Formate; Grid screens PEG 6K, PEG/LiCl, MPD - Screen Mme (all from Hampton) and The Classics (from Qiagen). First cubic crystals 20µm in size appeared in 50 days (Figure 3.36), belonging to space group I222 (lattice constants 81 Å, 149 Å, 158 Å, 90°, 90°, 90°) in Qiagen-The Classics kit with conditions 0.1 M tri-sodium citrate, 20% isopropanol, 20% PEG4000 pH 5.6.

The crystals were fished using standard protocol by Cherezov et al. [131] into MiTeGen cryoloops and flash frozen in liquid nitrogen without cryoprotectant. The

diffraction quality was tested at ESRF ID23-1 beamline and the Bragg peaks were tractable to the resolution up to 5 Å.

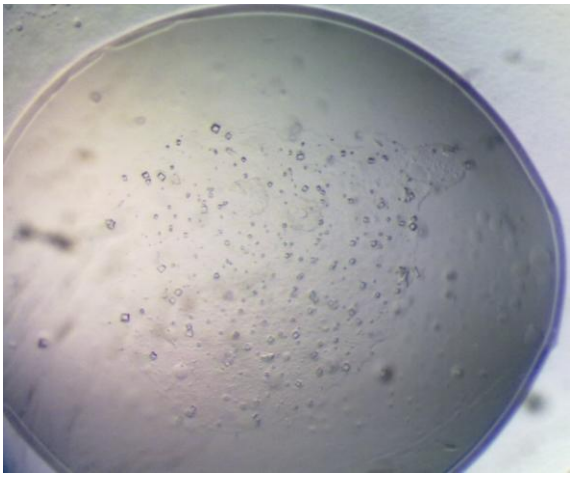

Figure 3.36 A photo of NarQ-1-231 crystals obtained by in surfo crystallization method

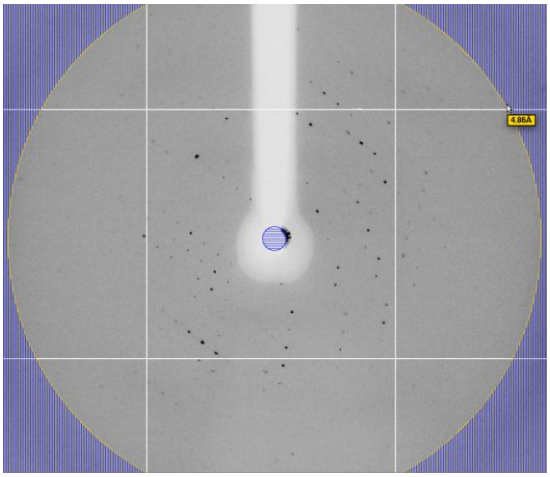

Figure 3.37 Diffraction pattern of NarQ-1-231 crystal

These experiments have confirmed that this construct is suitable for crystallization. Since the membrane proteins solubilized in DDM detergent usually don't form well-diffracting crystals, there is obviously still some room for quality improvement. The next setup was done for *in meso* crystallization. The protein solution in buffer 300 mM NaCl, 20 mM Tris pH 8, 2% DDM, was used to make crystallization setups. The protein/lipid mixture was mixed with lipid monooleoyl by 2:3 ratio using connected syringes. The meso-phase was formed after 1-2 days. After the phase formation, the protein/lipid/detergent mixture was dispensed using Formulatrix NT8 robot by 50 nl into each crystallization drop. Mother solution was dispensed by 800 nl into each drop. The following crystallization kits were used: Qiagen Cubic Phase I, Qiagen Cubic Phase II and Molecular Dimensions MemStart & MemSys. First crystals appeared after one month under various conditions in the kit Qiagen Cubic Phase II in probes containing 5% OG.

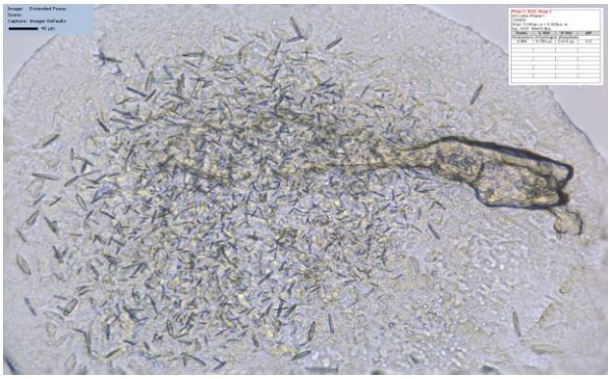

Figure 3.38 A photo of NarQ-1-231 crystals obtained by in surfo crystallization method

Main results and perspectives overview

- The structure of D75N mutant of SRII in a complex with HtrII was obtained with the resolution of 2 Å. The complex was crystallized using novel methods of nanovolume crystallization from mesophases using robotic technologies. The structure of the active site of SRII was analyzed. Possible mechanism of signal transfer in this complex is proposed.

- Different structures of the SRII/HtrII complex (resolution range 1.7-3.0 Å) have revealed two possible quaternary structures, which differ in the relative angle of the homodimer. They were called “V”-shape (for the structure initially observed in $P2_12_12$ space group) and ”U”-shape (for the structure initially observed in $I2_12_12_1$ space group). The relevance of this finding for understanding of the signal transduction mechanism in the complex is discussed.

- Various molecular constructs aiming to elucidate the structure of the cytoplasmic part of HtrII (and, particularly, the HAMP domain) were produced, expressed and purified. Unfortunately, the crystallization trials didn’t succeed for the moment of thesis preparation.

- Nitrate/nitrite receptors NarQ and NarX from *E.coli* were studied. Plasmid constructs containing membrane and cytoplasmic parts of the proteins were created. The proteins were expressed and purified. The first crystals diffracting to 5 Å were obtained. Crystallization optimization is ongoing at the moment.

Concluding remarks

Interactions between SRII and HtrII are of broad interest with respect to the mechanism of signal transduction in archaea and its close relationship to the chemotaxis in eubacteria. This thesis presents a new crystal form, D75N mutant and intermediate trapping study of sensory rhodopsin II in a complex with its transducer protein (HtrlI), both of which are cloned from the host halobacteria *N. pharaonis*. The major new finding of this work is a new structure of the complex in the space group $I2_12_12_1$ rather than $P2_12_12$ from which all earlier studies have been reported. A third crystal form, in $P6_4$, is also reported for a shorter HtrII construct (truncated at residue 135). Two SRII molecules in the dimer are inclined at an angle of about 15 degrees relative to each other in $I2_12_12_1$ whereas they are at an angle of 35 degrees in the earlier $P2_12_12$ crystal packing. This raises the question as: which crystal form most accurately models the packing of the SRII/HtrII complex in the native N. pharaonis membrane?

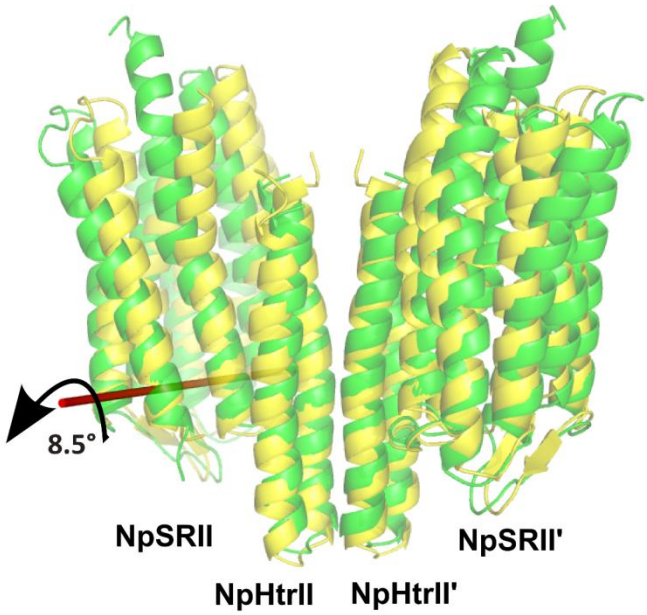

A view on the SRII/HtrII complex along the membrane. The "U"-shape structure is shown in yellow and the "V"-shape structure is shown in green. The red line indicates an axis of rigid body rotation during transformation of SRII from "V"-shape to "U"-shape.

Analysis of the homology model containing the HAMP domain indicates that the "U"-shape structure is a much better "candidate" for the ground state structure than the "V" shape. Another support of this idea is the fact that independent molecular dynamics studies have shown that the "V"-shape structure can transform into "U"-shape structure. The role of the

“V”-shape is not obvious. Taking into account various studies of interaction between the HAMP domain and SRII, especially EF loop, one can see that the connection between them loosens upon transition of the complex into active state. This is exactly the case of the “V”-shape where the HAMP domain is situated too far from SRII to form any hydrogen bonds or to have a strong electrostatic interaction. Therefore, it is suggested that “V”-shape might be an active form of the complex. If this is true then one should distinguish between spectroscopically distinct ground and M states on one side that are so far mostly characterized structurally by changes in the active site (first of all, isomerization state of the retinal), and “U” and “V”-shapes on the other side that appear in experiment under different crystallization conditions and cannot be interconverted in a single crystal. Ideally, if the theory is correct, in living systems the “U”-shape with all-*trans* retinal should represent the ground state and the “V”-shape with 13-*cis* retinal would represent the active state. The energy for such transition would then be converted from the energy of the incident photon, which is about 100 kT, while the energy of the mismatch between structures is estimated below 15 kT.

The D75N mutant of NpSRII-NpHtrII has been shown to exhibit wild-type phototaxis signaling activity *in vivo*, with the mutant complex modulating the motility system in a manner indistinguishable from the wild-type complex both in the dark and in the light. Meanwhile, the homologous complex from *H. salinarum* is constitutively active. The complex of NpSRII-D75N/NpHtrII was crystallized to the resolution of 2 Å that is sufficient for analyzing the hydrogen bond network in the active core of SRII. It was shown that in terms of hydrogen bonds number this mutant complex is in between the ground state and the M state of the wild type. Since no movements of helices were detected, it was suggested the existing hydrogen bonds network is sufficient to maintain SRII-D75N structure in the ground state.

Unfortunately, despite numerous efforts and embodied experiments, the structure of the HAMP domain couldn’t be solved. Structures of truncated HtrII in complex with SRII revealed only the membrane part of the proteins. Various constructs of water-soluble parts of HtrII also didn’t result in any crystals. The most probable reason is domain’s thermal instability and unfolding under low-salt conditions.

NarQ and NarX proteins represent an important family of transmembrane histidine kinases. They contain one HAMP domain and in their structure in general are highly similar to HtrII. As the genes come from *E.coli*, investigation of their structure and mechanism of functioning is of high practical importance. Moreover, in these systems the HAMP domain

structure may be more robust and easier to obtain in a folded state. By now the first crystals diffracting to 5 Å were obtained.

References

[1] M. Caffrey, V. Cherezov, Crystallizing membrane proteins using lipidic mesophases., Nature Protocols. 4 (2009) 706–31.

[2] A. Deniaud, E. Moiseeva, V. Gordeliy, E. Pebay-Peyroula, Crystallography of membrane proteins: from crystallization to structure., Methods in Molecular Biology (Clifton, N.J.). 654 (2010) 79–103.

[3] E.M. Landau, J.P. Rosenbusch, Lipidic cubic phases: a novel concept for the crystallization of membrane proteins., Proceedings of the National Academy of Sciences of the United States of America. 93 (1996) 14532–5.

[4] A.M. Stock, V.L. Robinson, P.N. Goudreau, Two-component signal transduction., Annual Review of Biochemistry. 69 (2000) 183–215.

[5] V.L. Robinson, D.R. Buckler, A.M. Stock, A tale of two components: a novel kinase and a regulatory switch., Nature Structural Biology. 7 (2000) 626–33.

[6] R. Moukhametzianov, J.P. Klare, R. Efremov, C. Baeken, A. Göppner, J. Labahn, et al., Development of the signal in sensory rhodopsin and its transfer to the cognate transducer., Nature. 440 (2006) 115–9.

[7] V.I. Gordeliy, J. Labahn, R. Moukhametzianov, R. Efremov, J. Granzin, R. Schlesinger, et al., Molecular basis of transmembrane signalling by sensory rhodopsin II-transducer complex., Nature. 419 (2002) 484–7.

[8] T. Tanaka, S.K. Saha, C. Tomomori, R. Ishima, D. Liu, K.I. Tong, et al., NMR structure of the histidine kinase domain of the E. coli osmosensor EnvZ., Nature. 396 (1998) 88–92.

[9] C. Tomomori, T. Tanaka, R. Dutta, H. Park, S.K. Saha, Y. Zhu, et al., Solution structure of the homodimeric core domain of Escherichia coli histidine kinase EnvZ., Nature Structural Biology. 6 (1999) 729–34.

[10] H. Otto, Substitution of Amino Acids Asp-85, Asp-212, and Arg-82 in Bacteriorhodopsin Affects the Proton Release Phase of the Pump and the pK of the Schiff Base, Proceedings of the National Academy of Sciences. 87 (1990) 1018–1022.

[11] P.R. Robinson, G.B. Cohen, E.A. Zhukovsky, D.D. Oprian, Constitutively active mutants of rhodopsin, Neuron. 9 (1992) 719–725.

[12] A.K. Dioumaev, J.M. Wang, Z. Bálint, G. Váró, J.K. Lanyi, Proton transport by proteorhodopsin requires that the retinal Schiff base counterion Asp-97 be anionic., Biochemistry. 42 (2003) 6582–7.

[13] J.S. Parkinson, Signaling mechanisms of HAMP domains in chemoreceptors and sensor kinases., Annual Review of Microbiology. 64 (2010) 101–22.

[14] E. Bordignon, J.P. Klare, M. Doebber, A.A. Wegener, S. Martell, M. Engelhard, et al., Structural Analysis of a HAMP Domain, Journal of Biological Chemistry. 280 (2005) 38767–38775.

[15] M. V Airola, K.J. Watts, B.R. Crane, Identifying divergent HAMP domains and poly-HAMP chains., The Journal of Biological Chemistry. 285 (2010) le7; author reply 1e8.

[16] I.Y. Gushchin, V.I. Gordeliy, S. Grudinin, Role of the HAMP Domain Region of Sensory Rhodopsin Transducers in Signal Transduction., Biochemistry. 50 (2010) 574–580.

[17] M. V Airola, K.J. Watts, A.M. Bilwes, B.R. Crane, Structure of concatenated HAMP domains provides a mechanism for signal transduction., Structure (London, England : 1993). 18 (2010) 436–48.

[18] M. Hulko, F. Berndt, M. Gruber, J.U. Linder, V. Truffault, A. Schultz, et al., The HAMP domain structure implies helix rotation in transmembrane signaling., Cell. 126 (2006) 929–40.

[19] T. Mascher, J.D. Helmann, G. Unden, Stimulus perception in bacterial signal-transducing histidine kinases., Microbiology and Molecular Biology Reviews : MMBR. 70 (2006) 910–38.

[20] J.J. Falke, G.L. Hazelbauer, Transmembrane signaling in bacterial chemoreceptors, Trends in Biochemical Sciences. 26 (2001) 257–265.

[21] L.A. Alex, M.I. Simon, Protein histidine kinases and signal tranduction in prokaryotes and eukaryotes, Trends in Genetics. 10 (1994) 133–138.

[22] A. Khorchid, M. Ikura, Bacterial histidine kinase as signal sensor and transducer., The International Journal of Biochemistry & Cell Biology. 38 (2006) 307–12.

[23] J. Cheung, W.A. Hendrickson, Structural analysis of ligand stimulation of the histidine kinase NarX., Structure (London, England : 1993). 17 (2009) 190–201.

[24] P.M. Wolanin, P.A. Thomason, J.B. Stock, Histidine protein kinases: key signal transducers outside the animal kingdom., Genome Biology. 3 (2002) REVIEWS3013.

[25] R. Dutta, L. Qin, M. Inouye, Histidine kinases: diversity of domain organization, Molecular Microbiology. 34 (1999) 633–640.

[26] C.E. Noriega, H.-Y. Lin, L.-L. Chen, S.B. Williams, V. Stewart, Asymmetric cross-regulation between the nitrate-responsive NarX-NarL and NarQ-NarP two-component regulatory systems from Escherichia coli K-12., Molecular Microbiology. 75 (2010) 394–412.

[27] F.D. Russo, T.J. Silhavy, The essential tension: opposed reactions in bacterial two-component regulatory systems, Trends in Microbiology. 1 (1993) 306–310.

[28] W.F. Loomis, G. Shaulsky, N. Wang, Histidine kinases in signal transduction pathways of eukaryotes., Journal of Cell Science. 110 (Pt 1 (1997) 1141–5.

[29] R. V Swanson, S.C. Schuster, M.I. Simon, Expression of CheA fragments which define domains encoding kinase, phosphotransfer, and CheY binding activities., Biochemistry. 32 (1993) 7623–9.

[30] H. Park, S.K. Saha, M. Inouye, Two-domain reconstitution of a functional protein histidine kinase., Proceedings of the National Academy of Sciences of the United States of America. 95 (1998) 6728–32.

[31] A.M. Bilwes, L.A. Alex, B.R. Crane, M.I. Simon, Structure of CheA, a signal-transducing histidine kinase., Cell. 96 (1999) 131–41.

[32] D.J. Bretl, C. Demetriadou, T.C. Zahrt, Adaptation to environmental stimuli within the host: two-component signal transduction systems of Mycobacterium tuberculosis., Microbiology and Molecular Biology Reviews : MMBR. 75 (2011) 566–82.

[33] A.K. Sharma, J.L. Spudich, W.F. Doolittle, Microbial rhodopsins: functional versatility and genetic mobility., Trends in Microbiology. 14 (2006) 463–9.

[34] T.M. Bridges, C.W. Lindsley, G-protein-coupled receptors: from classical modes of modulation to allosteric mechanisms., ACS Chemical Biology. 3 (2008) 530–41.

[35] W.D. Hoff, K.H. Jung, J.L. Spudich, Molecular mechanism of photosignaling by archaeal sensory rhodopsins., Annual Review of Biophysics and Biomolecular Structure. 26 (1997) 223–58.

[36] D. Oesterhelt, The structure and mechanism of the family of retinal proteins from halophilic archaea., Current Opinion in Structural Biology. 8 (1998) 489–500.

[37] T. Knöpfel, M.Z. Lin, A. Levskaya, L. Tian, J.Y. Lin, E.S. Boyden, Toward the second generation of optogenetic tools., The Journal of Neuroscience : the Official Journal of the Society for Neuroscience. 30 (2010) 14998–5004.

[38] H.U. Ferris, S. Dunin-Horkawicz, L.G. Mondéjar, M. Hulko, K. Hantke, J. Martin, et al., The mechanisms of HAMP-mediated signaling in transmembrane receptors., Structure (London, England : 1993). 19 (2011) 378–85.

[39] J. Wang, J. Sasaki, A.-L. Tsai, J.L. Spudich, HAMP Domain Signal Relay Mechanism in a Sensory Rhodopsin-Transducer Complex., The Journal of Biological Chemistry. 287 (2012) 21316–25.

[40] A.A. Wegener, J.P. Klare, M. Engelhard, H.J. Steinhoff, Structural insights into the early steps of receptor-transducer signal transfer in archaeal phototaxis., The EMBO Journal. 20 (2001) 5312–9.

[41] A.A. Wegener, I. Chizhov, M. Engelhard, H.J. Steinhoff, Time-resolved detection of transient movement of helix F in spin-labelled pharaonis sensory rhodopsin II., Journal of Molecular Biology. 301 (2000) 881–91.

[42] C.-S. Yang, O. Sineshchekov, E.N. Spudich, J.L. Spudich, The Cytoplasmic Membrane-proximal Domain of the HtrII Transducer Interacts with the E-F Loop of Photoactivated Natronomonas pharaonis Sensory Rhodopsin II, Journal of Biological Chemistry. 279 (2004) 42970–42976.

[43] S. Hippler-Mreyen, Probing the Sensory Rhodopsin II Binding Domain of its Cognate Transducer by Calorimetry and Electrophysiology, Journal of Molecular Biology. 330 (2003) 1203–1213.

[44] Y. Sudo, H. Okuda, M. Yamabi, Y. Fukuzaki, M. Mishima, N. Kamo, et al., Linker region of a halobacterial transducer protein interacts directly with its sensor retinal protein., Biochemistry. 44 (2005) 6144–52.

[45] M. Etzkorn, K. Seidel, L. Li, S. Martell, M. Geyer, M. Engelhard, et al., Complex formation and light activation in membrane-embedded sensory rhodopsin II as seen by solid-state NMR spectroscopy., Structure (London, England : 1993). 18 (2010) 293–300.

[46] I. Chizhov, G. Schmies, R. Seidel, J.R. Sydor, B. Lüttenberg, M. Engelhard, The photophobic receptor from Natronobacterium pharaonis: temperature and pH dependencies of the photocycle of sensory rhodopsin II., Biophysical Journal. 75 (1998) 999–1009.

[47] G. Schmies, B. Lüttenberg, I. Chizhov, M. Engelhard, a Becker, E. Bamberg, Sensory rhodopsin II from the haloalkaliphilic natronobacterium pharaonis: light-activated proton transfer reactions., Biophysical Journal. 78 (2000) 967–76.

[48] H. Luecke, B. Schobert, J.K. Lanyi, E.N. Spudich, J.L. Spudich, Crystal structure of sensory rhodopsin II at 2.4 angstroms: insights into color tuning and transducer interaction., Science (New York, N.Y.). 293 (2001) 1499–503.

[49] M. Engelhard, B. Scharf, F. Siebert, Protonation changes during the photocycle of sensory rhodopsin II from Natronobacterium pharaonis., FEBS Letters. 395 (1996) 195–8.

[50] E.N. Spudich, W. Zhang, M. Alam, J.L. Spudich, Constitutive signaling by the phototaxis receptor sensory rhodopsin II from disruption of its protonated Schiff base-Asp-73 interhelical salt bridge., Proceedings of the National Academy of Sciences of the United States of America. 94 (1997) 4960–5.

[51] J. Sasaki, T. Nara, E.N. Spudich, J.L. Spudich, Constitutive activity in chimeras and deletions localize sensory rhodopsin II/HtrII signal relay to the membrane-inserted domain, Molecular Microbiology. 66 (2007) 1321–1330.

[52] T. Takahashi, B. Yan, P. Mazur, F. Derguini, K. Nakanishi, J.L. Spudich, Color regulation in the archaebacterial phototaxis receptor phoborhodopsin (sensory rhodopsin II), Biochemistry. 29 (1990) 8467–8474.

[53] E. Pebay-Peyroula, A. Royant, E.M. Landau, J. Navarro, Structural basis for sensory rhodopsin function., Biochimica Et Biophysica Acta. 1565 (2002) 196–205.

[54] R. Efremov, Study of structure and mechanism of functioning of retinal membrane proteins: crystallization and trapping of protein intermediate states in crystals, MIPT, 2005.

[55] J. Sasaki, J.L. Spudich, Signal transfer in haloarchaeal sensory rhodopsin- transducer complexes., Photochemistry and Photobiology. 84 (2008) 863–8.

[56] J. Sasaki, A. Tsai, J.L. Spudich, Opposite displacement of helix F in attractant and repellent signaling by sensory rhodopsin-Htr complexes., The Journal of Biological Chemistry. 286 (2011) 18868–77.

[57] K. Hayashi, Y. Sudo, J. Jee, M. Mishima, H. Hara, N. Kamo, et al., Structural analysis of the phototactic transducer protein HtrII linker region from Natronomonas pharaonis., Biochemistry. 46 (2007) 14380–90.

[58] J.O. Moore, W.A. Hendrickson, Structural analysis of sensor domains from the TMAO-responsive histidine kinase receptor TorS., Structure (London, England : 1993). 17 (2009) 1195–204.

[59] K. Tsutsui, Y. Shichida, Multiple functions of Schiff base counterion in rhodopsins., Photochemical & Photobiological Sciences : Official Journal of the European Photochemistry Association and the European Society for Photobiology. 9 (2010) 1426–34.

[60] M. Han, B.S. DeDecker, S.O. Smith, Localization of the retinal protonated Schiff base counterion in rhodopsin., Biophysical Journal. 65 (1993) 899–906.

[61] L.S. Brown, A.K. Dioumaev, R. Needleman, J.K. Lanyi, Connectivity of the retinal Schiff base to Asp85 and Asp96 during the bacteriorhodopsin photocycle: the local-access model., Biophysical Journal. 75 (1998) 1455–65.

[62] R. Needleman, M. Chang, B. Ni, G. Varo, J. Fornes, S. White, et al., Properties of Asp212----Asn bacteriorhodopsin suggest that Asp212 and Asp85 both participate in a counterion and proton acceptor complex near the Schiff base, J. Biol. Chem. 266 (1991) 11478–11484.

[63] S. Rouhani, J.P. Cartailler, M.T. Facciotti, P. Walian, R. Needleman, J.K. Lanyi, et al., Crystal structure of the D85S mutant of bacteriorhodopsin: model of an O-like photocycle intermediate., Journal of Molecular Biology. 313 (2001) 615–28.

[64] H.J. Butt, K. Fendler, E. Bamberg, J. Tittor, D. Oesterhelt, Aspartic acids 96 and 85 play a central role in the function of bacteriorhodopsin as a proton pump., The EMBO Journal. 8 (1989) 1657–63.

[65] P. Rath, E. Spudich, D.D. Neal, J.L. Spudich, K.J. Rothschild, Asp76 is the Schiff base counterion and proton acceptor in the proton-translocating form of sensory rhodopsin I., Biochemistry. 35 (1996) 6690–6.

[66] C. Ganea, J. Tittor, E. Bamberg, D. Oesterhelt, Chloride- and pH-dependent proton transport by BR mutant D85N, Biochimica Et Biophysica Acta (BBA) - Biomembranes. 1368 (1998) 84–96.

[67] J. Tittor, D. Oesterhelt, E. Bamberg, Bacteriorhodopsin mutants D85N, D85T and D85,96N as proton pumps, Biophysical Chemistry. 56 (1995) 153–157.

[68] M. Sato, T. Kikukawa, T. Araiso, H. Okita, K. Shimono, N. Kamo, et al., Roles of Ser130 and Thr126 in chloride binding and photocycle of pharaonis halorhodopsin., Journal of Biochemistry. 134 (2003) 151–8.

[69] K. Inoue, J. Sasaki, J.L. Spudich, M. Terazima, Laser-induced transient grating analysis of dynamics of interaction between sensory rhodopsin II D75N and the HtrII transducer., Biophysical Journal. 92 (2007) 2028–40.

[70] C.S. Yang, J.L. Spudich, Light-induced structural changes occur in the transmembrane helices of the Natronobacterium pharaonis HtrII transducer., Biochemistry. 40 (2001) 14207–14.

[71] V. Stewart, Nitrate- and nitrite-responsive sensors NarX and NarQ of proteobacteria, Biochemical Society Transactions. 31 (n.d.) 1–10.

[72] E. Wallin, G. von Heijne, Genome-wide analysis of integral membrane proteins from eubacterial, archaean, and eukaryotic organisms., Protein Science : a Publication of the Protein Society. 7 (1998) 1029–38.

[73] K.M. Giacomini, S.-M. Huang, D.J. Tweedie, L.Z. Benet, K.L.R. Brouwer, X. Chu, et al., Membrane transporters in drug development., Nature Reviews. Drug Discovery. 9 (2010) 215–36.

[74] B. Byrne, S. Iwata, Membrane protein complexes, Current Opinion in Structural Biology. 12 (2002) 239–243.

[75] S. Faham, J.U. Bowie, Bicelle crystallization: a new method for crystallizing membrane proteins yields a monomeric bacteriorhodopsin structure., Journal of Molecular Biology. 316 (2002) 1–6.

[76] K. Takeda, H. Sato, T. Hino, M. Kono, K. Fukuda, I. Sakurai, et al., A novel three-dimensional crystal of bacteriorhodopsin obtained by successive fusion of the vesicular assemblies., Journal of Molecular Biology. 283 (1998) 463–74.

[77] V. Cherezov, J. Clogston, M.Z. Papiz, M. Caffrey, Room to move: crystallizing membrane proteins in swollen lipidic mesophases., Journal of Molecular Biology. 357 (2006) 1605–18.

[78] M. Caffrey, C. Porter, Crystallizing membrane proteins for structure determination using lipidic mesophases., Journal of Visualized Experiments : JoVE. (2010).

[79] D.M. Rosenbaum, V. Cherezov, M. a Hanson, S.G.F. Rasmussen, F.S. Thian, T.S. Kobilka, et al., GPCR engineering yields high-resolution structural insights into beta2-adrenergic receptor function., Science (New York, N.Y.). 318 (2007) 1266–73.

[80] B. Wu, E.Y.T. Chien, C.D. Mol, G. Fenalti, W. Liu, V. Katritch, et al., Structures of the CXCR4 chemokine GPCR with small-molecule and cyclic peptide antagonists., Science (New York, N.Y.). 330 (2010) 1066–71.

[81] D.M. Rosenbaum, C. Zhang, J.A. Lyons, R. Holl, D. Aragao, D.H. Arlow, et al., Structure and function of an irreversible agonist-β(2) adrenoceptor complex., Nature. 469 (2011) 236–40.

[82] G. Katona, U. Andréasson, E.M. Landau, L.-E. Andréasson, R. Neutze, Lipidic Cubic Phase Crystal Structure of the Photosynthetic Reaction Centre from Rhodobacter sphaeroides at 2.35Å Resolution, Journal of Molecular Biology. 331 (2003) 681–692.

[83] Y. Misquitta, M. Caffrey, Detergents destabilize the cubic phase of monoolein: implications for membrane protein crystallization., Biophysical Journal. 85 (2003) 3084–96.

[84] E. Gouaux, It's not just a phase: crystallization and X-ray structure determination of bacteriorhodopsin in lipidic cubic phases., Structure (London, England : 1993). 6 (1998) 5–10.

[85] V. Cherezov, Lipidic cubic phase technologies for membrane protein structural studies., Current Opinion in Structural Biology. 21 (2011) 559–566.

[86] H. Qiu, M. Caffrey, The phase diagram of the monoolein/water system: metastability and equilibrium aspects, Biomaterials. 21 (2000) 223–234.

[87] K.B. Mullis, F.A. Faloona, Specific synthesis of DNA in vitro via a polymerase-catalyzed chain reaction., Methods in Enzymology. 155 (1987) 335–50.

[88] S.N. Ho, H.D. Hunt, R.M. Horton, J.K. Pullen, L.R. Pease, Site-directed mutagenesis by overlap extension using the polymerase chain reaction., Gene. 77 (1989) 51–9.

[89] H. Inoue, H. Nojima, H. Okayama, High efficiency transformation of Escherichia coli with plasmids., Gene. 96 (1990) 23–8.

[90] H. Schägger, G. von Jagow, Tricine-sodium dodecyl sulfate-polyacrylamide gel electrophoresis for the separation of proteins in the range from 1 to 100 kDa, Analytical Biochemistry. 166 (1987) 368–379.

[91] H. Goetz, M. Kuschel, T. Wulff, C. Sauber, C. Miller, S. Fisher, et al., Comparison of selected analytical techniques for protein sizing, quantitation and molecular weight determination., Journal of Biochemical and Biophysical Methods. 60 (2004) 281–93.

[92] S. Tayyab, S. Qamar, M. Islam, Size exclusion chromatography and size exclusion HPLC of proteins, Biochemical Education. 19 (1991) 149–152.

[93] R.M. Caprioli, T.B. Farmer, J. Gile, Molecular Imaging of Biological Samples: Localization of Peptides and Proteins Using MALDI-TOF MS, Analytical Chemistry. 69 (1997) 4751–4760.

[94] O. Vorm, P. Roepstorff, M. Mann, Improved Resolution and Very High Sensitivity in MALDI TOF of Matrix Surfaces Made by Fast Evaporation, Analytical Chemistry. 66 (1994) 3281–3287.

[95] A.G.W. Leslie, The integration of macromolecular diffraction data., Acta Crystallographica. Section D, Biological Crystallography. 62 (2006) 48–57.

[96] P. Evans, Scaling and assessment of data quality., Acta Crystallographica. Section D, Biological Crystallography. 62 (2006) 72–82.

[97] R.G. Fisher, R.M. Sweet, Treatment of diffraction data from protein crystals twinned by merohedry: erratum, Acta Crystallographica Section A. 37 (1981) 137–137.

[98] T.O. Yeates, Detecting and overcoming crystal twinning., Methods in Enzymology. 276 (1997) 344–58.

[99] N. 4 Collaborative Computational Project, The CCP4 suite: programs for protein crystallography., Acta Crystallographica. Section D, Biological Crystallography. 50 (1994) 760–3.

[100] R. Efremov, R. Moukhametzianov, G. Büldt, V. Gordeliy, Physical detwinning of hemihedrally twinned hexagonal crystals of bacteriorhodopsin., Biophysical Journal. 87 (2004) 3608–13.

[101] V. Borshchevskiy, Study of Mechanism of proton transport in bacteriorhodopsin: obtaining high quality X-Ray structures of functional states, MIPT, 2011.

[102] P. Evans, A. McCoy, An introduction to molecular replacement., Acta Crystallographica. Section D, Biological Crystallography. 64 (2008) 1–10.

[103] T. Blundell, L. Johnson, Protein Crystallography, (1976).

[104] R.W. Grosse-Kunstleve, P.D. Adams, Patterson correlation methods: a review of molecular replacement with CNS, Acta Crystallographica Section D Biological Crystallography. 57 (2001) 1390–1396.

[105] R. Moukhametzianov, X-ray Crystallographic Study on the Mechanisms of Bacteriorhodopsin and the Sensory Rhodopsin / Transducer Complex, 2006.

[106] P.H. Zwart, P. V Afonine, R.W. Grosse-Kunstleve, L.-W. Hung, T.R. Ioerger, A.J. McCoy, et al., Automated structure solution with the PHENIX suite., Methods in Molecular Biology (Clifton, N.J.). 426 (2008) 419–35.

[107] A. Vagin, A. Teplyakov, MOLREP : an Automated Program for Molecular Replacement, Journal of Applied Crystallography. 30 (1997) 1022–1025.

[108] G. Langer, S.X. Cohen, V.S. Lamzin, A. Perrakis, Automated macromolecular model building for X-ray crystallography using ARP/wARP version 7., Nature Protocols. 3 (2008) 1171–9.

[109] G.N. Murshudov, A.A. Vagin, E.J. Dodson, Refinement of macromolecular structures by the maximum-likelihood method., Acta Crystallographica. Section D, Biological Crystallography. 53 (1997) 240–55.

[110] P.D. Adams, P. V Afonine, G. Bunkóczi, V.B. Chen, I.W. Davis, N. Echols, et al., PHENIX: a comprehensive Python-based system for macromolecular structure solution., Acta Crystallographica. Section D, Biological Crystallography. 66 (2010) 213–21.

[111] I.W. Davis, L.W. Murray, J.S. Richardson, D.C. Richardson, MOLPROBITY: structure validation and all-atom contact analysis for nucleic acids and their complexes., Nucleic Acids Research. 32 (2004) W615–9.

[112] A.T. Brünger, P.D. Adams, G.M. Clore, W.L. DeLano, P. Gros, R.W. Grosse-Kunstleve, et al., Crystallography & NMR system: A new software suite for macromolecular structure determination., Acta Crystallographica. Section D, Biological Crystallography. 54 (1998) 905–21.

[113] I. Gushchin, A. Reshetnyak, V. Borshchevskiy, A. Ishchenko, E. Round, S. Grudinin, et al., Active state of sensory rhodopsin II: structural determinants for signal transfer and proton pumping., Journal of Molecular Biology. 412 (2011) 591–600.

[114] A. Royant, P. Nollert, K. Edman, R. Neutze, E.M. Landau, E. Pebay-Peyroula, et al., X-ray structure of sensory rhodopsin II at 2.1-A resolution., Proceedings of the National Academy of Sciences of the United States of America. 98 (2001) 10131–6.

[115] W. Avenue, N. Haven, Crystallization of membrane proteins Christian Ostermeier and Hartmut Michelt, (1995) 697–701.

[116] A. Ishchenko, E. Round, V. Borshchevskiy, S. Grudinin, I. Gushchin, J.P. Klare, et al., Ground State Structure of D75N Mutant of Sensory Rhodopsin II in Complex with its Cognate Transducer, Journal of Photochemistry and Photobiology B: Biology. null (2013).

[117] M. Hein, I. Radu, J.P. Klare, M. Engelhard, F. Siebert, Consequences of counterion mutation in sensory rhodopsin II of Natronobacterium pharaonis for photoreaction and receptor activation: an FTIR study., Biochemistry. 43 (2004) 995–1002.

[118] J. Holterhues, E. Bordignon, D. Klose, C. Rickert, J.P. Klare, S. Martell, et al., The signal transfer from the receptor NpSRII to the transducer NpHtrII is not hampered by the D75N mutation., Biophysical Journal. 100 (2011) 2275–82.

[119] V.I. Borshchevskiy, E.S. Round, A.N. Popov, G. Büldt, V.I. Gordeliy, X-ray-radiation-induced changes in bacteriorhodopsin structure., Journal of Molecular Biology. 409 (2011) 813–25.

[120] K. Nishikata, S. Fuchigami, M. Ikeguchi, A. Kidera, Molecular modeling of the HAMP domain of sensory rhodopsin II transducer from Natronomonas pharaonis, Biophysics. 6 (2010) 27–36.

[121] Y. Sudo, M. Iwamoto, K. Shimono, N. Kamo, Pharaonis phoborhodopsin binds to its cognate truncated transducer even in the presence of a detergent with a 1:1 stoichiometry., Photochemistry and Photobiology. 74 (2001) 489–94.

[122] Y. Sudo, M. Yamabi, M. Iwamoto, K. Shimono, N. Kamo, Interaction of Natronobacterium pharaonis phoborhodopsin (sensory rhodopsin II) with its cognate transducer probed by increase in the thermal stability., Photochemistry and Photobiology. 78 (2003) 511–6.

[123] K. Nishikata, M. Ikeguchi, A. Kidera, Comparative Simulations of the Ground State and the M-Intermediate State of the Sensory Rhodopsin II-Transducer Complex with a HAMP Domain Model., Biochemistry. 51 (2012) 5958–5966.

[124] C. Nielsen, M. Goulian, O.S. Andersen, Energetics of inclusion-induced bilayer deformations., Biophysical Journal. 74 (1998) 1966–83.

[125] J.K. Lanyi, Bacteriorhodopsin., Annual Review of Physiology. 66 (2004) 665–88.

[126] V. Borshchevskiy, R. Efremov, E. Moiseeva, G. Büldt, V. Gordeliy, Overcoming merohedral twinning in crystals of bacteriorhodopsin grown in lipidic mesophase., Acta Crystallographica. Section D, Biological Crystallography. 66 (2010) 26–32.

[127] K. Takeda, Y. Matsui, N. Kamiya, S. Adachi, H. Okumura, T. Kouyama, Crystal Structure of the M Intermediate of Bacteriorhodopsin: Allosteric Structural Changes Mediated by Sliding Movement of a Transmembrane Helix, Journal of Molecular Biology. 341 (2004) 1023–1037.

[128] Y. Sudo, J.L. Spudich, Three strategically placed hydrogen-bonding residues convert a proton pump into a sensory receptor., Proceedings of the National Academy of Sciences of the United States of America. 103 (2006) 16129–34.

[129] A. Remeeva, Thesis, Institut de Biologie Structurale J.P. Ebel, 2013.

[130] F.W. Studier, Protein Production by Auto-Induction in High-Density Shaking Cultures, Growth (Lakeland). 234 (2005).

[131] W. Liu, V. Cherezov, Crystallization of membrane proteins in lipidic mesophases., Journal of Visualized Experiments : JoVE. (2011).

Appendix I

Table 1. *Crystallographic data collection and refinement statistics for the wild type complex SRII/HtrII*

	Ground State, HtrII truncated at resid. 157	**M State, HtrII truncated at resid. 157**	**Ground State, HtrII truncated at resid. 135**
Data collection			
Space group	$I2_12_12_1$	$I2_12_12_1$	$P6_4$
Cell dimensions			
a, b, c (Å)	49.64, 113.66, 125.99	49.56, 113.78, 125.39	66.31, 66.31, 170.08
α, β, γ (°)	90, 90, 90	90, 90, 90	90,90,120
Resolution (Å)	28.0-1.9 (1.97-1.90*)	36.0-1.9 (1.97-1.90*)	34.0-2.5 (2.59-2.50*)
Rmerge (%)	7.0 (39.3*)	5.1 (14.4*)	9.0 (39.6*)
I / σI	13.4 (2.4*)	18.7 (3.8*)	11.16 (2.1*)
Completeness (%)	99.4 (99.8*)	98.6 (95.6*)	77.6 (73.4*)
Redundancy	3.8 (3.5*)	3.4 (3.3*)	5.2 (5.5*)
Refinement			
Resolution (Å)	22-1.9	36-1.9	34-2.5
No. reflections	28430 (1423**)	28034 (1402**)	20997 (1080**)
Rwork / Rfree (%)	19.66 / 21.83	20.15 / 23.24	19.32 / 23.37
No. atoms			
Protein	2090	4180 (2090***)	2034
Ligand/ion	171	191 (171***)	110
Water	56	110 (54***)	26
B-factors			

Protein	22.70	24.30 (23.90***)	56.10
Ligand/ion	41.70	44.40 (48.50***)	69.70
Water	32.20	33.60 (32.90***)	59.70
R.m.s. deviations			
Bond lengths (Å)	0.011	0.010	0.012
Bond angles (°)	1.23	1.30	1.87

*Values in parentheses are for high-resolution shell.

** Number of reflection not used for refinement (free reflections)

*** Number of atoms whose position was refined (atoms of active-state model)

Rmerge=$\sum h \sum i |I(h,i) - \langle I(h) \rangle| / \sum h \sum i |I(h,i)| \times 100$ %, where I(h,i) is the intensity value of the ith measurement of h and <I(h)> is the corresponding mean value of h for all I measurements of h. The summation is over all measurements.

Rwork = $\sum \left| Fo - Fc \right| / \sum \left| Fo \right| \times 100$ %.

Rfree was calculated for 5% of observed reflections, omitted from the refinement and Rwork calculation and picked randomly within thin resolution shells.

Table 2. *Crystallographic data collection and refinement statistics for the complex SRII-D75N/HtrII*

	SRII-D75N/HtrII
Data collection	
Space group	$I2_12_121$
Cell dimensions	
a, b, c (Å)	49.47, 113.67, 126.19
α, β, γ (°)	90, 90, 90
Resolution (Å)	42-2.05 (2.12-2.05)*

Rmerge (%)	6.1 (40.6)
I / σI	15.0 (2.6)*
Completeness (%)	99.86(100.00)
Redundancy	3.7 (3.5)*
Refinement	
Resolution (Å)	42-2.05
No. reflections	22752 (1132**)
Rwork / Rfree (%)	20.26/22.29
No. atoms	
Protein	2053
Ligand/ion	102
Water	70
B-factors	
Protein	25.10
Ligand/ion	38.30
Water	40.10
R.m.s. deviations	
Bond lengths (Å)	0.011
Bond angles (°)	1.13

---

*Values in parentheses are for highest-resolution shell.

** Number of reflection not used for refinement (free reflections)

*** Number of atoms whose position was refined (atoms of active-state model)

Rmerge=$\sum h \sum i |I(h,i) - \langle I(h) \rangle| / \sum h \sum i |I(h,i)| \times 100$ %, where I(h,i) is the intensity value of the ith measurement of h and $\langle I(h) \rangle$ is the corresponding mean value of h for all I measurements of h. The summation is over all measurements.

$$Rwork = \sum | Fo - Fc | / | \sum Fo | \times 100\ \%.$$

Rfree was calculated for 5% of observed reflections, omitted from the refinement and Rwork calculation, picked randomly within thin resolution shells.

Appendix II

Amino-acid sequences of protein constructs (together with expression tags)

SRII:

VGLTTLFWLGAIGMLVGTLAFAWAGRDAGSGERRYYVTLVGISGIAAVAYV
VMALGVGWVPVAERTVFAPRYIDWILTTPLIVYFLGLLAGLDSREFGIVITLNT
VVMLAGFAGAMVPGIERYALFGMGAVAFLGLVYYLVGPMTESASQRSSGIKS
LYVRLRNLTVILWAIYPFIWLLGPPGVALLTPTVDVALIVYLDLVTKVGFGFIA
LDAAATLRAEHGESLAGVDTDAPAVADENSHHHHHHH

HtrII-1-134:

MSLNVSRLLLPSRVRHSYTGKMGAVFIFVGALTVLFGAIAYGEVTAAAATGD
AAAVQEAAVSAILGLIILLGINLGLVAATLFGDTAASLSTLAAKASRMGDGDL
DVELETRREDEIGDLYAAFDEMRQSVRTSCITGDALVALPEGESVRIADIVPGA
RPNSDNAIDLKVLDRHGNPVLADRLFHSGEHPVYTVRTVEGLRVTGTANHPL
LCLVDVAGVPTLLWKLIDEIKPGDYAVIQRSAFSVDCAGFARGKPEFAPTTYT
VGVPGLVRFLEAHHRDPDAQAIADELTDGRFYYAKVASVTDAGVQPVYSLR
VDTADHAFITNGFVSHATGLTGLNSGLTTNPGVSAWQVNTAYTAGQLVTYN
GKTYKCLQPHTSLAGWEPSNVPALWQLQ

HtrII-83-210:

MGGDTAASLSTLAAKASRMGDGDLDVELETRREDEIGDLYAAFDEMRQSVR
TSLEDAKNAREDAEQAQKRAEEINTELQAEAERFGEVMDRCADGDFTQRLDA
ETDNEAMQSIEGSFNEMMDGIEALVGLEHHHHHH

HtrII-83-157:

MKIEEGKLVIGSLEGCFAKGTNVLMADGSIECIENIEVGNKVMGKDGRPREVI
KLPRGRETMYSVVQKSQHRAHKSDSSREVPELLKFTCNATHELVVRTPRSVR
RLSRTIKGVEYFEVITFEMGQKKAPDGRIVELVKEVSKSYPISEGPERANELVE
SYRKASNKAYFEWTIEARDLSLLGSHVRKATYQTYAPILYENDHFFDYMQKS
KFHLTIEGPKVLAYLLGLWIGDGLSDRATFSVDSRDTSLMERVTEYAEKLNLC
AEYKDRKEPQVAKTVNLYSKVVRGASTNPGVSAWQVNTAYTAGQLVTYNG
KTYKCLQPHTSLAGWEPSNVPALWQLQGGHGGIRNNLNTENPLWDAIVGLGF
LKDGVKNIPSFLSTDNIGTRETFLAGLIDSDGYVTDEHGIKATIKTIHTSVRDGL

VSLARSLGLVVSVNAEPAKVDMNVTKHKISYAIYMSGGDVLLNVLSKCAGSK
KFRPAPAAAFARECRGFYFELQELKEDDYYGITLSDDSDHQFLLGSQVVVQN
GGDTAASLSTLAAKASRMGDGDLDVELETRREDEIGDLYAAFDEMRQSVRTS
LEDAKNAREDAEQAQKRAEEINT

HtrII-83-135:

MKIEEGKLVIGSLEGCFAKGTNVLMADGSIECIENIEVGNKVMGKDGRPREVI
KLPRGRETMYSVVQKSQHRAHKSDSSREVPELLKFTCNATHELVVRTPRSVR
RLSRTIKGVEYFEVITFEMGQKKAPDGRIVELVKEVSKSYPISEGPERANELVE
SYRKASNKAYFEWTIEARDLSLLGSHVRKATYQTYAPILYENDHFFDYMQKS
KFHLTIEGPKVLAYLLGLWIGDGLSDRATFSVDSRDTSLMERVTEYAEKLNLC
AEYKDRKEPQVAKTVNLYSKVVRGASTNPGVSAWQVNTAYTAGQLVTYNG
KTYKCLQPHTSLAGWEPSNVPALWQLQGGHGGIRNNLNTENPLWDAIVGLGF
LKDGVKNIPSFLSTDNIGTRETFLAGLIDSDGYVTDEHGIKATIKTIHTSVRDGL
VSLARSLGLVVSVNAEPAKVDMNVTKHKISYAIYMSGGDVLLNVLSKCAGSK
KFRPAPAAAFARECRGFYFELQELKEDDYYGITLSDDSDHQFLLGSQVVVQN
GGDTAASLSTLAAKASRMGDGDLDVELETRREDEIGDLYAAFDEMRQSVRTS

HtrII-83-534:

MGGDTAASLSTLAAKASRMGDGDLDVELETRREDEIGDLYAAFDEMRQSVR
TSLEDAKNAREDAEQAQKRAEEINTELQAEAERFGEVMDRCADGDFTQRLDA
ETDNEAMQSIEGSFNEMMDGIEALVGRIERFADAVSEDAEAVRANAESVMEA
SEDVNRAVQNISDAAGDQTETVQQIALEMDDVSATTEEVAASADDIAKTARQ
AAETGEAGRETAETAITEMNEVESRTEQAVASMEELNEDVREIGEVSEMIADI
AEQTNILALNASIEAARADGNSEGFAVVADEVKALAEETKAATEEIDDLIGTV
QDRTQTTVDDIRETSDQVSEGVETVEDTVDALERIVDSVERTNDGIQEINQSTD
AQADAAQKATTMVEDMAATSEQTASDAETAAETTETQAESVKEVFDLIDGLS
EQADTLSETLRRTDTEEASAADLDDQPTLAAGDDLEHHHHHH

NarQ-1-231:

MIVKRPVSASLARAFFYIVLLSILSTGIALLTLASSLRDAEAINIAGSLRMQSYR
LGYDLQSGSPQLNAHRQLFQQALHSPVLTNLNVWYVPEAVKTRYAHLNANW
LEMNNRLSKGDLPWYQANINNYVNQIDLFVLALQHYAERKMLLVVAISLAG
GIGIFTLVFFTLRRIRHQVVAPLNQLVTASQRIEHGQFDSPPLDTNLPNELGLLA
KTFNQMSSELHKLYRSLEHHHHHH

NarX-1-225:

MLKRCLSPLTLVNQVALIVLLSTAIGLAGMAVSGWLVQGVQGSAHAINKAGS
LRMQSYRLLAAVPLSEKDKPLIKEMEQTAFSAELTRAAERDGQLAQLQGLQD
YWRNELIPALMRAQNRETVSADVSQFVAGLDQLVSGFDRTTEMRIETVVLVH
RVMAVFMALLLVFTIIWLRARLLQPWRQLLAMASAVSHRDFTQRANISGRNE
MAMLGTALNNMSAELAELEHHHHHH

Appendix III

PDB Accession codes

4GY6 NpSRII/HtrII-157 ground state

4GYA NpSRII/HtrII-135 ground state

4GY8 NpSRII/HtrII-157 M state

4J1D NpSRII/HtrIIG83F-135 ground state

4GYC NpSRII-D75N/NpHtrII ground state

Abstract

Membrane proteins are one of the main components of cell membranes and have a variety of functions. Studies of membrane proteins are of big importance for understanding the key processes that maintain a cell in a viable state. Despite the well-established importance and wide interest, the number of the structures of membrane proteins available at the moment is small. The rate of appearance of membrane protein structures is lagging considerably from that for water-soluble proteins. The reasons for that are difficulties that researchers encounter of all stages of protein preparation.

Two-component signaling systems is an important class of proteins. In contrast to eukaryota, most prokaryotic signal transduction pathways use schemes of phosphate transfer involving two conserved components, a histidine protein kinase and a response regulator protein. To the moment, hundreds of such systems were found in eubacteria, archaea, and a few eukaryotic organisms. These systems serve as a basic stimulus-response coupling mechanism to allow organisms to sense and respond to changes in many different environmental conditions. Though many advances in the field of signal transduction in two-component signal transduction have been made recently, there is still a strong demand for robust model systems where molecular mechanism of signal transduction can be studied. The complex of two membrane proteins from Halobacterium *N.pharaonis*, Sensory Rhodopsin II (SRII) with its cognate Transducer (HtrII) is an example of such system. It is serving as a phototaxis receptor that helps halobacteria to avoid harmful UV light. Sensory rhodopsin II belongs to the family of archaeal retinal proteins. HtrII is highly homologous to bacterial chemoreceptors. It consists of transmembrane domain, linker domain, methylation region involved in adaptation and kinase domain.

The X-Ray structures of SRII/HtrII give a unique insight into the complex of two transmembrane proteins. These structures elucidate initial steps of signal transduction in SRII and possible mechanism to transfer the signal to HtrII. NMR structures of cytoplasmic domain of osmotic sensor EnvZ from *E.coli* have shown the design of kinase domain that is highly conserved among all histidine kinases. Despite some structural information available there is still no detailed molecular mechanism of functioning of the complex from the initial step of retinal isomerization to phosphate group transition to the kinase CheA. This work is aimed to elucidate some of these steps in more detail and to show by means of X-Ray structural analysis the key features of protein structures that are prerequisite for efficient signal transduction.

All halobacterial retinal proteins share common features of the signal transduction mechanism. One of these features is a proton transfer from the Schiff base to the counterion after retinal isomerization. Various studies have shown that the mutation of the counterion to a neutral amino acid residue is critical for the function of most of them. In the case of SRII/HtrII complex, physiological experiments have shown that Asp75-to-Asn75 mutation doesn't inhibit the signal transduction that is seen as persistent rate of cell motion reversals upon light illumination. This fact is important for understanding signal transduction mechanism in these systems. The structure described in this thesis shows the change in the hydrogen network of SRII-D75N/HtrII complex with respect to the wild type complex. Comparison with the ground and M states of the wild type has helped to elucidate how the signal transduction process might evolve in the D75N mutant protein.

Intense crystallization under various conditions has resulted into another finding that might be very important for understanding of the mechanism of functioning. Crystals of different space groups were produced and the structures in these space groups were compared to the previously published structures in the $P2_12_12$ space group. A striking difference in the arrangement of the SRII and HtrII proteins in the complex were observed. Whereas in the $P2_12_12$ space group the proteins form a crevice with an opening towards cytoplasmic side ("V"-shape), in newly obtained structure of $I2_12_12_1$ space group proteins are roughly parallel to each other ("U"-shape). This thesis contains a discussion about which of the quaternary structures of the complex represents the functional complex that occurs *in vivo*.

Histidine kinase chemoreceptors are another representative of two-component signal transduction systems. NarQ and NarX belong to the family of histidine kinase receptors and react to nitrate or nitrite to regulate anaerobic respiration in various bacteria. This study has revealed some approaches that can be used in studying these very important proteins. First crystals were obtained. The membrane domain of the nitrate/nitrite receptor NarQ from *E.coli* was successfully expressed, purified and crystallized. At the moment these crystals require additional optimization.

Abstract

Membranproteine sind ein Hauptbestandteil von Zellmembranen und erfüllen dort unterschiedliche Funktionen. Die Untersuchung von Membranproteinen ist von großer Bedeutung für das Verständnis der Prozesse, die eine Zelle am Leben halten. Obwohl die wichtige Rolle von Membranproteinen bekannt und von großem Interesse ist, ist die Struktur der meisten Membranproteine bisher nicht untersucht. Die Aufklärung der Struktur von Membranproteinen macht deutlich langsamere Fortschritte als die wasserlöslicher Proteine. Dies ist auf Schwierigkeiten in allen Phasen der Proteinpräparation zurückzuführen.

Zweikomponenten-Signaltransduktionsproteine sind eine wichtige Proteinklasse. Anders als bei Eukaryoten kommt in den meisten Prokaryoten bei der Signaltransduktion ein Schema des Phosphattransfers zum Tragen, an dem zwei konservierte Proteinkomponenten beteiligt sind: eine Histidinkinase und ein Antwortregulator. Bis heute wurden hunderte solcher Systeme in Eubakterien, Archaeen, sowie in einigen eukaryotischen Organismen gefunden. Diese Systeme dienen als einfacher Mechanismus der Kopplung zwischen Stimulus und Antwort, der es Organismen erlaubt, Veränderungen verschiedener Umweltbedingungen wahrzunehmen und auf sie zu reagieren. Obwohl bei der Erforschung der Signaltransduktion in Zweikomponentensystemen in letzter Zeit viele Fortschritte gemacht wurden, besteht noch immer ein großer Bedarf an zuverlässigen Modellsystemen, mit denen die molekularen Mechanismen der Signaltransduktion untersucht werden können. Ein aus zwei Membranproteinen – dem sensorischen Rhodopsin II (SRII) und dem zugehörigen Transducer (HtrII) – bestehender Komplex in dem Halobakterium *N. pharaonis* ist ein Beispiel für ein solches System. Als Phototaxis-Rezeptor hilft dieser Komplex Halobakterien bei der Vermeidung schädlichen UV-Lichts. Das Sensor Rhodopsin II gehört zur Familie der archaealen Retinalproteine. HtrII weist eine starke Homologie zu bakteriellen Chemorezeptoren auf. Es besteht aus einer Transmembrandomäne, einem Linkerbereich, einer Methylierungsdomäne, die an der Adaption beteiligt ist, und einer Kinasedomäne.

Die Röntgenstrukturen von SRII/HtrII geben einen einzigartigen Einblick in den Komplex aus zwei Transmembranproteinen. Diese Strukturinformationen erklären die ersten Schritte der Signaltransduktion in SRII und einen möglichen Mechanismus der Signalübermittlung an HtrII. NMR-Strukturinformationen der zytoplasmatischen Domäne des osmosensorischen EnvZ aus *E. coli* zeigen den Aufbau der Kinasedomäne. Obwohl mehrere Strukturinformationen vorliegen, sind die Details der Funktionsweise des Komplexes auf molekularer Ebene, von der Isomerisierung des Retinals zum Übergang einer

Phosphatgruppe zur Kinase CheA, noch immer unbekannt. Diese Arbeit soll einen Beitrag zur Aufklärung einiger dieser Schritte leisten und mit Hilfe der Röntgenstrukturanalyse die wichtigsten Eigenschaften von Proteinstrukturen zeigen, die eine effiziente Signaltransduktion möglich machen.

Der Mechanismus der Signaltransduktion weist bei allen halobakteriellen Retinalproteinen einige Gemeinsamkeiten auf. Eine dieser Gemeinsamkeiten ist ein Protonentransfer von der Schiff Base zum Gegenion, der nach der Isomerisierung des Retinals stattfindet. Verschiedene Studien haben gezeigt, dass die Mutation des Gegenions zu einem neutralen Aminosäurerest in vielen Fällen kritisch für die Funktion ist. Im Fall des SRII/HtrII-Komplexes haben physiologische Versuche gezeigt, dass die Mutation von Asp75 zu Asn75 die Signaltransduktion, die als persistente Rate der Umkehrung von Zellbewegungen bei Lichteinfall gilt, nicht hemmt. Diese Tatsache ist wichtig, um den Mechanismus der Signaltransduktion in diesen Systemen zu verstehen. Die in dieser Arbeit beschriebene Struktur zeigt die Veränderung im Wasserstoffnetzwerk vom SRII-D75N/HtrII-Komplex im Vergleich zum Wildtyp-Komplex. Ein Vergleich mit dem Grundzustand und dem M-Zustand des Wildtyps konnte Hinweise darauf geben, wie die Signaltransduktion in der D75N-Proteinvariante möglicherweise abläuft.

Die intensive Kristallisierung unter verschiedenen Bedingungen hat zu einem weiteren Ergebnis geführt, das für das Verständnis des Funktionsmechanismus ebenfalls von großer Bedeutung sein könnte. Es wurden Kristalle hergestellt, die unterschiedliche Raumgruppen aufwiesen, und die Strukturinformationen für diese Raumgruppen wurden mit den vorher veröffentlichen Daten zur Raumgruppe $P2_12_12$ verglichen. Dabei wurde ein auffallender Unterschied in der Anordnung der SRII- und HtrII-Proteine innerhalb des Komplexes festgestellt. Während die Proteine in der Raumgruppe $P2_12_12$ einen "Spalt" bilden, der zur zytoplasmatischen Seite hin offen ist ("V-Form"), sind sie in der neuen Struktur der Raumgruppe $I2_12_12_1$ etwa parallel angeordnet ("U-Form"). In dieser Arbeit wird diskutiert, welche der Quartärstrukturen des Komplexes den *in vivo* vorkommenden funktionalen Komplex darstellt.

Histidinkinasen sind ein weiteres Beispiel für Zweikomponentensysteme zur Signaltransduktion. NarQ und NarX sind solche Histidinkinasen, die als Rezeptor für Nitrat und Nitrit dienen, d. h. auf diese Substanzen reagieren, um die anaerobe Atmung in verschiedenen Bakterien zu regulieren. Diese Arbeit zeigt einige Ansätze, die bei der Untersuchung dieser sehr wichtigen Proteine zur Anwendung kommen können. Dazu wurden

zunächst Kristalle gewonnen. Die Membrandomäne des Nitrat/Nitrit-Rezeptors NarQ aus *E. coli* wurde erfolgreich exprimiert, gereinigt und kristallisiert. Derzeit erfordern diese Kristalle jedoch noch weitere Optimierung.

Jül-4362
Juni 2013
ISSN 0944-2952